
Mitigating Data Scarcity in Time Series Analysis: A Foundation Model with Series-Symbol Data Generation

Wenxuan Wang¹ Kai Wu¹ Yujian Betterest Li¹ Dan Wang² Xiaoyu Zhang³ Jing Liu¹

Abstract

Foundation models for time series analysis (TSA) have attracted significant attention. However, challenges such as data scarcity and data imbalance continue to hinder their development. To address this, we consider modeling complex systems through symbolic expressions that serve as semantic descriptors of time series. Building on this concept, we introduce a series-symbol (S2) dual-modality data generation mechanism, enabling the unrestricted creation of high-quality time series data paired with corresponding symbolic representations. Leveraging the S2 dataset, we develop *SymTime*, a pre-trained foundation model for TSA. *SymTime* demonstrates competitive performance across five major TSA tasks when fine-tuned with downstream task, rivaling foundation models pre-trained on real-world datasets. This approach underscores the potential of dual-modality data generation and pretraining mechanisms in overcoming data scarcity and enhancing task performance.

1. Introduction

researchers (Liang et al., 2024; Wang et al., 2024c). In recent years, with the rapid advancement of deep learning, foundation models for TSA have garnered widespread attention due to their superior generalization capabilities, scalability and advantages in few-shot learning (Zhou et al., 2023). Presently, pre-training methods such as mask time series modeling (MTM) (Zhao et al., 2024; Dong et al., 2024), contrastive learning (Wang et al., 2023c), and generative modeling (Liu et al., 2024d) have given rise to a series of foundation models for time series, achieving significant

results in TSA tasks.

Coupled with issues of data privacy (Farayola et al., 2024; Wang et al., 2023c), existing time series datasets are smaller compared to those in the fields of computer vision (CV) and natural language processing (NLP). Besides, current large-scale time series datasets face significant data imbalance issues, with certain types such as finance and healthcare still being relatively scarce (see Appendix B.2). According to scaling laws (Bahri et al., 2024), this can lead to performance bias in the time series foundation models, reducing their generalization capabilities on out-of-distribution data (Yao et al., 2025).

To address the issue of data scarcity and data imbalance, this paper, starting from the nature and mechanisms of time series, posits that time series are representations of complex dynamical systems (Torres et al., 2021; Li et al., 2023a). On one hand, the intricate patterns within natural systems can be captured through observed numerical data (Meidani et al., 2023); for instance, the time series of body temperature fluctuations throughout a day is derived from observations of the human system. On the other hand, complex systems can be expressed abstractly using mathematical symbols and formulas (Kamienny et al., 2022), with ordinary differential equations (ODE) and partial differential equations (PDE) being the most common methods for modeling complex systems (Doering, 2018). Symbols provide semantic information for modeling complex systems (Bartlett et al., 2024). Therefore, as time series serve as the dynamic representation of observing complex systems, they can form a pairing relationship with the symbols used to model these systems.

To this end, we provide a series-symbol (S2) dual-modality data generation mechanism. This allows us to unrestrictedly produce high-quality time series and their paired symbolic data, constructing a large-scale S2 dataset. Then, we pretrain a time series foundation model *SymTime* with symbolic semantic information on this dataset. We train a Transformer-based time series encoder and a symbol encoder composed of a pre-trained large language model (LLM) (Radford et al., 2019) through MTM and mask language modeling (MLM) (Devlin et al., 2019) to learn the basic representations of series and symbols respectively. Subsequently, using momentum distillation (Li et al., 2021; Lin & Hu, 2024), we

¹School of Artificial Intelligence, Xidian University, Xi’an, Shaanxi, China ²The State Key Laboratory of Integrated Services Networks, Xi’an, Shaanxi, China ³School of Network and Information Security, Xidian University, Xi’an, Shaanxi, China. Correspondence to: Kai Wu <kwu@xidian.edu.cn>, Dan Wang <danwang@xidian.edu.cn>.

introduce contrastive losses between series and symbols through the added [CLS] token to further learn the cross-modal pairing representations and knowledge between series and symbols. To encapsulate our work, the contributions are as follows:

- We posit that time series are representations of complex dynamical systems and symbolic expressions can be regarded as the semantic information of time series. Based on this, we provide a method for the infinite generation of high-quality dual-modality series-symbol data. The size of the S2 dataset directly correlates with model performance on downstream tasks, and our S2 data can evenly cover the basic representations of all types of time series.
- Using synthetic S2 datasets, we construct the dual-modality time series pretrained foundation model, *SymTime*, using mask modeling and contrastive learning, thereby obtaining a pre-trained model with symbolic semantic information and cross-modal representations. Compared to foundation models pre-trained on real datasets, *SymTime* achieves competitive results in the five major TSA tasks.
- Additionally, we observe that: 1) *SymTime* achieves better performance with a smaller model parameter count and memory capacity than existing foundation models in forecasting; 2) *SymTime* successfully learns fundamental time series representations, enabling zero-shot imputation.

2. Related Work

In CV and NLP (Radford et al., 2021), pre-trained foundation models (PTFMs) have been demonstrated to adapt to a variety of downstream tasks after fine-tuning on specific datasets, exhibiting excellent generalization and scalability (Chen et al., 2024). Inspired by this, recent years have seen significant progress in PTFMs for TSA (Ahmed et al., 2023; Liang et al., 2024), with the emergence of various pre-training methods. MOIRAI, through MTM and reconstruction, has been pre-trained on large datasets (27B), yielding a universal forecasting model with significant zero-shot advantages (Woo et al., 2024). Timer, after generative pre-training on large datasets (1B), has performed well in forecasting (Liu et al., 2024d). TimeGPT trained an encoder-decoder Transformer with 100B data (Garza et al., 2024). COMET, using multi-level contrastive learning on a large ECG dataset, has obtained a medical time series PTFMs with few-shot advantages (Wang et al., 2023c).

As discussed in Appendix B.2, these baseline models still face challenges related to data scarcity and data imbalance. In the next section, we introduce the proposed data generation mechanism and the corresponding dual-modality

foundation model designed to address these issues. The review of other topics can be found in Appendix E.

3. Main Methods

3.1. Series-Symbol (S2) Dataset Generation

The pre-training of *SymTime* relies on a large synthetic series-symbol (S2) dataset. The specific generation process is shown in Figure 1 (left). Firstly, we construct a multivariate input-output symbolic expression $f(\cdot)$ through random sampling (Lample & Charton, 2020). Then, we use the randomly generated sampling series $X \in \mathbb{R}^{M \times L}$ to forward propagate through the symbolic expression to obtain the generated series $Y = f(X) \in \mathbb{R}^{N \times L}$, where N and M represent the dimensions of the input and output series respectively, and L is the length of the series.

Sampling of Functions. We first determine the dimensions of the input and output series and randomly select the number of binary operators from a uniform distribution. Then, we construct a binary tree with symbolic variables and constants as leaf nodes, and binary operators as two-child nodes to form the basic framework of the symbolic expression (Meidani et al., 2023). Finally, we enhance the diversity of the expressions by inserting unary operators as one-child nodes and applying affine transformations randomly (Kamienny et al., 2022). After determining the framework of the tree, we select specific operators for all nodes from the uniform distribution $\mathcal{U}(+, -, \times)$ and $\mathcal{U}(\text{inv}, \text{abs}, \text{pow}2, \text{pow}3, \text{sqrt}, \text{sin}, \text{cos}, \text{tan}, \text{arctan}, \text{log}, \text{exp})$, and randomly initialize leaf nodes with random constants and variables. The symbolic expression can be read out via in-order traversal.

Generating Inputs and Outputs. To better align the generated series with time series characteristics, we sample multi-channel input series X from both mixed distributions (MD) (Kamienny et al., 2022) and randomly parameterized ARMA(p, q) models (Chujai et al., 2013). We first select the distribution number in MD or the order (p, q) in ARMA model from the uniform distribution (Shumway et al., 2017; Lample & Charton, 2020). Then, we randomly initialize the parameters of the MD (including the mean and variance of a normal distribution, as well as the range of a uniform distribution) or the ARMA model (including autoregressive and moving average components). We can obtain the sampling series X through forward propagation. Finally, we standardize each channel and obtain the generated series $Y = f(X)$ through the symbolic expressions. To ensure data quality, we discard samples outside the domain of $f(\cdot)$ and excessively large generated values (Meidani et al., 2023).

Details and specific processes for data generation are provided in Appendix A. Through the two processes mentioned, we can obtain a large number of multi-channels series along with their corresponding symbolic expressions. We concate-

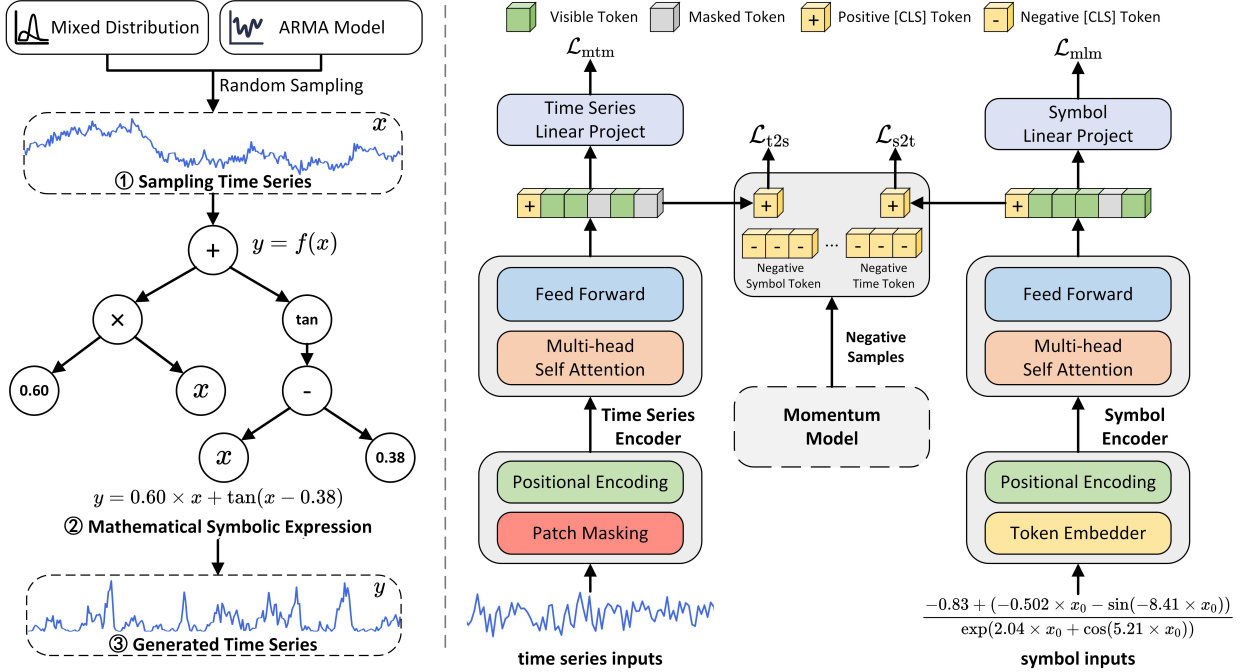


Figure 1. S2 dataset generation mechanism (left) and SymTime network architecture (right).

nate the time series and divide it into patches for the time series encoder (Nie et al., 2023), and tokenize the symbolic expressions for the symbolic encoder (Sanh et al., 2020). We generated a total of 25M series-symbol pairs in S2 dataset, with the total series length of 50B.

3.2. Model Architecture and Pre-training Objectives

As shown in Figure 1 (right), SymTime mainly consists of three components: a time series encoder, a symbolic encoder, and momentum models (He et al., 2020), each with its own distinct pre-training objectives.

Time Series Encoder and Mask Time Series Modeling.

We employ a 6-layer Transformer as the time series encoder. An input time series is first divided into non-overlapping patches $P = \{p_1, p_2, \dots, p_n\}$ using a sliding window approach (Nie et al., 2023; Jin et al., 2024). Then, we add random masks to these patches and embed them into the time series encoder to learn the basic representation of the series (He et al., 2022), obtaining the corresponding embedded sequence $T = \{t_{cls}, t_1, t_2, \dots, t_n\}$, where t_{cls} is the [CLS] token added by the model (Devlin et al., 2019). Our training objective is to restore the masked patch p_j^M through the final linear mapping layer. The MTM loss is as follows:

$$\mathcal{L}_{mtm} = \frac{1}{N} \sum_{j \in M_T} \|p_j - \hat{p}_j\|^2, \quad (1)$$

where M_T is the set of masked patches, and \hat{p}_j represents the patch reconstructed by the time series encoder and linear

projection (Lin et al., 2024). This approach allows the time series encoder to learn the representation of the time series.

Symbol Encoder and Mask Language Modeling. We treat symbolic expressions as natural language and use a 6-layer DistilBert as the symbolic encoder to learn their representations (Sanh et al., 2020). We first randomly replace the words in the symbolic expressions with [Mask] (Devlin et al., 2019) and input them into the symbolic encoder for representation learning, obtaining the embedded sequence: $S = \{s_{cls}, s_1, \dots, s_m\}$, where s_{cls} is the [CLS] token added by the model. We have DistilBert predict the masked tokens using bidirectional information. Let \hat{s} denote a masked token, and $p^{\text{mask}}(\hat{s})$ denote the model’s predicted probability for the masked token. The MLM minimizes a cross-entropy \mathbf{H} loss:

$$\mathcal{L}_{mlm} = \frac{1}{N} \sum_{j \in M_S} \mathbf{H}(y_j, p_j^{\text{mask}}(\hat{s})), \quad (2)$$

where M_S is the set of masked words in the symbolic expression, and y_j is a one-hot vocabulary distribution with a probability of 1 for the ground-truth token.

Series-Symbol Contrastive Learning. In order to enable the time series encoder to learn the semantic information of symbolic expressions, we employ contrastive learning to associate the dual encoders in SymTime, allowing them to learn better unimodal representations. Specifically, SymTime will learn an inner product similarity function (Radford et al., 2021): $\text{sim} = g_t(t_{cls})^T g_s(s_{cls})$, where

t_{cls} and s_{cls} are the [CLS] tokens added during the embedding of time series and symbolic expressions, respectively. They represent the features of the entire input series and input symbols. g_t and g_s are linear projections that map the [CLS] embeddings of to a normalized low-dimensional space. Paired series-symbol representations should have higher similarity (Li et al., 2021). Inspired by MoCo (He et al., 2020), we use a momentum model to obtain a large and consistent dictionary for contrastive learning. The normalized series and symbol features generated by the momentum model are denoted as $g'_t(t'_{\text{cls}})$ and $g'_s(s'_{\text{cls}})$, respectively. We denote $\text{sim}(t, s) = g_t(t_{\text{cls}})^T g'_s(s'_{\text{cls}})$ and $\text{sim}(s, t) = g_s(s_{\text{cls}})^T g'_t(t'_{\text{cls}})$. Then, for each pair of series and symbol, the softmax similarity (Li et al., 2021; Wang et al., 2023b; Duan et al., 2024) from series to symbol and from symbol to series can be defined as follow:

$$p^{t2s}(t) = \frac{\exp(\text{sim}(t, s_m)/\tau)}{\sum_{m=1}^M \exp(\text{sim}(t, s_m)/\tau)}, \quad (3)$$

$$p^{s2t}(s) = \frac{\exp(\text{sim}(s, t_m)/\tau)}{\sum_{m=1}^M \exp(\text{sim}(s, t_m)/\tau)}, \quad (4)$$

where τ is a learnable temperature parameter (Wang et al., 2023c; He et al., 2020). Let $y^{t2s}(t)$ and $y^{s2t}(s)$ represent the one-hot similarity, with positive pairs having a probability of 1 and negative pairs having 0 (He et al., 2020). The contrastive loss for time series-symbol is formulated as the cross-entropy \mathbf{H} between similarity p and the true labels y :

$$\mathcal{L}_{\text{tsc}} = \frac{1}{2} \mathbb{E} [\mathbf{H}(y^{t2s}(t), p^{t2s}(t)) + \mathbf{H}(y^{s2t}(s), p^{s2t}(s))]. \quad (5)$$

By employing this method, the dual-encoder `SymTime` can align the representations of the two encoders by bringing positively correlated series-symbol pairs closer together in the representation space (Wang et al., 2023b).

3.3. Momentum Distillation for Masked Data Learning

Since we obtain the [CLS] token from masked data for contrastive learning, even with a low masking ratio, it still has an impact on the representation. Inspired by ALBEF (Li et al., 2021), we treat the mask as noise added to the series and symbol. Therefore, we use momentum distillation (Lin & Hu, 2024) to overcome the impact of masking on data representation. We train `SymTime` not only with true labels of series-symbol pairs (Equation 5) (Radford et al., 2021) but also from the pseudo-targets generated by the momentum model (He et al., 2020; Gou et al., 2021). This allows our encoder’s predictions to match the predictions of the momentum models. Let the similarity functions generated by the momentum encoders be $\text{sim}'(t, s) = g_t(t'_{\text{cls}})^T g_s(s'_{\text{cls}})$ and $\text{sim}'(s, t) = g_s(s'_{\text{cls}})^T g_t(t'_{\text{cls}})$. We compute soft pseudo targets $q^{t2s}(t)$ and $q^{s2t}(s)$ by replacing sim with sim' in

Equations 3 and 4. Then, the momentum distillation loss can be defined as:

$$\mathcal{L}_{\text{tsc}}^{\text{mod}} = \frac{1}{2} \mathbb{E} [\mathbf{KL}(q^{t2s}(t) \| p^{t2s}(t)) + \mathbf{KL}(q^{s2t}(s) \| p^{s2t}(s))], \quad (6)$$

where \mathbf{KL} denotes the Kullback-Leibler divergence. We introduce a scaling coefficient α to balance \mathcal{L}_{tsc} and $\mathcal{L}_{\text{tsc}}^{\text{mod}}$. Ultimately, all the pre-training objectives of `SymTime` can be expressed as:

$$\mathcal{L} = \mathcal{L}_{\text{mtm}} + \mathcal{L}_{\text{mlm}} + \alpha \mathcal{L}_{\text{tsc}} + (1 - \alpha) \mathcal{L}_{\text{tsc}}^{\text{mod}}. \quad (7)$$

3.4. Model Fine-tuning for Downstream Tasks

Through MTM and series-symbol contrastive learning, we pre-train the time series encoder to imbue it with semantic information from symbols (Zerveas et al., 2021; Meidani et al., 2023). When fine-tuning on downstream tasks, we use this encoder as the backbone to extract universal representations of time series. For the input multivariate time series, we first perform instance normalization to address data offset (Kim et al., 2022). Subsequently, we will adopt different strategies according to different tasks. For classification tasks, we divide the time series into patches through sliding window (Nie et al., 2023; Wang et al., 2024d). Then, we input them into the encoder to extract features and project the outputs into the classification space through linear mapping. For other reconstruction tasks (forecasting, imputation and anomaly detection) (Wu et al., 2024b), we first decompose the input series into two parts: trend and period. Then, the trend is output through linear mapping. We divide the period part into different patches and input them into the encoder in a channel-independent manner. After linear mapping, we reintegrate the trend and period to get the final output.

4. Experiments

In our experiments, we first validate the effectiveness of the time series encoder and the series-symbol pre-training method on 5 mainstream TSA tasks. Details about the pre-training can be found in Appendix D.3. These specific downstream tasks include long-term forecasting (Section 4.1), short-term forecasting (Section 4.2), classification (Section 4.3), imputation (Section 4.3), and anomaly detection (Section 4.5). We use the same benchmarks as TimesNet (Wu et al., 2023) for our experiments, with specific details in Appendix D.1. Then, in Section 4.6, we conduct ablation studies on the pre-training objectives of `SymTime` on long and short term forecasting. Subsequently, in Section 4.7, we analyze the complexity of the model and demonstrate that the time series encoder in `SymTime` learns the semantic information of the symbols. Finally, We demonstrate that through MTM and contrastive learning, `SymTime` has a certain ability of zero-shot imputation and can distinguish the

Table 1. The model architecture of the time series and symbolic encoders in SymTime.

Encoder	Layers	d_{model}	d_{ff}	Heads	Params
Time	6	512	2048	8	19M
Symbol	6	786	3072	12	67M

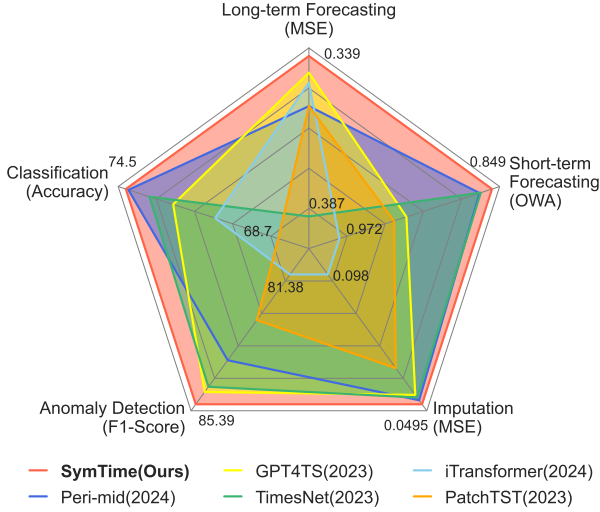


Figure 2. Model performance comparison with the state-of-the-art models in terms of five tasks.

symbolic semantics of simple series. The model architecture of the time series and symbolic encoders are shown in Table 1.

Baselines. The baselines including **Transformer-based models**: PatchTST (Nie et al., 2023), iTransformer (Liu et al., 2024b), Autoformer (Wu et al., 2021), ETSformer (Woo et al., 2023), FEDformer (Zhou et al., 2022a), Non-stationary Transformer (Liu et al., 2022b), Crossformer (Zhang & Yan, 2023), Informer (Zhou et al., 2021), Anomaly Transformer (Xu et al., 2022), Peri-midFormer (Wu et al., 2024b); **LLM-based models**: GPT4TS (Zhou et al., 2023), Time-LLM (Jin et al., 2024), S^2 IP-LLM (Pan et al., 2024); **CNN-based models**: TimesNet (Wu et al., 2023), TSLANet (Eldele et al., 2024), Rocket (Dempster et al., 2020), InceptionTime (InTime) (Ismail Fawaz et al., 2020) and MICN (Wang et al., 2023a); **MLP-based models**: DLinear (Zeng et al., 2023), LightTS (Zhang et al., 2022), TimeMixer (Wang et al., 2024b) and FilterNet (Yi et al., 2024). We also compare with the **pre-trained foundation models**: Moirai (Woo et al., 2024), Timer (Liu et al., 2024d), UniTS (Gao et al., 2024) and Moment (Goswami et al., 2024). Some models can be applied to all 5 TSA tasks, while others are suitable for only one or some specific tasks.

Main Results. Figure 2 displays the comprehensive comparison results between SymTime and other foundation

models, it excels across all 5 downstream tasks.

4.1. Long-term Forecasting

Setup. Time series forecasting, which analyzes historical data patterns to predict future trends, is crucial for financial market analysis, inventory management, energy demand and other fields (Wang et al., 2025; Liu et al., 2025). We adopt 8 real-world benchmark datasets for long-term forecasting, including ETTm1, ETTm2, ETTh1, ETTh2 (Zhou et al., 2021), Weather (Wetterstation), ECL (UCI), Traffic (PeMS) and Exchange (Lai et al., 2018). The forecasting lengths are set to $\{96, 192, 336, 720\}$. To ensure fairness in the comparison, we set the look-back window length of SymTime and all other models to 96, except Moirai and Timer are 672 and S^2 IP-LLM is 512.

Results. Table 2 clearly demonstrates that SymTime achieves excellent performance in long-term forecasting tasks. Our model surpasses Peri-midFormer, GPT4TS and TimesNet, which are foundation models for the 5 major tasks, as well as Moirai and Timer, two general forecasting models. SymTime approaches and surpasses the customized time series forecasting model Time-LLM in terms of MSE and MAE metrics. However, Time-LLM relies on a large-scale LLM as its backbone, whereas SymTime can achieve comparable results through pre-training on synthetic datasets and fine-tuning with a more lightweight model.

4.2. Short-term Forecasting

Setup. We adopt M4 benchmark (Spyros Makridakis, 2018) for short-term forecasting, which contains the yearly, quarterly and monthly collected univariate marketing data. Then, we use symmetric mean absolute error (SMAPE), mean absolute scaled error (MASE) and overall weighted average (OWA) to measure the forecasting performance, which are calculated as detailed in Appendix D.2.

Results. Table 3 indicates that SymTime after pre-training, surpasses TimeMixer, Peri-midFormer and TimesNet on the short-term forecasting tasks in terms of SMAPE, MASE and OWA metrics, achieving state-of-the-art performance. Specifically, SymTime performs well on Yearly, Quarterly and Monthly datasets, demonstrating its capability to capture not only the trends of annual variations but also the cyclic characteristics of seasonal and monthly encoding.

4.3. Classification

Setup. Time series classification is crucial for the identification and diagnosis of patterns in complex systems and plays a significant role in various fields such as financial analysis, medical diagnosis and industrial monitoring (Ismail Fawaz et al., 2019). Using the experimental setup from TimesNet (Wu et al., 2023), we test SymTime’s discriminative ability

Table 2. Long-term forecasting task. The results are averaged from four different series length {96, 192, 336, 720}. (* means former.) See Appendix G.1. **Red**: best, **Blue**: second best.

Model	SymTime (Ours)		Peri-mid* (2024b)		Moriai (2024)		Timer (2024d)		Time-LLM (2024)		TSLANet (2024)		S2IP-LLM (2024)		GPT4TS (2023)		TimeMixer (2024b)	
	MSE	MAE	MSE	MAE	MSE	MAE	MSE	MAE	MSE	MAE	MSE	MAE	MSE	MAE	MSE	MAE	MSE	MAE
ETTm1	0.372	0.392	0.409	0.410	0.398	0.417	0.388	0.402	0.369	0.394	0.377	0.397	0.374	0.404	0.369	0.395	0.382	0.397
ETTm2	0.283	0.328	0.290	0.328	0.296	0.348	0.405	0.408	0.275	0.324	0.283	0.327	0.266	0.325	0.264	0.328	0.279	0.325
ETTh1	0.430	0.436	0.455	0.446	0.441	0.454	0.434	0.444	0.438	0.445	0.448	0.441	0.456	0.454	0.434	0.440	0.453	0.441
ETTh2	0.375	0.405	0.400	0.416	0.402	0.411	0.428	0.441	0.369	0.407	0.355	0.391	0.362	0.405	0.359	0.403	0.388	0.408
Weather	0.247	0.276	0.262	0.283	0.265	0.299	0.329	0.358	0.247	0.269	0.259	0.352	0.243	0.274	0.265	0.285	0.253	0.280
ECL	0.187	0.276	0.178	0.267	0.167	0.252	0.177	0.267	0.180	0.269	0.199	0.283	0.191	0.283	0.206	0.291	0.185	0.274
Traffic	0.457	0.291	0.458	0.295	0.424	0.289	0.436	0.284	0.418	0.306	0.463	0.310	0.417	0.306	0.491	0.320	0.499	0.306
Exchange	0.359	0.401	0.388	0.417	0.373	0.417	0.382	0.425	0.376	0.414	0.368	0.414	0.472	0.478	0.370	0.411	0.403	0.423
Average	0.339	0.351	0.355	0.358	0.346	0.361	0.372	0.378	0.334	0.353	0.344	0.364	0.348	0.366	0.345	0.359	0.355	0.357

Table 3. Short-term forecasting task on M4. The prediction lengths are {6, 48} and results are weighted averaged from several datasets under different sample intervals. (* means former, TMixer is TimeMixer). See Appendix G.2 for full results. **Red**: best, **Blue**: second best.

Models	SymTime (Ours)	Peri-mid* (2024b)	S2IP-LLM (2024)	Time-LLM (2024)	GPT4TS (2023)	TMixer (2024b)	PatchTST (2023)	iTrans* (2024b)	TimesNet (2023)	DLinear (2023)	LightTS (2022)	FED* (2022a)	In* (2021)
SMAPE	11.785	11.897	12.514	12.584	12.367	11.885	12.866	13.233	11.888	12.500	11.962	12.605	15.018
MASE	1.584	1.607	1.726	1.763	1.767	1.598	1.734	1.850	1.607	1.678	1.609	1.677	2.096
OWA	0.849	0.859	0.913	0.915	0.918	0.856	0.928	0.972	0.858	0.899	0.862	0.903	1.102

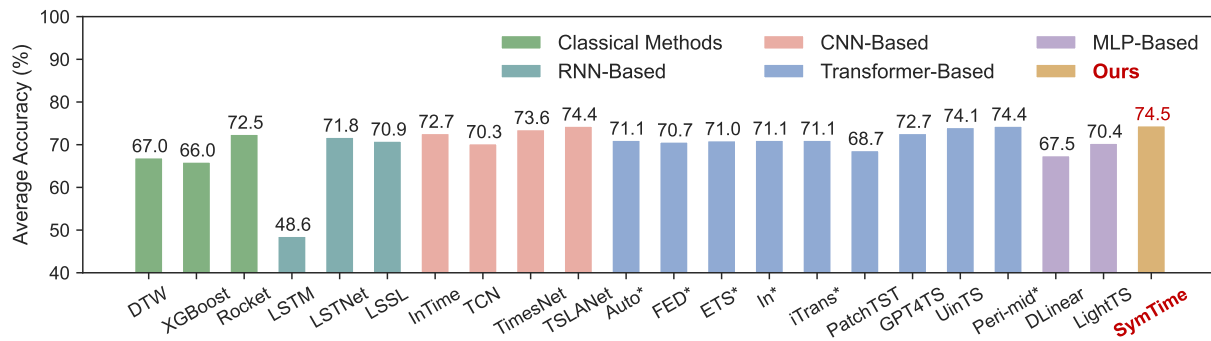


Figure 3. Comparison of the average accuracy of SymTime and other baselines on 10 UEA datasets. See Appendix G.3 for full results.

on 10 UEA multivariate time series classification datasets (Bagnall et al., 2018), including categories such as Industry, Face Detection, ECG, Voice and Transportation.

Results. As shown in Figure 3, SymTime achieves an average accuracy of 74.5%, surpassing all baselines, indicating that SymTime is competitive in classification tasks.

4.4. Imputation

Setup. Sensors monitoring complex systems in the real world may experience distortions or malfunctions, leading to partial missing data in the collected time series. Therefore, time series imputation is crucial for the recovery of complete datasets. We verify SymTime’s imputation capabilities on 6 datasets: ETTm1, ETTm2, ETTh1, ETTh2

(Zhou et al., 2021), Weather (Wetterstation) and ECL (UCI). To test the model’s imputation ability under varying degrees of missing data, we add random masks at proportions of {12.5%, 25%, 37.5%, 50%} in point level on time series of length 96. Since SymTime was pre-trained by randomly masking patches level for series reconstruction and masks are added randomly in point level in the imputation task. Considering the differences between these masking approaches and the potential disruption of the series’s original trends and periodic features at higher mask rates, we adopt per-interpolation for the masked series from (Wu et al., 2024b). Analysis and ablation experiments regarding this method are presented in Appendix D.7.

Results. Table 4 shows that SymTime outperforms Peri-midFormer, GPT4TS and TimesNet in overall performance

establishing *SymTime* as the latest state-of-the-art approach. Although *SymTime*'s performance on the ETT series of datasets is not as strong as GPT4TS, it achieves more significant effects on datasets with a higher number of channels, such as ECL and Weather.

4.5. Anomaly Detection

Setup. Time series anomaly detection is crucial for rapidly identifying anomalies in critical areas, aiding in risk prevention and decision optimization. Due to the difficulty in annotating time series anomalies, we focus primarily on unsupervised anomaly detection. We conduct experiments on 5 widely used anomaly detection datasets: SMD and SMAP (Su et al., 2019), MSL (Hundman et al., 2018), SWaT (Mathur & Tippenhauer, 2016), PSM (Abdulaal et al., 2021), encompassing service monitoring, space & earth exploration, and water treatment applications. We adopt the same data preprocessing method as the Anomaly Transformer (Xu et al., 2022), dividing the data into non-overlapping segments of length 100 for reconstruction. Specifically, normal data is used for model training and we employ a simple reconstruction loss to help the model learn the distribution of normal data (Wu et al., 2024b). In subsequent testing phases, reconstructed outputs exceeding a specified threshold are considered anomalies.

Results. Table 5 indicates that *SymTime* surpasses previous state-of-the-art methods such as TimesNet and GPT4TS and achieves commendable performance on the SMD and SWaT datasets. However, due to UniTS employing real data and downstream task-relevant pre-training, there is a slight performance difference between *SymTime* and UniTS.

4.6. Ablation Experiments

Setup. We conduct ablation studies on *SymTime*'s pre-training objectives and the size of the pre-training dataset using the ETT long-term forecasting dataset (Zhou et al., 2021). First, we establish 8 different control groups based on whether pre-training is performed, freezing the model and various pre-training losses: (1) Freeze, (2) w/o Pre-train, (3) w/o MTM, (4) w/o MLM, (5) w/o T2S, (6) w/o S2T, (7) w/o Symbol and (8) w/o Distill. Specific explanations for the above control groups are provided in Appendix D.5. We use the average MSE of the prediction lengths {96, 192, 336, 720} on the ETTh1 and ETTh2 datasets as the evaluation metric, with the average results shown in Figure 4 (a). Then, we set the sizes of the pre-training datasets to {0, 10B, 20B, 30B, 40B, 50B}, where 0 indicates no pre-training. We subsequently observe the changes in the model's MSE with the size of the pre-training dataset, with specific results shown in Figure 4 (b). We apply the same experimental configuration for ablation studies on short-term forecasting tasks, with detailed results and analy-

sis provided in Appendix D.6.

Results. Figure 4 (a) indicates that pre-training with the standard configuration significantly enhances *SymTime*'s performance in long-term forecasting. Moreover, removing the symbolic component and relying solely on MTM losses to learn representations of time series can moderately degrade model performance. This suggests that the semantic information provided by the symbol encoder and contrastive learning improves the time series encoder's performance in long-term forecasting (Liu et al., 2024c). Additionally, eliminating any single pre-training objective can also impact model performance to some extent. Figure 4 (b) shows that as the size of the pre-training dataset increases, the model's performance on downstream tasks also improves, highlighting the importance of a large-scale and comprehensively representative dataset for model pre-training. However, on ETTm1 and ETTm2 datasets, a slight saturation trend is observed once the data volume reaches 40B.

4.7. Discussion

Complexity Analysis. We analyze the complexity of the model on the long-term forecasting ETTh1 dataset, with results shown in Figure 5. We consider the parameter count, the GPU memory required for forward and backward propagation when the batch size is 1, the MSE as an evaluation metric. *SymTime* achieves better performance with a smaller model parameter count and memory capacity than existing foundation models in forecasting. Although *SymTime*'s performance is slightly lower than Time-LLM in the final experimental results of all datasets, its complexity is also significantly lower than Time-LLM. The computational load and complexity of our model are reasonable and acceptable in the vast majority of application scenarios.

Statistical Characterization of S2 dataset. We quantify the range of representations that the S2 dataset can cover through statistical metrics (including stationarity (Elliott et al., 1992), forecastability (Goerg, 2013), seasonality and entropy (Cao et al., 2004)), proving that our unrestricted data generation mechanism can evenly cover the basic representations of all types of time series, thereby solving the data scarcity problem. See Appendix B.3 for full results.

Zero-shot Imputation. After large-scale masked time series modeling (Equation 1), *SymTime* successfully learned the basic representation of time series and has the ability of zero-shot imputation for S2 out-of-domain data and real-world time series data. See Appendix C for full results.

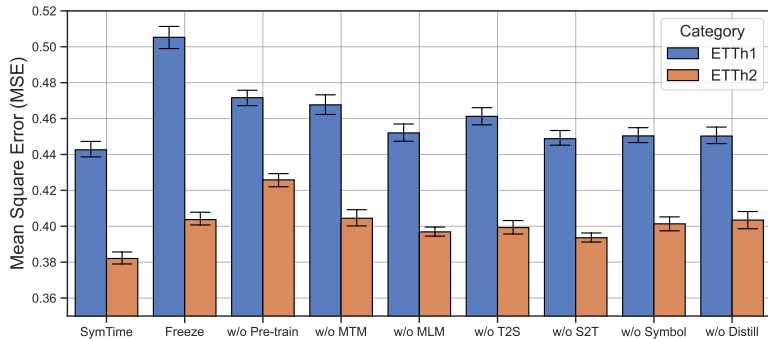
Series-Symbol Representation Learning. Through contrastive learning (Equation 5), our time series encoder is able to distinguish series of simple unary symbolic expressions, proving that our encoder has learned the semantic information of the symbols (Wang et al., 2024a). Specific

Table 4. Imputation task, where we randomly mask {12.5%, 25%, 37.5%, 50%} time points of length-96 time series. The results averaged from 4 different mask ratios. (* means former.) See Appendix G.4 for full results. **Red**: best, **Blue**: second best.

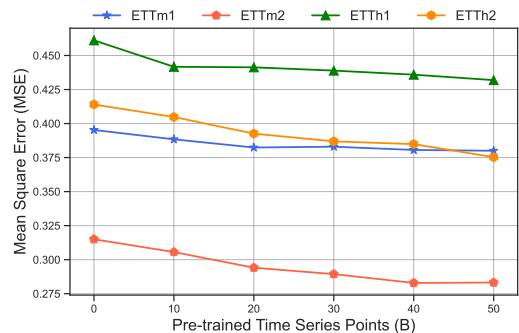
Model	SymTime (Ours)		GPT4TS (2023)		TimesNet (2023)		Peri-mid* (2024b)		Moment (2024)		iTrans* (2024b)		PatchTST (2023)		DLinear (2023)		LightTS (2022)	
Metric	MSE	MAE	MSE	MAE	MSE	MAE	MSE	MAE	MSE	MAE	MSE	MAE	MSE	MAE	MSE	MAE	MSE	MAE
ETTm1	0.036	0.116	0.028	0.109	0.027	0.107	0.036	0.116	0.074	0.168	0.072	0.185	0.049	0.143	0.090	0.204	0.068	0.182
ETTm2	0.026	0.088	0.022	0.088	0.022	0.089	0.026	0.087	0.031	0.108	0.082	0.191	0.030	0.101	0.102	0.212	0.068	0.176
ETTh1	0.095	0.201	0.093	0.200	0.089	0.199	0.091	0.196	0.139	0.234	0.148	0.269	0.126	0.231	0.169	0.283	0.159	0.278
ETTh2	0.058	0.148	0.052	0.147	0.050	0.148	0.057	0.147	0.061	0.159	0.139	0.254	0.066	0.164	0.163	0.273	0.143	0.258
ECL	0.054	0.151	0.093	0.212	0.094	0.211	0.063	0.169	0.094	0.211	0.099	0.224	0.078	0.192	0.128	0.256	0.108	0.238
Weather	0.028	0.038	0.032	0.058	0.030	0.056	0.029	0.041	0.035	0.075	0.052	0.114	0.033	0.057	0.053	0.116	0.047	0.106
Average	0.049	0.124	0.053	0.136	0.052	0.135	0.050	0.126	0.072	0.159	0.099	0.206	0.064	0.148	0.118	0.224	0.099	0.206

Table 5. Anomaly detection task, where we calculate the F1-score (as %) for each dataset. (* means former.) A higher value of F1-score indicates a better performance. See Appendix G.5 for full results. **Red**: best, **Blue**: second best.

Model	SymTime (Ours)	UniTS (2024)	Peri-mid* (2024b)	GPT4TS (2023)	TimesNet (2023)	PatchTST (2023)	LightTS (2022)	DLinear (2023)	iTrans* (2024b)	Anomaly (2022)	Stationary (2022b)	Cross* (2023)	In* (2021)	Auto* (2021)
SMD	84.62	83.69	84.08	84.49	84.37	84.62	82.53	79.76	80.19	85.49	82.97	77.22	77.88	71.17
MSL	81.77	81.16	80.68	82.03	81.14	78.70	78.95	81.87	72.47	83.31	76.68	80.59	81.07	82.22
SMAP	69.87	74.00	67.53	68.85	69.05	68.82	69.21	67.30	66.72	71.18	69.02	67.12	73.26	73.97
SWaT	93.61	92.51	91.64	92.60	92.61	85.72	93.33	92.66	92.64	83.10	92.24	90.22	80.35	79.19
PSM	97.07	97.31	96.21	97.09	97.06	96.08	97.15	96.64	94.88	79.40	97.23	92.52	90.43	88.24
Avg F1	85.39	85.73	84.03	85.01	84.85	82.79	84.23	83.64	81.38	80.50	83.63	81.53	80.60	78.96



(a) Ablation on pre-training objectives.



(b) Ablation on the size of pre-training dataset.

Figure 4. Ablation experiments on long-term forecasting task.

results and analysis are provided in Appendix C.

5. Conclusion

To address the challenges of data scarcity and distribution imbalance in time series analysis, we introduce a dual-modality data generation mechanism that enables the unrestricted creation of high-quality time series data, along with corresponding symbolic representations. Leveraging this large-scale series-symbol synthetic dataset, we propose SymTime, a pre-trained foundation model that integrates both time series representations and symbolic semantic information. Our pre-trained model demonstrates exceptional performance across five major TSA tasks, highlighting the

effectiveness of both our data generation strategy and pre-training methodology. Looking ahead, we aim to scale up our approach by training larger models on synthetic datasets, further boosting performance on downstream tasks.

Impact Statement

The potential value of this work lies in its ability to mitigate fundamental challenges in TSA, such as the lack of sufficient labeled data and the issue of imbalanced datasets. By generating rich, diverse, and high-quality synthetic data, our approach not only addresses these issues but also opens new avenues for improving model generalization across a wide range of applications. Furthermore, the dual-modality

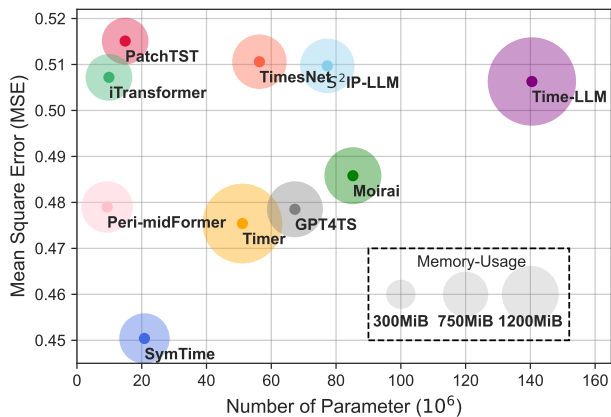


Figure 5. Complexity analysis on long time series prediction tasks (ETTh1 dataset, forecasting length is 720). Note that since the original backbone of Time-LLM (Jin et al., 2024) has too many parameters, we replaced it with GPT2 (Radford et al., 2019).

framework, which combines time series data with symbolic semantics, introduces a novel way of enriching the representation power of models, allowing them to better understand complex temporal dynamics and their underlying patterns.

We foresee that pre-training models on synthetic datasets, especially those that combine structured symbolic information with time series data, will become a key development trend in the TSA field. This could pave the way for more robust and scalable solutions in a variety of domains, including finance, healthcare, and climate modeling, where time series data is abundant, but labeled data is often scarce or hard to obtain.

References

- Abdulaal, A., Liu, Z., and Lancewicki, T. Practical approach to asynchronous multivariate time series anomaly detection and localization. In *Proceedings of the 27th ACM SIGKDD Conference on Knowledge Discovery & Data Mining*, KDD '21, pp. 2485–2494, New York, NY, USA, 2021. Association for Computing Machinery. ISBN 9781450383325. doi: 10.1145/3447548.3467174. URL <https://doi.org/10.1145/3447548.3467174>.
- Aghajanyan, A., Yu, L., Conneau, A., Hsu, W.-N., Hambarzumyan, K., Zhang, S., Roller, S., Goyal, N., Levy, O., and Zettlemoyer, L. Scaling laws for generative mixed-modal language models. In Krause, A., Brunskill, E., Cho, K., Engelhardt, B., Sabato, S., and Scarlett, J. (eds.), *Proceedings of the 40th International Conference on Machine Learning*, volume 202 of *Proceedings of Machine Learning Research*, pp. 265–279. PMLR, 23–29 Jul 2023. URL <https://proceedings.mlr.press/v202/aghajanyan23a.html>.
- Ahmed, S., Nielsen, I. E., Tripathi, A., Siddiqui, S., Ramachandran, R. P., and Rasool, G. Transformers in time-series analysis: A tutorial. *Circuits, Systems, and Signal Processing*, 42(12):7433–7466, 2023.
- Alon, U., Xu, F. F., He, J., Sengupta, S., Roth, D., and Neubig, G. Neuro-symbolic language modeling with automaton-augmented retrieval. In *ICML 2022 Workshop on Knowledge Retrieval and Language Models*, 2022. URL <https://openreview.net/forum?id=ZJZmKGM6UB>.
- Bagnall, A., Dau, H. A., Lines, J., Flynn, M., Large, J., Bostrom, A., Southam, P., and Keogh, E. The uea multivariate time series classification archive, 2018, 2018. URL <https://arxiv.org/abs/1811.00075>.
- Bahri, Y., Dyer, E., Kaplan, J., Lee, J., and Sharma, U. Explaining neural scaling laws. *Proceedings of the National Academy of Sciences*, 121(27):e2311878121, 2024.
- Bartlett, D. J., Desmond, H., and Ferreira, P. G. Exhaustive symbolic regression. *IEEE Transactions on Evolutionary Computation*, 28(4):950–964, 2024. doi: 10.1109/TEVC.2023.3280250.
- Berndt, D. J. and Clifford, J. Using dynamic time warping to find patterns in time series. In *Proceedings of the 3rd International Conference on Knowledge Discovery and Data Mining*, AAAIWS'94, pp. 359–370. AAAI Press, 1994.
- Cao, Y., Tung, W.-w., Gao, J. B., Protopopescu, V. A., and Hively, L. M. Detecting dynamical changes in time series using the permutation entropy. *Physical Review E*, 70(4):046217, 2004. doi: 10.1103/physreve.70.046217. URL <https://app.dimensions.ai/details/publication/pub.1060732058>.
- Chen, T. and Guestrin, C. Xgboost: A scalable tree boosting system. In *Proceedings of the 22nd ACM SIGKDD International Conference on Knowledge Discovery and Data Mining*, KDD '16, pp. 785–794, New York, NY, USA, 2016. Association for Computing Machinery. ISBN 9781450342322. doi: 10.1145/2939672.2939785. URL <https://doi.org/10.1145/2939672.2939785>.
- Chen, T., Kornblith, S., Norouzi, M., and Hinton, G. A simple framework for contrastive learning of visual representations. In *Proceedings of the 37th International Conference on Machine Learning*, ICML'20, 2020.
- Chen, X., Qiu, P., Zhu, W., Li, H., Wang, H., Sotiras, A., Wang, Y., and Razi, A. TimeMIL: Advancing multivariate time series classification via a time-aware multiple instance learning. In *Forty-first International Con-*

- ference on Machine Learning, 2024. URL <https://openreview.net/forum?id=AxmefV2NEf>.
- Chujai, P., Kerdprasop, N., and Kerdprasop, K. Time series analysis of household electric consumption with arima and arma models. In *Proceedings of the international multiconference of engineers and computer scientists*, volume 1, pp. 295–300, 2013.
- Cini, A., Mandic, D., and Alippi, C. Graph-based time series clustering for end-to-end hierarchical forecasting. In *Forty-first International Conference on Machine Learning*, 2024. URL <https://openreview.net/forum?id=nd47Za5jk5>.
- Cleveland, R. B., Cleveland, W. S., McRae, J. E., Terpening, I., et al. Stl: A seasonal-trend decomposition. *J. off. Stat*, 6(1):3–73, 1990.
- Das, A., Kong, W., Sen, R., and Zhou, Y. A decoder-only foundation model for time-series forecasting. In *Forty-first International Conference on Machine Learning*, 2024. URL <https://openreview.net/forum?id=jn2iTJas6h>.
- de Franca, F. O. and Aldeia, G. S. I. Interaction–transformation evolutionary algorithm for symbolic regression. *Evolutionary Computation*, 29(3):367–390, 09 2021. ISSN 1063-6560. doi: 10.1162/evco.a_00285. URL https://doi.org/10.1162/evco_a_00285.
- Dempster, A., Petitjean, F., and Webb, G. I. Rocket: exceptionally fast and accurate time series classification using random convolutional kernels. *Data Mining and Knowledge Discovery*, 34(5):1454–1495, 2020.
- Devlin, J., Chang, M.-W., Lee, K., and Toutanova, K. Bert: Pre-training of deep bidirectional transformers for language understanding, 2019. URL <https://arxiv.org/abs/1810.04805>.
- Doering, C. R. Modeling complex systems: Stochastic processes, stochastic differential equations, and fokker-planck equations. In *1990 Lectures in Complex Systems*, pp. 3–52. CRC Press, 2018.
- Dong, J., Wu, H., Zhang, H., Zhang, L., Wang, J., and Long, M. SimMTM: A simple pre-training framework for masked time-series modeling. In *Thirty-seventh Conference on Neural Information Processing Systems*, 2023. URL <https://openreview.net/forum?id=ginTcBUnL8>.
- Dong, J., Wu, H., Wang, Y., Qiu, Y.-Z., Zhang, L., Wang, J., and Long, M. Timesiam: A pre-training framework for siamese time-series modeling. In *Forty-first International Conference on Machine Learning*, 2024. URL <https://openreview.net/forum?id=wrTzLoqbCg>.
- Dooley, S., Khurana, G. S., Mohapatra, C., Naidu, S. V., and White, C. ForecastPFN: Synthetically-trained zero-shot forecasting. In *Thirty-seventh Conference on Neural Information Processing Systems*, 2023. URL <https://openreview.net/forum?id=tScBQRNgjk>.
- Duan, J., Zheng, W., Du, Y., Wu, W., Jiang, H., and Qi, H. MF-CLR: Multi-frequency contrastive learning representation for time series. In *Forty-first International Conference on Machine Learning*, 2024. URL <https://openreview.net/forum?id=ec07WOI1MD>.
- Eldele, E., Ragab, M., Chen, Z., Wu, M., and Li, X. Tslanet: Rethinking transformers for time series representation learning. In *ICML*, 2024. URL <https://openreview.net/forum?id=CGR3vpX63X>.
- Elliott, G., Rothenberg, T. J., and Stock, J. H. Efficient tests for an autoregressive unit root, 1992.
- Esterby, S. R. Review of methods for the detection and estimation of trends with emphasis on water quality applications. *Hydrological processes*, 10(2):127–149, 1996.
- Farayola, O. A., Olorunfemi, O. L., and Shoetan, P. O. Data privacy and security in it: a review of techniques and challenges. *Computer Science & IT Research Journal*, 5(3):606–615, 2024.
- Franceschi, J.-Y., Dieuleveut, A., and Jaggi, M. Unsupervised scalable representation learning for multivariate time series. In Wallach, H., Larochelle, H., Beygelzimer, A., d’Alché-Buc, F., Fox, E., and Garnett, R. (eds.), *Advances in Neural Information Processing Systems*, volume 32. Curran Associates, Inc., 2019. URL https://proceedings.neurips.cc/paper_files/paper/2019/file/53c6de78244e9f528eb3e1cda69699bb-Paper.pdf.
- Gao, S., Koker, T., Queen, O., Hartvigsen, T., Tsiligkaridis, T., and Zitnik, M. UniTS: A unified multi-task time series model. In *The Thirty-eighth Annual Conference on Neural Information Processing Systems*, 2024. URL <https://openreview.net/forum?id=nB0YBptWW>.
- Garza, A., Challu, C., and Mergenthaler-Canseco, M. Timegpt-1, 2024. URL <https://arxiv.org/abs/2310.03589>.
- Godahewa, R. W., Bergmeir, C., Webb, G. I., Hyndman, R., and Montero-Manso, P. Monash time series forecasting archive. In *Thirty-fifth Conference on Neural Information Processing Systems Datasets and Benchmarks Track (Round 2)*, 2021. URL <https://openreview.net/forum?id=wEclmgAjU->.

- Goerg, G. Forecastable component analysis. In Dasgupta, S. and McAllester, D. (eds.), *Proceedings of the 30th International Conference on Machine Learning*, volume 28 of *Proceedings of Machine Learning Research*, pp. 64–72, Atlanta, Georgia, USA, 17–19 Jun 2013. PMLR. URL <https://proceedings.mlr.press/v28/goerg13.html>.
- Goswami, M., Szafer, K., Choudhry, A., Cai, Y., Li, S., and Dubrawski, A. MOMENT: A family of open time-series foundation models. In *Forty-first International Conference on Machine Learning*, 2024. URL <https://openreview.net/forum?id=FVvf69a5rx>.
- Gou, J., Yu, B., Maybank, S. J., and Tao, D. Knowledge distillation: A survey. *International Journal of Computer Vision*, 129(6):1789–1819, 2021.
- Gu, A., Goel, K., and Re, C. Efficiently modeling long sequences with structured state spaces. In *International Conference on Learning Representations*, 2022. URL <https://openreview.net/forum?id=uYLFoz1vlAC>.
- Han, L., Ye, H.-J., and Zhan, D.-C. SIN: Selective and interpretable normalization for long-term time series forecasting. In *Forty-first International Conference on Machine Learning*, 2024. URL <https://openreview.net/forum?id=cUMOVfOIVE>.
- He, K., Fan, H., Wu, Y., Xie, S., and Girshick, R. Momentum contrast for unsupervised visual representation learning. In *Proceedings of the IEEE/CVF conference on computer vision and pattern recognition*, pp. 9729–9738, 2020.
- He, K., Chen, X., Xie, S., Li, Y., Dollár, P., and Girshick, R. Masked autoencoders are scalable vision learners. In *Proceedings of the IEEE/CVF conference on computer vision and pattern recognition*, pp. 16000–16009, 2022.
- Hochreiter, S. and Schmidhuber, J. Long short-term memory. *Neural Computation*, 9(8):1735–1780, 11 1997. ISSN 0899-7667. doi: 10.1162/neco.1997.9.8.1735. URL <https://doi.org/10.1162/neco.1997.9.8.1735>.
- Hundman, K., Constantinou, V., Laporte, C., Colwell, I., and Soderstrom, T. Detecting spacecraft anomalies using lstms and nonparametric dynamic thresholding. *KDD '18*, pp. 387–395, New York, NY, USA, 2018. Association for Computing Machinery. ISBN 9781450355520. doi: 10.1145/3219819.3219845. URL <https://doi.org/10.1145/3219819.3219845>.
- Ilbert, R., Odonnat, A., Feofanov, V., Virmaux, A., Paolo, G., Palpanas, T., and Redko, I. SAMformer: Unlocking the potential of transformers in time series forecasting with sharpness-aware minimization and channel-wise attention. In *Forty-first International Conference on Machine Learning*, 2024. URL <https://openreview.net/forum?id=8kLzL5QBh2>.
- Ismail Fawaz, H., Forestier, G., Weber, J., Idoumghar, L., and Muller, P.-A. Deep learning for time series classification: a review. *Data mining and knowledge discovery*, 33(4):917–963, 2019.
- Ismail Fawaz, H., Lucas, B., Forestier, G., Pelletier, C., Schmidt, D. F., Weber, J., Webb, G. I., Idoumghar, L., Muller, P.-A., and Petitjean, F. Inceptiontime: Finding alexnet for time series classification. *Data Mining and Knowledge Discovery*, 34(6):1936–1962, 2020.
- Jin, M., Wang, S., Ma, L., Chu, Z., Zhang, J. Y., Shi, X., Chen, P.-Y., Liang, Y., Li, Y.-F., Pan, S., and Wen, Q. Time-LLM: Time series forecasting by reprogramming large language models. In *The Twelfth International Conference on Learning Representations*, 2024. URL <https://openreview.net/forum?id=Unb5CVptae>.
- junxin lu and Sun, S. CaudiTS: Causal disentangled domain adaptation of multivariate time series. In *Forty-first International Conference on Machine Learning*, 2024. URL <https://openreview.net/forum?id=lsavZkUjFZ>.
- Kamienny, P.-A., d’Ascoli, S., Lample, G., and Charton, F. End-to-end symbolic regression with transformers. In Oh, A. H., Agarwal, A., Belgrave, D., and Cho, K. (eds.), *Advances in Neural Information Processing Systems*, 2022. URL https://openreview.net/forum?id=GoOuIrdHG_Y.
- Kaplan, J., McCandlish, S., Henighan, T., Brown, T. B., Chess, B., Child, R., Gray, S., Radford, A., Wu, J., and Amodei, D. Scaling laws for neural language models, 2020. URL <https://arxiv.org/abs/2001.08361>.
- Kim, T., Kim, J., Tae, Y., Park, C., Choi, J.-H., and Choo, J. Reversible instance normalization for accurate time-series forecasting against distribution shift. In *International Conference on Learning Representations*, 2022. URL <https://openreview.net/forum?id=cGDakQo1C0p>.
- Kingma, D. P. and Ba, J. Adam: A method for stochastic optimization, 2017. URL <https://arxiv.org/abs/1412.6980>.
- Kitaev, N., Kaiser, L., and Levskaya, A. Reformer: The efficient transformer. In *International Conference*

- on *Learning Representations*, 2020. URL <https://openreview.net/forum?id=rkgNKkHtvB>.
- Lai, G., Chang, W.-C., Yang, Y., and Liu, H. Modeling long- and short-term temporal patterns with deep neural networks. In *The 41st International ACM SIGIR Conference on Research & Development in Information Retrieval, SIGIR '18*, pp. 95–104, New York, NY, USA, 2018. Association for Computing Machinery. ISBN 9781450356572. doi: 10.1145/3209978.3210006. URL <https://doi.org/10.1145/3209978.3210006>.
- Lample, G. and Charton, F. Deep learning for symbolic mathematics. In *International Conference on Learning Representations*, 2020. URL <https://openreview.net/forum?id=S1eZYeHFDS>.
- Li, J., Selvaraju, R. R., Gotmare, A. D., Joty, S., Xiong, C., and Hoi, S. Align before fuse: Vision and language representation learning with momentum distillation. In Beygelzimer, A., Dauphin, Y., Liang, P., and Vaughan, J. W. (eds.), *Advances in Neural Information Processing Systems*, 2021. URL <https://openreview.net/forum?id=OJLaKwiXSbx>.
- Li, Y., Wu, K., and Liu, J. Discover governing differential equations from evolving systems. *Physical Review Research*, 5:023126, May 2023a.
- Li, Z., Qi, S., Li, Y., and Xu, Z. Revisiting long-term time series forecasting: An investigation on linear mapping, 2023b. URL <https://arxiv.org/abs/2305.10721>.
- Liang, Y., Wen, H., Nie, Y., Jiang, Y., Jin, M., Song, D., Pan, S., and Wen, Q. Foundation models for time series analysis: A tutorial and survey. In *Proceedings of the 30th ACM SIGKDD Conference on Knowledge Discovery and Data Mining*, pp. 6555–6565, 2024.
- Lin, R. and Hu, H. Multi-task momentum distillation for multimodal sentiment analysis. *IEEE Transactions on Affective Computing*, 15(2):549–565, 2024. doi: 10.1109/TAFFC.2023.3282410.
- Lin, S., Lin, W., Wu, W., Chen, H., and Yang, J. SparseTSF: Modeling long-term time series forecasting with *1k* parameters. In *Forty-first International Conference on Machine Learning*, 2024. URL <https://openreview.net/forum?id=54NSHO0lFe>.
- Liu, C., Wan, Z., Ouyang, C., Shah, A., Bai, W., and Arcucci, R. Zero-shot ECG classification with multimodal learning and test-time clinical knowledge enhancement. In *Forty-first International Conference on Machine Learning*, 2024a. URL <https://openreview.net/forum?id=ZvJ2lQQKjz>.
- Liu, S., Yu, H., Liao, C., Li, J., Lin, W., Liu, A. X., and Dastdar, S. Pyraformer: Low-complexity pyramidal attention for long-range time series modeling and forecasting. In *International Conference on Learning Representations*, 2022a. URL <https://openreview.net/forum?id=0EXmFzUn5I>.
- Liu, Y., Wu, H., Wang, J., and Long, M. Non-stationary transformers: Exploring the stationarity in time series forecasting. In Oh, A. H., Agarwal, A., Belgrave, D., and Cho, K. (eds.), *Advances in Neural Information Processing Systems*, 2022b. URL <https://openreview.net/forum?id=ucNDIDRNjjv>.
- Liu, Y., Hu, T., Zhang, H., Wu, H., Wang, S., Ma, L., and Long, M. itransformer: Inverted transformers are effective for time series forecasting. In *The Twelfth International Conference on Learning Representations*, 2024b. URL <https://openreview.net/forum?id=JePFAI8fah>.
- Liu, Y., Qin, G., Huang, X., Wang, J., and Long, M. Autotimes: Autoregressive time series forecasters via large language models. In *The Thirty-eighth Annual Conference on Neural Information Processing Systems*, 2024c. URL <https://openreview.net/forum?id=FOvZztntlH>.
- Liu, Y., Zhang, H., Li, C., Huang, X., Wang, J., and Long, M. Timer: Generative pre-trained transformers are large time series models. In *Forty-first International Conference on Machine Learning*, 2024d. URL <https://openreview.net/forum?id=bYRYb7DMNo>.
- Liu, Y., Qin, G., Huang, X., Wang, J., and Long, M. Timer-xl: Long-context transformers for unified time series forecasting. In *The Thirteenth International Conference on Learning Representations*, 2025. URL <https://arxiv.org/abs/2410.04803>.
- Loshchilov, I. and Hutter, F. Decoupled weight decay regularization. In *International Conference on Learning Representations*, 2019. URL <https://openreview.net/forum?id=Bkg6RiCqY7>.
- Mathur, A. P. and Tippenhauer, N. O. Swat: a water treatment testbed for research and training on ics security. In *2016 International Workshop on Cyber-physical Systems for Smart Water Networks (CySWater)*, pp. 31–36, 2016. doi: 10.1109/CySWater.2016.7469060.
- Meidani, K., Shojaee, P., Reddy, C., and Farimani, A. B. SNIP: Bridging mathematical symbolic and numeric realms with unified pre-training. In *NeurIPS 2023 AI for Science Workshop*, 2023. URL <https://openreview.net/forum?id=Nn43zREWvX>.

- Müller, S., Hollmann, N., Arango, S. P., Grabocka, J., and Hutter, F. Transformers can do bayesian inference. In *International Conference on Learning Representations*, 2022. URL <https://openreview.net/forum?id=KSugKcbNf9>.
- Nagler, T. Statistical foundations of prior-data fitted networks. In Krause, A., Brunskill, E., Cho, K., Engelhardt, B., Sabato, S., and Scarlett, J. (eds.), *Proceedings of the 40th International Conference on Machine Learning*, volume 202 of *Proceedings of Machine Learning Research*, pp. 25660–25676. PMLR, 23–29 Jul 2023. URL <https://proceedings.mlr.press/v202/nagler23a.html>.
- Newbold, P. Arima model building and the time series analysis approach to forecasting. *Journal of forecasting*, 2(1):23–35, 1983.
- Nie, Y., Nguyen, N. H., Sinthong, P., and Kalagnanam, J. A time series is worth 64 words: Long-term forecasting with transformers. In *The Eleventh International Conference on Learning Representations*, 2023. URL <https://openreview.net/forum?id=Jbdc0vTOcol>.
- Pan, Z., Jiang, Y., Garg, S., Schneider, A., Nevmyvaka, Y., and Song, D. S²ip-llm: Semantic space informed prompt learning with llm for time series forecasting. In *Forty-first International Conference on Machine Learning*, 2024. URL <https://arxiv.org/abs/2403.05798>.
- PeMS. Traffic. <http://pems.dot.ca.gov/>.
- Radford, A., Wu, J., Child, R., Luan, D., Amodei, D., Sutskever, I., et al. Language models are unsupervised multitask learners. *OpenAI blog*, 1(8):9, 2019.
- Radford, A., Kim, J. W., Hallacy, C., Ramesh, A., Goh, G., Agarwal, S., Sastry, G., Askell, A., Mishkin, P., Clark, J., et al. Learning transferable visual models from natural language supervision. In *International conference on machine learning*, pp. 8748–8763. PMLR, 2021.
- Sanh, V., Debut, L., Chaumond, J., and Wolf, T. Distilbert, a distilled version of bert: smaller, faster, cheaper and lighter, 2020. URL <https://arxiv.org/abs/1910.01108>.
- Selva, J., Johansen, A. S., Escalera, S., Nasrollahi, K., Moeslund, T. B., and Clapés, A. Video transformers: A survey. *IEEE Transactions on Pattern Analysis and Machine Intelligence*, 45(11):12922–12943, 2023.
- Shi, X., Wang, S., Nie, Y., Li, D., Ye, Z., Wen, Q., and Jin, M. Time-moe: Billion-scale time series foundation models with mixture of experts. In *The Thirteenth International Conference on Learning Representations*, 2025. URL <https://arxiv.org/abs/2409.16040>.
- Shumway, R. H., Stoffer, D. S., Shumway, R. H., and Stoffer, D. S. Arima models. *Time series analysis and its applications: with R examples*, pp. 75–163, 2017.
- singh chib, P., Nath, A., Kabra, P., Gupta, I., and Singh, P. MS-TIP: Imputation aware pedestrian trajectory prediction. In *Forty-first International Conference on Machine Learning*, 2024. URL <https://openreview.net/forum?id=s4Hy0L4mml>.
- Spyros Makridakis. M4 dataset, 2018. URL <https://github.com/M4Competition/M4-methods/tree/master/Dataset>.
- Su, Y., Zhao, Y., Niu, C., Liu, R., Sun, W., and Pei, D. Robust anomaly detection for multivariate time series through stochastic recurrent neural network. *KDD '19*, pp. 2828–2837, New York, NY, USA, 2019. Association for Computing Machinery. ISBN 9781450362016. doi: 10.1145/3292500.3330672. URL <https://doi.org/10.1145/3292500.3330672>.
- Taga, E. O., Ildiz, M. E., and Oymak, S. TimePFN: Effective multivariate time series forecasting with synthetic data. In *NeurIPS Workshop on Time Series in the Age of Large Models*, 2024. URL <https://openreview.net/forum?id=A9iqHtj3dk>.
- Torres, L., Blevins, A. S., Bassett, D., and Eliassi-Rad, T. The why, how, and when of representations for complex systems. *SIAM Review*, 63(3):435–485, 2021.
- Turrero, C. M., Bouvier, M., Breitenstein, M., Zanuttigh, P., and Parret, V. ALERT-transformer: Bridging asynchronous and synchronous machine learning for real-time event-based spatio-temporal data. In *Forty-first International Conference on Machine Learning*, 2024. URL <https://openreview.net/forum?id=8ZDFn7BDaH>.
- UCI. Electricity. <https://archive.ics.uci.edu/ml/datasets/ElectricityLoadDiagrams20112014>.
- Udrescu, S.-M. and Tegmark, M. Ai feynman: A physics-inspired method for symbolic regression. *Science Advances*, 6(16):eaay2631, 2020. doi: 10.1126/sciadv.aay2631. URL <https://www.science.org/doi/abs/10.1126/sciadv.aay2631>.
- Varambally, S., Ma, Y., and Yu, R. Discovering mixtures of structural causal models from time series data. In *Forty-first International Conference on Machine Learning*, 2024. URL <https://openreview.net/forum?id=chJAUdam3i>.
- Vaswani, A. Attention is all you need. *Advances in Neural Information Processing Systems*, 2017.

- Virgolin, M., Alderliesten, T., Witteveen, C., and Bosman, P. A. Improving model-based genetic programming for symbolic regression of small expressions. *Evolutionary computation*, 29(2):211–237, 2021.
- Wang, C., Qi, Q., Wang, J., Sun, H., Zhuang, Z., Wu, J., Zhang, L., and Liao, J. Chattime: A unified multimodal time series foundation model bridging numerical and textual data, 2024a. URL <https://arxiv.org/abs/2412.11376>.
- Wang, H., Peng, J., Huang, F., Wang, J., Chen, J., and Xiao, Y. MICN: Multi-scale local and global context modeling for long-term series forecasting. In *The Eleventh International Conference on Learning Representations*, 2023a. URL <https://openreview.net/forum?id=zt53IDUR1U>.
- Wang, S., Wu, H., Shi, X., Hu, T., Luo, H., Ma, L., Zhang, J. Y., and ZHOU, J. Timemixer: Decomposable multi-scale mixing for time series forecasting. In *The Twelfth International Conference on Learning Representations*, 2024b. URL <https://openreview.net/forum?id=7oLshfEIC2>.
- Wang, S., Li, J., Shi, X., Ye, Z., Mo, B., Lin, W., Ju, S., Chu, Z., and Jin, M. Timemixer++: A general time series pattern machine for universal predictive analysis. In *The Thirteenth International Conference on Learning Representations*, 2025. URL <https://arxiv.org/abs/2410.16032>.
- Wang, W., Bao, H., Dong, L., Bjorck, J., Peng, Z., Liu, Q., Aggarwal, K., Mohammed, O. K., Singhal, S., Som, S., et al. Image as a foreign language: Beit pretraining for vision and vision-language tasks. In *Proceedings of the IEEE/CVF Conference on Computer Vision and Pattern Recognition*, pp. 19175–19186, 2023b.
- Wang, Y., Han, Y., Wang, H., and Zhang, X. Contrast everything: A hierarchical contrastive framework for medical time-series. In *Thirty-seventh Conference on Neural Information Processing Systems*, 2023c. URL <https://openreview.net/forum?id=sQBHlCmzp>.
- Wang, Y., Wu, H., Dong, J., Liu, Y., Long, M., and Wang, J. Deep time series models: A comprehensive survey and benchmark, 2024c. URL <https://arxiv.org/abs/2407.13278>.
- Wang, Y., Wu, H., Dong, J., Qin, G., Zhang, H., Liu, Y., Qiu, Y.-Z., Wang, J., and Long, M. Timexer: Empowering transformers for time series forecasting with exogenous variables. In *The Thirty-eighth Annual Conference on Neural Information Processing Systems*, 2024d. URL <https://openreview.net/forum?id=INAeUQ041T>.
- Wattenberg, M., Viégas, F., and Johnson, I. How to use t-sne effectively. *Distill*, 2016. doi: 10.23915/distill.00002. URL <http://distill.pub/2016/misread-tsne>.
- Welleck, S., West, P., Cao, J., and Choi, Y. Symbolic brittleness in sequence models: on systematic generalization in symbolic mathematics. In *Proceedings of the AAAI Conference on Artificial Intelligence*, volume 36, pp. 8629–8637, 2022.
- Wetterstation. Weather. <https://www.bgc-jena.mpg.de/wetter/>.
- Woo, G., Liu, C., Sahoo, D., Kumar, A., and Hoi, S. ETSformer: Exponential smoothing transformers for time-series forecasting, 2023. URL https://openreview.net/forum?id=5m_3whfo483.
- Woo, G., Liu, C., Kumar, A., Xiong, C., Savarese, S., and Sahoo, D. Unified training of universal time series forecasting transformers. In *Forty-first International Conference on Machine Learning*, 2024. URL <https://openreview.net/forum?id=Yd8eHMY1wz>.
- Wu, H., Xu, J., Wang, J., and Long, M. Autoformer: Decomposition transformers with auto-correlation for long-term series forecasting. In Beygelzimer, A., Dauphin, Y., Liang, P., and Vaughan, J. W. (eds.), *Advances in Neural Information Processing Systems*, 2021. URL <https://openreview.net/forum?id=J4gRj6d5Qm>.
- Wu, H., Hu, T., Liu, Y., Zhou, H., Wang, J., and Long, M. Timesnet: Temporal 2d-variation modeling for general time series analysis. In *The Eleventh International Conference on Learning Representations*, 2023. URL https://openreview.net/forum?id=ju_Uqw384Oq.
- Wu, K., Li, Y. B., Lou, J., Zhang, X., Wang, H., and Liu, J. Rapid plug-in defenders. In *The Thirty-eighth Annual Conference on Neural Information Processing Systems*, 2024a. URL <https://openreview.net/forum?id=UMPedMhKWm>.
- Wu, Q., Yao, G., Feng, Z., and Yang, S. Peri-midformer: Periodic pyramid transformer for time series analysis. In *The Thirty-eighth Annual Conference on Neural Information Processing Systems*, 2024b. URL <https://openreview.net/forum?id=5iUxMVJVEV>.
- Xiao, Y., BAI, L., Xue, W., Chen, H., Chen, K., kang chen, Han, T., and Ouyang, W. Towards a self-contained data-driven global weather forecasting framework. In *Forty-first International Conference on Machine Learning*, 2024. URL <https://openreview.net/forum?id=Y2WorV5ag6>.

- Xu, C., Jiang, H., and Xie, Y. Conformal prediction for multi-dimensional time series by ellipsoidal sets. In *Forty-first International Conference on Machine Learning*, 2024. URL <https://openreview.net/forum?id=uN39Tt9P8b>.
- Xu, J., Wu, H., Wang, J., and Long, M. Anomaly transformer: Time series anomaly detection with association discrepancy, 2022. URL <https://arxiv.org/abs/2110.02642>.
- Yao, Q., Yang, C.-H. H., Jiang, R., Liang, Y., Jin, M., and Pan, S. Towards neural scaling laws for time series foundation models. In *The Thirteenth International Conference on Learning Representations*, 2025. URL <https://arxiv.org/abs/2410.12360>.
- Yi, K., Fei, J., Zhang, Q., He, H., Hao, S., Lian, D., and Fan, W. Filternet: Harnessing frequency filters for time series forecasting. In *The Thirty-eighth Annual Conference on Neural Information Processing Systems*, 2024. URL <https://openreview.net/forum?id=ugL2D9idAD>.
- Zeng, A., Chen, M., Zhang, L., and Xu, Q. Are transformers effective for time series forecasting? In *Proceedings of the Thirty-Seventh AAAI Conference on Artificial Intelligence, AAAI'23/IAAI'23/EAAI'23*. AAAI Press, 2023. ISBN 978-1-57735-880-0. doi: 10.1609/aaai.v37i9.26317. URL <https://doi.org/10.1609/aaai.v37i9.26317>.
- Zerveas, G., Jayaraman, S., Patel, D., Bhamidipaty, A., and Eickhoff, C. A transformer-based framework for multivariate time series representation learning. In *Proceedings of the 27th ACM SIGKDD conference on knowledge discovery & data mining*, pp. 2114–2124, 2021.
- Zhang, T., Zhang, Y., Cao, W., Bian, J., Yi, X., Zheng, S., and Li, J. Less is more: Fast multivariate time series forecasting with light sampling-oriented mlp structures, 2022. URL <https://arxiv.org/abs/2207.01186>.
- Zhang, Y. and Yan, J. Crossformer: Transformer utilizing cross-dimension dependency for multivariate time series forecasting. In *The Eleventh International Conference on Learning Representations*, 2023. URL <https://openreview.net/forum?id=vSVLM2j9eie>.
- Zhao, S., Jin, M., Hou, Z., Yang, C., Li, Z., Wen, Q., and Wang, Y. Himtm: Hierarchical multi-scale masked time series modeling with self-distillation for long-term forecasting. In *Proceedings of the 33rd ACM International Conference on Information and Knowledge Management*, pp. 3352–3362, 2024.
- Zhou, F., Chen, M., Wang, Z., Luo, F., Luo, X., Huang, W., Chen, Y., and Zhao, Y. A radviz-based visualization for understanding fuzzy clustering results. In *Proceedings of the 10th International Symposium on Visual Information Communication and Interaction, VINCI '17*, pp. 9–15, New York, NY, USA, 2017. Association for Computing Machinery. ISBN 9781450352925. doi: 10.1145/3105971.3105980. URL <https://doi.org/10.1145/3105971.3105980>.
- Zhou, H., Zhang, S., Peng, J., Zhang, S., Li, J., Xiong, H., and Zhang, W. Informer: Beyond efficient transformer for long sequence time-series forecasting. In *Proceedings of the AAAI conference on artificial intelligence*, volume 35, pp. 11106–11115, 2021.
- Zhou, T., Ma, Z., Wen, Q., Wang, X., Sun, L., and Jin, R. Fedformer: Frequency enhanced decomposed transformer for long-term series forecasting. In *International conference on machine learning*, pp. 27268–27286. PMLR, 2022a. URL <https://arxiv.org/abs/2201.12740>.
- Zhou, T., Ma, Z., xue wang, Wen, Q., Sun, L., Yao, T., Yin, W., and Jin, R. FiLM: Frequency improved legendre memory model for long-term time series forecasting. In Oh, A. H., Agarwal, A., Belgrave, D., and Cho, K. (eds.), *Advances in Neural Information Processing Systems*, 2022b. URL <https://openreview.net/forum?id=zTQdHSQUQWc>.
- Zhou, T., Niu, P., Wang, X., Sun, L., and Jin, R. One fits all: Power general time series analysis by pretrained LM. In *Thirty-seventh Conference on Neural Information Processing Systems*, 2023. URL <https://openreview.net/forum?id=gMS6FVZvmF>.

A. Series-Symbol (S2) Pre-training Data Details

In this section, we primarily detail the S2 dataset generation process. Section A.1 describes the generation of symbolic expressions. Subsequently, A.2 explains the process of generating sampling series from mixed distributions and random ARMA series. Then, A.3 presents the series-symbol data we generated. Finally, in Section A.4, we provide a detailed introduction to the usage of the S2 dataset for `SymTime` pre-training. Some of the mathematical symbols used and their explanations are shown in Table 6.

Table 6. Some symbols used in data generation and their explanations.

SYMBOLS	EXPLANATION	SYMBOLS	EXPLANATION
X	SAMPLING SERIES	Y	GENERATED SERIES
$f(\cdot)$	SYMBOLIC EXPRESSION	e_t	WHITE NOISE SEQUENCE
M	THE INPUT CHANNELS NUMBER	N	THE OUTPUT CHANNELS NUMBER
\mathcal{U}	UNIFORM DISTRIBUTION	\mathcal{N}	NORMAL DISTRIBUTION
p	THE ORDER OF THE AR PROCESS	q	THE ORDER OF THE MA PROCESS
ϕ_p	THE PARAMETERS OF THE AR PROCESS	θ_q	THE PARAMETER OF THE MA PROCESS

A.1. Sampling of Functions

Since the structure of mathematical expressions is inherently tree-like (Meidani et al., 2023), where constants and variables can be considered leaf nodes, and binary operators can be seen as root nodes with two child nodes, while unary operators can be regarded as root nodes with a single child node (Kamienny et al., 2022; Lample & Charton, 2020). Therefore, we construct a binary tree using input variables and binary operators as the basic framework for symbolic expressions (Welleck et al., 2022). Subsequently, we randomly insert unary operators within the binary tree and introduce constants through affine transformations to increase the diversity and complexity of the expressions (Bartlett et al., 2024; Meidani et al., 2023; Kamienny et al., 2022). The specific process is illustrated below. The three key steps are shown in Figure 6.

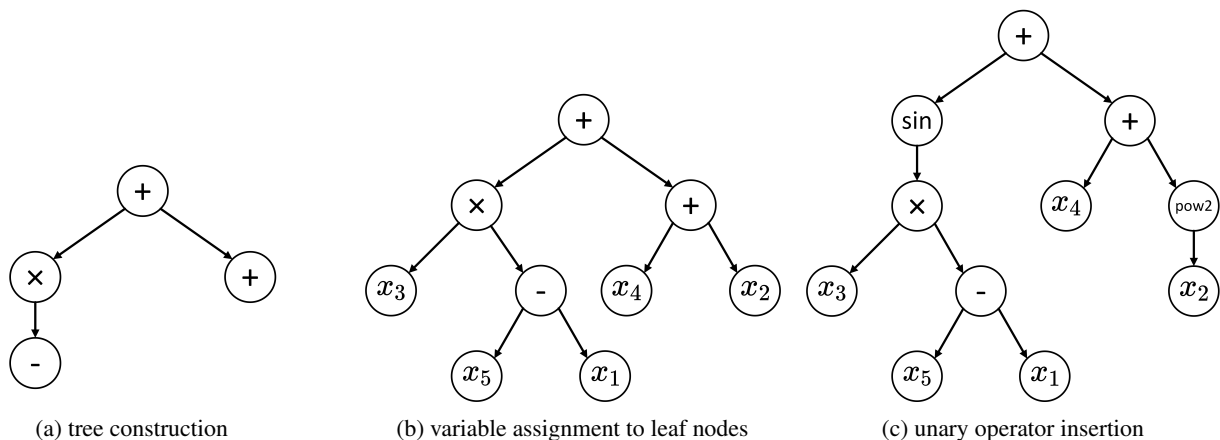


Figure 6. The process of building a binary tree when sampling symbolic expressions.

Input and Output Dimension Selection. To learn the features of numerical series and symbolic expressions, previous works generated the dimensions M for sampling series and N for generated series from uniform distributions $\mathcal{U}(1, M_{\max})$ and $\mathcal{U}(1, N_{\max})$ (Meidani et al., 2023; Kamienny et al., 2022; Alon et al., 2022). However, this paper traverses $[1, M_{\max}]$ and $[1, N_{\max}]$ directly to cover representations of multivariate time series, considering $M_{\max} = 6$ and $N_{\max} = 12$ due to the complexity and uncertainty of data generation. An input series dimension of M implies the construction of expressions with M variable nodes x_1, x_2, \dots, x_M . An output series dimension of N indicates sampling N expressions $y_i = f_i(x_1, x_2, \dots, x_M), i = 1, 2, \dots, N$, yielding N channel-related generated series (Lample & Charton, 2020).

Binary Operator Quantity Selection. After determining the input and output dimensions, we sample the number of binary

operators b from $\mathcal{U}(b_{\min}, b_{\max})$ (Kamienny et al., 2022). These binary operators will serve as the root nodes of binary trees, forming the basic skeleton of the tree. Subsequently, for each binary operator node, we randomly draw the specific operation for the corresponding position from $\mathcal{U}(+, -, \times)$. This step ensures the diversity and complexity of the generated expressions (Meidani et al., 2023; Virgolin et al., 2021; de Franca & Aldeia, 2021).

Tree Construction and Variable Assignment to Leaf Nodes. Based on the number of binary operators obtained through random sampling, we construct a binary tree to simulate the structure of mathematical functions (Meidani et al., 2023). The binary operators will act as the root nodes, forming the basic skeleton of the binary tree (Kamienny et al., 2022; Lample & Charton, 2020), which is shown in Figure 6 (a). After obtaining the basic skeleton of the binary tree, input variables x_1, x_2, \dots, x_M are inserted as leaf nodes into the binary tree, ensuring that each leaf node corresponds to a variable. This process is shown in Figure 6 (b).

Unary Operator Insertion. After inserting the leaf nodes to form a complete binary tree, we select the number of unary operators u from $\mathcal{U}(u_{\min}, u_{\max})$ and insert unary operators at random positions in the binary tree. The available unary operators include $\{\text{inv}, \text{abs}, \text{pow2}, \text{pow3}, \text{sqrt}, \text{sin}, \text{cos}, \text{tan}, \text{arctan}, \text{log}, \text{exp}\}$ (Meidani et al., 2023; Kamienny et al., 2022). This process is shown in Figure 6 (c).

Affine Transformation. To further diversify the generated symbolic expressions, we perform random affine transformations on each random variable x_d and unary operator u_d in the binary tree. Specifically, we replace x_d and u_d with $ax_d + b$ and $au_d + b$, respectively, where a and b are random constants (Meidani et al., 2023; Kamienny et al., 2022). For example, we perform an affine transformation on the unary operation function $\tan(\cdot)$ to obtain $a \times \tan(\cdot) + b$, where a and b are constants.

A.2. Generating Inputs and Outputs Series

After obtaining the symbolic expression $f_i(\cdot)$, we generate a sampling series $X = [x_1, x_2, \dots, x_M] \in \mathbb{R}^{M \times L}$ and obtain the generated series $Y = [y_1, y_2, \dots, y_N] \in \mathbb{R}^{N \times L}$ through forward propagation of the symbolic expression, where $y_i = f_i(X) = f_i(x_1, x_2, \dots, x_M)$, $i = 1, 2, \dots, N$. In order to ensure the quality and diversity of the data, previous works generated sampling series from mixed distributions (Meidani et al., 2023; Kamienny et al., 2022; Lample & Charton, 2020). To make the generated series data more representative of time series, the data in this paper is not only sampled from mixed distributions but also generated from autoregressive moving average (ARMA) models (Shumway et al., 2017; Chujai et al., 2013) with random parameters. The ARMA(p, q) model consists of moving average (MA) and autoregressive (AR) processes (Newbold, 1983), which can be expressed as:

$$Y_t = \phi_1 Y_{t-1} + \phi_2 Y_{t-2} + \dots + \phi_p Y_{t-p} + e_t - \theta_1 e_{t-1} - \theta_2 e_{t-2} - \dots - \theta_q e_{t-q}, \quad (8)$$

where p and q represent the orders of the AR and MA models, respectively, ϕ_p and θ_q are the parameters of the AR and MA processes (Chujai et al., 2013), and $e_t \sim \mathcal{N}(0, 1)$ denotes the observed white noise sequence. Since ARMA possess both the temporal correlation of the AR process and the randomness of the MA process, series obtained from mixed distributions and ARMA sampling better reflect the characteristics of time series.

To ensure the quality of the generated series Y , if the sampling series value x_i falls outside the domain of the expression $f(\cdot)$ or if the generated target value y_i is excessively large, exceeding 10^4 , then the sample is discarded and resampled (Meidani et al., 2023; Kamienny et al., 2022; Xu et al., 2024). This measure ensures the proper generation of data. Furthermore, for each random seed, we traverse all input and output channels to generate symbolic expressions, and each expression is sampled only once. The specific process for generating the sampling series X is as follows.

Mixture Distribution Number and ARMA(p, q) Model Order Selection. Our generated series originate from either a mixed distribution (Meidani et al., 2023; Kamienny et al., 2022; Xu et al., 2024) or a randomly parameterized ARMA(p, q) model (Shumway et al., 2017). Thus, the initial step involves randomly deciding with probability P whether to employ mixed distribution sampling or the ARMA(p, q) model, with this paper setting $P \leq 0.5$ for the mixed distribution and $P > 0.5$ for ARMA(p, q). When opting for the mixed distribution, we select the number of distributions k from the uniform distribution $\mathcal{U}(1, k_{\max})$ and determine the weights for each distribution $\{w_j \sim \mathcal{U}(0, 1)\}_{j=1}^k$, normalizing them so that $\sum_j w_j = 1$ (Meidani et al., 2023). For the ARMA(p, q) model, we independently choose the orders of the AR and MA components, p and q , from the uniform distributions $\mathcal{U}(1, p_{\max})$ and $\mathcal{U}(1, q_{\max})$, respectively.

Generation of Distribution and Parameters. When utilizing a mixed distribution, we select the mean μ_j and variance σ_j for the j -th mixed distribution from $\mathcal{N}(0, 1)$ and $\mathcal{U}(0, 1)$, respectively. Ultimately, we randomly determine a Gaussian

distribution $\mathcal{N}(\mu_j, \sigma_j^2)$ or a uniform distribution $\mathcal{U}(0, \mu_j)$ (Meidani et al., 2023). When employing the ARMA(p, q) model, we randomly generate the parameters $\theta_1, \theta_2, \dots, \theta_q$ for the MA process from $\mathcal{U}(-1, 1)$. Similarly, we generate the parameters $\phi_1, \phi_2, \dots, \phi_p$ for the AR process from the uniform distribution $\mathcal{U}(-1, 1)$ (Shumway et al., 2017). However, to ensure the stationarity of the sampling series X , we need to ensure that the characteristic equation of the AR process has a stationary solution (Chujai et al., 2013). Specifically, we impose the following constraints on the parameters of the AR process:

$$\left. \begin{array}{l} \phi_1 + \phi_2 + \dots + \phi_p < 1 \\ |\phi_p| < 1 \end{array} \right\}. \quad (9)$$

Input Point Generation and Normalization. After determining the parameters for the mixed distribution and the ARMA(p, q) model, we generate the corresponding sampling series X and normalize it on each dimension. Finally, we obtain the generated series $Y = f(X)$ through the symbolic expression. The length of the sampling series is 256.

A.3. Series-Symbol Data Display

The symbolic expressions with text format are shown as follow:

Symbolic expression of Figure 7 (a)

```
y1 = (-0.795 add ((-0.675 mul ((0.999 add (-6.7 mul x1)))*2) add ((-0.798 mul inv((-5.99 add (-0.751 mul x1)))) sub (9.68 mul sqrt((-7.37 add (0.756 mul x1))))))
```

Symbolic expression of Figure 7 (c)

```
y1 = (-3.39 add (((0.56 mul (inv((-98.9 add (58.2 mul x2))) mul ((-19.7000 mul x1) sub (31.9000 mul x2)))) sub (40.4000 mul x1)) add (0.71 mul (((7.13 mul x2) sub (-1.68 mul (x1 mul sqrt((-92.8000 add (0.054 mul (x2 mul ((0.327 mul x2) sub (2.3 mul x2)))))))))) mul x1))))
y2 = (1.0 add ((68.9 mul x2) sub ((80.9 mul (x1 mul (x1 mul ((6.1000 mul x2) sub ((34.2 mul sqrt((64.4 add (29.2000 mul x1)))) add (-5.24 mul x1)))))) add (6.78 mul x2) sub (((0.5730 mul x1) sub ((2.34 mul x2) sub (-6.72 mul x1))) add (0.966 mul sqrt((76.8000 add (-7.79 mul x1))))))
```

Symbolic expression of Figure 7 (e)

```
y1 = (0.795 add ((0.42 mul x3) sub ((4.39 mul x1) add (((0.1430 mul x2) sub (-5.28 mul x3) add (((-0.028 mul (((1.27 mul x3) sub ((0.331 mul x2) sub (2.99 mul x3) add (-0.932 mul ((0.606 mul x1) sub (0.967 mul x3)) mul x3)))) sub (-0.609 mul x3))) add (-1.25 mul x1)) mul x1)) sub (77.3000 mul x1)) sub (1.93 mul x3))) sub (16.7 mul x3))))
y2 = (-9.2900 add ((0.398 mul (((-49.7 mul x1) sub ((5.93 mul sin((6.54 add (-0.045 mul x1)))) add ((62.3000 mul inv(((0.138 mul x2) add (29.0 mul x1)))) add (8.75 mul x2)))) add ((-0.9500 mul x3) add (-8.1 mul x1)) mul x3)) add ((-9.74 mul x3) add (((-0.9 mul x3) sub (4.45 mul sqrt((-0.373 add (-0.151 mul x3)))) add (-54.6 mul x3)) sub (-0.758 mul ((85.3000 add (8.74 mul x3))*2))))))
```

```
y3 = (-0.975 add ((-54.4000 mul sqrt((-0.722 add (-9.33 mul x2)))) sub (1.45 mul ((66.4 add (-9.65 mul x1))*2)))
```

Symbolic expression of Figure 7 (g)

```
y1 = (-7.17 add (0.537 mul x1))
```

```
y2 = (-0.843 add (48.8000 mul x1))
```

```
y3 = (57.3000 add (((-0.449 mul x2) add (-1.32 mul x3)) add ((-0.9400 mul x4) add (0.51 mul x1))))
```

```
y4 = (-0.2040 add (((-6.6000 mul inv((0.88 add (58.1 mul x4)))) sub ((-23.0 mul x4) add ((-91.0 mul x3) sub (-93.6000 mul x2)))) sub ((-6.6000 mul x4) sub (0.9580 mul ((x3 mul x3) mul ((-0.45 mul x2) sub (((-9.09 mul x4) sub ((8.93 mul sqrt((-26.6 mul x4) add (-0.907 mul x1)))) add (-6.2 mul x4)) sub (-0.078 mul x4)) sub (-16.5 mul x2))))))
```

In Figure 7, we show the visualization of the generated series from 1 input channel and 1 output channel to 4 input channels

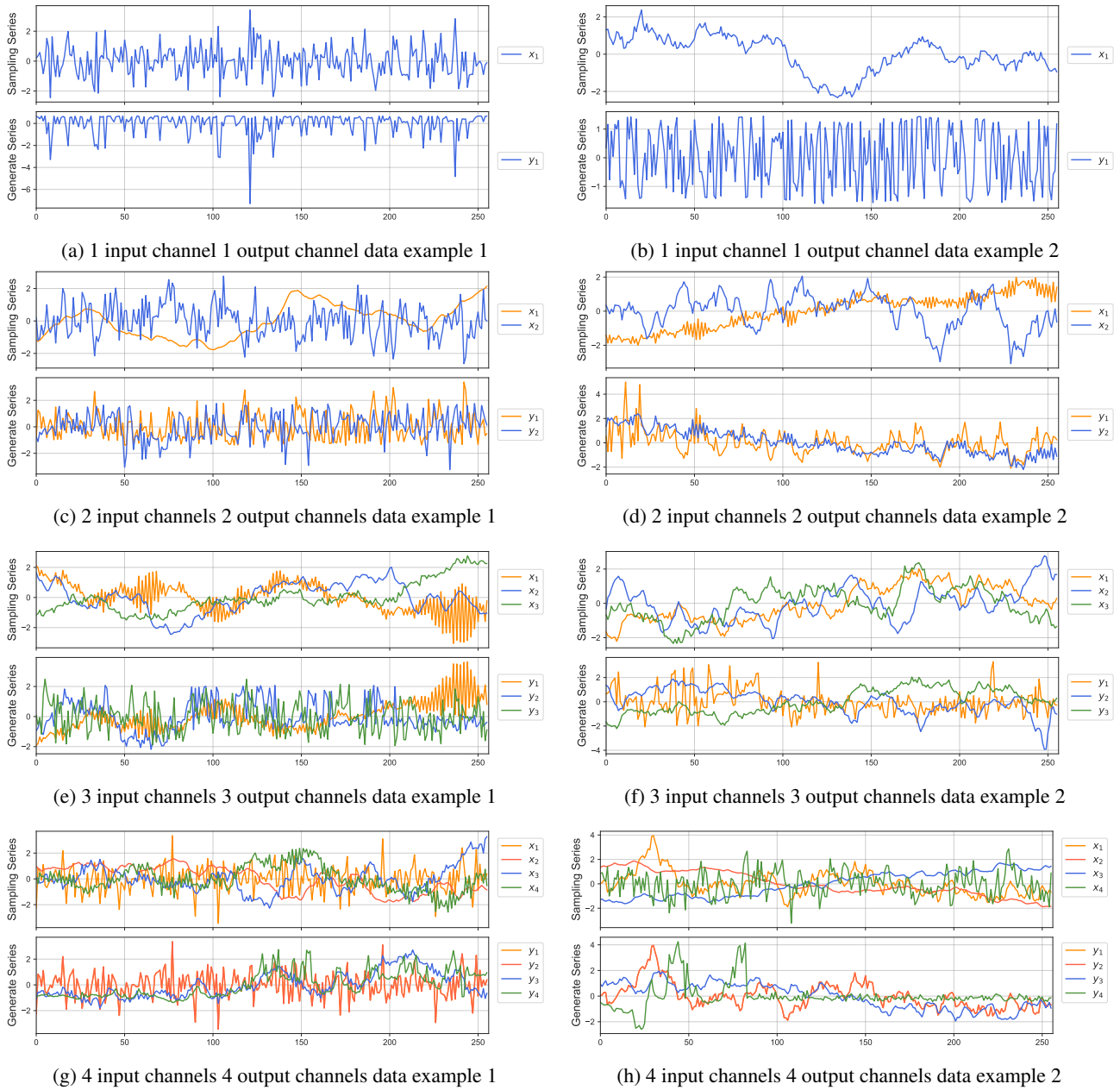


Figure 7. Visualization of series from 1 input channel 1 output channel to 4 input channels 4 output channels.

and 4 output channels. We show two sets of cases for each input and output channel. The symbolic expressions $f(\cdot)$ for the generated series in (a), (c), (e) and (g) in Figure 7 are shown above.

A.4. Composition and Usage of the Series-Symbol Dataset

We set the maximum number of input channels and the maximum number of output channels to 6 and 12 respectively to generate symbolic expressions and series. Each symbolic expression is sampled only once. We generated a total of 25M pairs of series and symbols. The cumulative series length is 50B. The data number of each input channel and output channel in the dataset is shown in Figure 8.

When pre-training `SymTime` with S2 dataset, we start by combining the sampled and generated series and then segmenting

them into patches using a sliding window (Nie et al., 2023; Jin et al., 2024). The sliding window’s kernel size and step size are both set to 16. Due to the requirement for mask time series modeling (MTM) (Dong et al., 2023; Zhao et al., 2024), there is no overlap between adjacent patches. Given the varying number of input and output channels in the data, the series from the maximum input and output channels can be segmented into up to 288 patches ($18 \times 256/16$) (Selva et al., 2023). For series with fewer than 288 patches, we pad them with zeros to align the length. Next, for symbolic expressions in natural language form (Devlin et al., 2019; Meidani et al., 2023; Pan et al., 2024; Wu et al., 2021; Wang et al., 2024a), we set a maximum length of 512 characters and perform tokenization. Ultimately, the time series patches and natural language tokens are fed into the time series encoder and the LLM of the Transformer architecture, respectively.

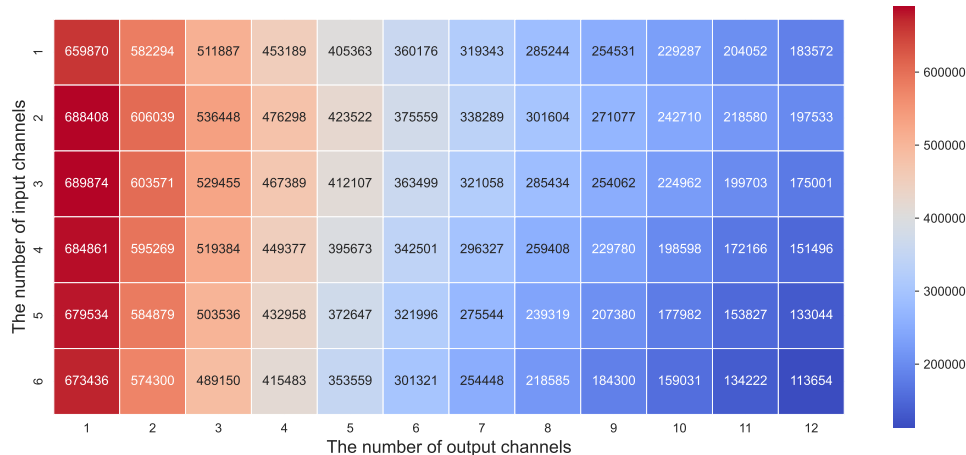


Figure 8. The number of samples in each part of the S2 dataset.

B. Analysis of Series-Symbol (S2) Dataset and Model Pre-training

In Appendix A, we provide a detailed introduction to the generation process, composition and usage of the S2 dataset (Meidani et al., 2023; Kamienny et al., 2022; Lample & Charton, 2020). In this section, we first conduct a random sampling analysis of the statistical characteristics of the S2 dataset, including stationarity (Elliott et al., 1992) and predictability (Goerg, 2013; Liu et al., 2024d). Then, we present the composition of four existing large-scale time series pre-training datasets. It is evident that all current real-world time series datasets face significant data imbalance issues, leading to performance biases in the foundation models pre-trained on them. However, the S2 data generation method provided in this paper can unrestrictedly supply high-quality time series data, thus covering almost all time series representations.

B.1. Statistics Analysis

Table 7. Results of the stationarity and forecastability tests for the S2 dataset.

INPUTS	OUTPUTS	ADF	P VALUE	FORECAST	INPUTS	OUTPUTS	ADF	P VALUE	FORECASTABILITY
1	1	-12.77	0.0538	0.3155	1	6	-11.48	0.0619	0.3375
2	2	-11.89	0.0568	0.3199	2	6	-11.46	0.0733	0.3218
3	3	-12.40	0.0544	0.3328	3	6	-11.43	0.0625	0.3244
4	4	-11.66	0.0617	0.3491	4	6	-11.53	0.0640	0.3428
5	5	-11.38	0.0628	0.3140	5	6	-12.32	0.0597	0.3284
6	6	-12.43	0.0625	0.3262	6	8	-11.52	0.0555	0.3246
6	10	-11.65	0.0619	0.3287	6	12	-11.66	0.0520	0.3310

Stationarity. Stationarity is one of the fundamental properties of time series (Shumway et al., 2017; Chujai et al., 2013). This attribute ensures that the statistical characteristics of time series data remain consistent across different time points, which is crucial for building effective predictive models and making reliable statistical inferences. To this end, we employ the Augmented Dickey-Fuller (ADF) (Elliott et al., 1992) test to examine the stationarity of the data, thereby determining

Table 8. Time-300B time series dataset from Time-MoE (Shi et al., 2025).

	Energy	Finance	Health	Nature	Sales	Synthetic	Transport	Web	Other	Total
# Obs.	15.98B	413.70K	471.04K	279.72B	26.38M	9.22B	2.13B	1.80B	20.32M	309.09B
%	5.17%	5.17%	0.0001%	90.50%	0.008%	2.98%	0.69%	0.58%	0.006%	100%

Table 9. UTSD time series dataset from Timer (Liu et al., 2024d), where Envir. means Environment, Trans. means Transport, Fin. means Finance, Mise. means Multiple Sources.

	Energy	Envir.	Health	IoT	Nature	Trans.	Web	Cloud	Sales	Fin.	Mise.
# Obs.	16.86B	70.45M	233.M	165M	201B	4.9B	157M	2.15B	198M	0.33M	56.52M
%	7.461%	0.031%	0.103%	0.073%	89%	2.17%	0.07%	0.95%	0.088%	0.00%	0.025%

Table 10. LOTSA time series dataset from Moirai (Woo et al., 2024).

	Energy	Transport	Climate	CloudOps	Web	Sales	Nature	Finance	Health	Total
# Obs.	16.36B	4.90B	4.19B	1.52B	428M	198M	28.55M	24.92M	1.59M	27.65B
%	59.17%	17.73%	15.15%	5.49%	1.55%	0.72%	0.09%	0.10%	0.01%	100%

Table 11. Time series datasets from neural scaling laws (Yao et al., 2025)

	Transport	Climate	Energy	CloudOps	Health	Sales	Web	Total
# Obs.	4.82B	4.73B	2.34B	2.15B	240M	140M	600M	14.46B
%	33.31%	32.71%	16.15%	14.86%	1.61%	0.96%	0.40%	100%

whether the generated S2 dataset is suitable for deep neural networks (DNNs) to learn representations of time series.

Forecastability. The forecastability of a time series refers to the ability and accuracy to forecast future values based on historical data and statistical models (Newbold, 1983; Liu et al., 2024d). For certain specific time series and complex systems, such as stock markets, it is often challenging to predict their subsequent developments. Therefore, it is necessary to test whether the S2 dataset is non-chaotic and learnable. Forecastability is calculated by subtracting the entropy of the series’ Fourier decomposition as adopted from (Goerg, 2013) and (Liu et al., 2024d), where a higher forecastability value indicates better predictability. Please note that since the method provided by (Goerg, 2013) is only applicable to multivariate time series, we merge the input channels and output channels together for calculation.

Test Methods and Results. For the multiple input-output channels presented in the Table 7, we randomly selected 1,000 samples to calculate their average ADF statistics, p-values, and Forecastability metrics. The results indicate that the average p-value from the ADF test across all samples is greater than 0.05, suggesting that the majority of the generated series in the S2 dataset are non-stationary time series, posing a challenge in modeling and learning (Elliott et al., 1992). However, the Forecastability metric, which is greater than 0.3 for all tested samples, indicates that the generated series Y is not produced by a chaotic system and is, overall, predictable.

B.2. Analysis of Existing Large-scale Datasets for Time Series Pre-training

Large-scale datasets are crucial for building foundation models. Almost all deep learning models today are data-driven, relying on training data (Zhou et al., 2021; Ismail Fawaz et al., 2020; He et al., 2022; Wu et al., 2024a). Therefore, when constructing a pre-trained foundation model for time series, a large-scale and comprehensively representative pre-training dataset is indispensable (Woo et al., 2024; Liu et al., 2024d; Wang et al., 2023b; Radford et al., 2021; Chen et al., 2020). The scaling laws of neural networks indicate that the learning effectiveness of deep neural networks is primarily influenced by three factors: the number of model parameters, the size of the training dataset, and the amount of computational resources

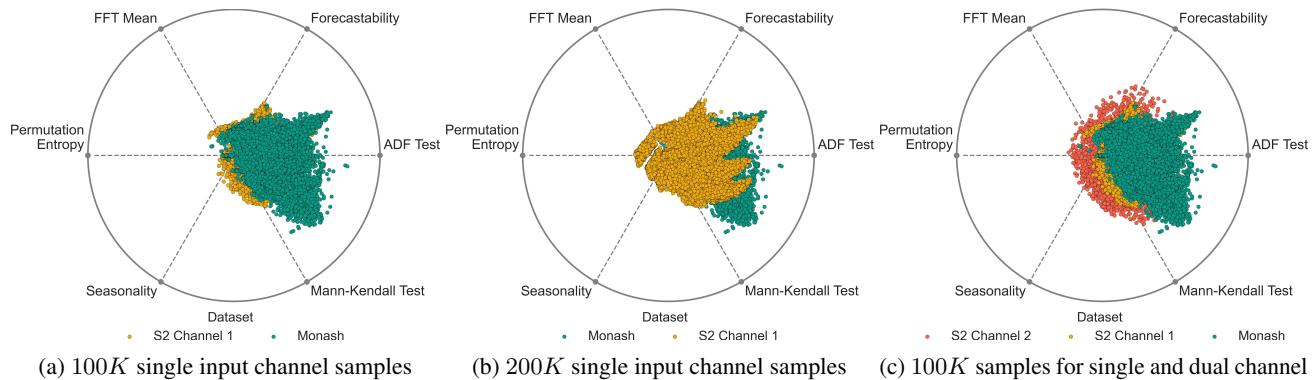


Figure 9. The Radviz visualization of S2 and Monash datasets.

(Bahri et al., 2024; Yao et al., 2025; Kaplan et al., 2020; Aghajanyan et al., 2023). Expanding the scale of the pre-training dataset can effectively improve the model’s generalization capability and performance, and the performance gains from increasing data volume are independent of the model architecture and training methods (Yao et al., 2025; Xiao et al., 2024; Liu et al., 2024a; Turrero et al., 2024). Consequently, an increasing number of models are adopting the approach of training larger-scale models on large-scale pre-training datasets to achieve better performance (Cini et al., 2024). This paper surveys the pre-training datasets used by the three current mainstream pre-trained foundation models—Time-MoE (Shi et al., 2025), Moirai (Woo et al., 2024), and Timer (Liu et al., 2024d)—as well as the datasets utilized in the study of time series scaling laws (Yao et al., 2025), which are shown in Tables 8, 9, 10 and 11.

Imbalanced domain distribution issues in large-scale time series datasets. The distribution of data across various domains indicates that the four large-scale time series pre-training datasets all face issues with imbalanced domain data distribution. For instance, domains such as Nature, Energy and Transport have the most datasets (Zhou et al., 2021), while others like Sales, IoT, Web, Finance and Multiple Sources suffer from extremely low data volumes due to difficulties in data collection or data privacy concerns. According to the scaling laws of neural networks, the imbalance in the pre-training dataset distribution can lead to significant performance biases in in-domain and out-of-domain forecasting tasks for the trained foundation models (Yao et al., 2025; Cini et al., 2024), meaning there is a considerable performance gap between domains with less data and those with more data. To address this, this paper proposes an unrestricted method for generating high-quality time series data to alleviate the scarcity and imbalanced distribution of data in time series analysis domains.

B.3. S2 Dataset Statistical Characterization Coverage Experiments

Metric. To further examine the diversity of the artificially synthesized data in the S2 dataset, we conduct a sampling assessment from six dimensions: stationarity, predictability, frequency domain characteristics, complexity, seasonality intensity, and trend characteristics. For each dimension, we select corresponding statistical indicators for dataset evaluation and quantification, as detailed below: **(1) Augmented Dickey-Fuller (ADF) Test:** Consistent with section B.1, we employ the ADF test to assess the stationarity of time series, using its test statistic as an indicator of time series stationarity (Elliott et al., 1992; Liu et al., 2024d). **(2) Forecastability:** Based on (Goerg, 2013) method, we determine whether a time series is chaotic or can be accurately predicted through machine learning models by using Fourier decomposition and entropy (Liu et al., 2024d). Note that since the method provided by (Goerg, 2013) is only applicable to multivariate time series, we invert the sampled single-channel time series to form a dual-channel series to calculate the indicator. **(3) FFT Mean:** We utilize the average of the Fourier transform power spectrum to evaluate the frequency domain characteristics of time series. This indicator can be used to measure the overall intensity of time series and assess the energy distribution. **(4) Permutation Entropy:** This indicator assesses the dynamic complexity of a time series by analyzing its permutation patterns (Cao et al., 2004). We set the embedding dimension $m = 3$ and time delay $\tau = 1$, and calculate its specific value using Shannon Entropy in Equation 10. See (Cao et al., 2004) for more detailed calculation. **(5) Seasonality:** We decompose the time series into trend, seasonal and residual components using the Seasonal-Trend Decomposition using LOESS (STL) algorithm (Cleveland et al., 1990). Then, we calculate the intensity of the seasonal component in the time series according to Equation 11. **(6) Mann-Kendall Test:** This is a non-parametric statistical method used to detect monotonic trends in time series (Esterby, 1996). The basic principle is to compare the size relationship between each data point and other data points in the

time series. Therefore, this method does not rely on a specific distribution of data and is not affected by outliers. We use the statistical test results of this method as the evaluation indicator, where -1 indicates a downward trend, 1 indicates an upward trend, and 0 indicates no obvious trend.

$$\text{Permutation} = - \sum_{j=1}^K P_j \times \ln P_j, \quad (10)$$

$$\left\{ \begin{array}{l} Y_t = T_t + S_t + R_t \\ \text{Seasonality} = \max \left\{ 0, 1 - \frac{\text{Var}(R_t)}{\text{Var}(S_t + R_t)} \right\} \end{array} \right\}, \quad (11)$$

where, P_i represents the frequency of the i -th permutation model in the permutation entropy, and $K = m!$ is the total number of permutation patterns (Cao et al., 2004). Y_t represents the original time series, T_t , S_t and R_t are the trend, seasonal and residual components decomposed by the STL algorithm (Cleveland et al., 1990) respectively. $\text{Var}(\cdot)$ means calculating the variance of a series.

Setup. We use the six evaluation metric mentioned above as 6 dimensions (Liu et al., 2024d; Cleveland et al., 1990; Goerg, 2013), and employ Radviz plots for high-dimensional space visualization (Zhou et al., 2017). Each time series segment is considered as a sample to calculate its statistical indicators, which are projected as coordinates in the high-dimensional space onto the Radviz plot. We compare the statistical characterization of the S2 dataset and the Monash real-world time series dataset to analyze the quality of our synthetic dataset (Godaheva et al., 2021). Monash covers time series representing various domains such as weather (Wetterstation), traffic (PeMS), electricity (UCI), tourism (singh chib et al., 2024), medicine (Liu et al., 2024a), and energy (Zhou et al., 2021). We uniformly sample 200K samples with a length of 256 from each sub-dataset of Monash and calculate their statistical metric. Since the S2 dataset consists of series-symbol sample pairs with different input and output channels, we randomly sample 100K samples with a length of 256 from the single-input-channel samples of the S2 dataset and calculate their statistical representations. The high-dimensional visualization results in the Radviz plot are shown in Figure 9 (a). Subsequently, we randomly sample 200K samples from the single-input-channel samples in the S2 dataset, and the Radviz visualization result is shown in Figure 9 (b). Finally, we randomly sample 100K samples from both the single-input-channel and dual-input-channel samples in the S2 dataset, and the Radviz visualization result is shown in Figure 9 (c).

Results. The results in Figure 9 (a) show that our synthetic S2 dataset and the real-world time series dataset have a large overlap in statistical characterization (Meidani et al., 2023; Liu et al., 2024d; Lample & Charton, 2020; Kamienny et al., 2022). Therefore, S2 dataset is very close to the real dataset in terms of stationarity, predictability, frequency domain characteristics, complexity, seasonality intensity, and trend characteristics. Pre-training models with the S2 dataset allows learning the basic representations of time series (Goswami et al., 2024; Woo et al., 2024). Moreover, since our S2 dataset generation method can provide high-quality series-symbol data unrestrictedly, it essentially covers the entire representation space of time series. As shown in Figure 9 (b), when the sampling data increases from 100K to 200K, the coverage of representation also expands, and some data representations even surpass the Monash dataset (Godaheva et al., 2021). However, all time series samples in the single-input channel are obtained through sampling from only one input series, i.e., all generated data y is obtained through an expression with only one input variable $f(x_1)$, thus limiting its diversity to some extent. To address this, in Figure 9 (c), we sample 100K samples each from both single-channel and dual-channel time series and the results show that the diversity of dual-channel time series samples is significantly higher than that of single-input channel samples. By increasing the number of input channels or input variables, we can sample more diverse and complex symbolic expressions $f(x_1, x_2, \dots, x_n)$, thereby obtaining more diverse time series (Meidani et al., 2023; Kamienny et al., 2022). This experiment demonstrates that our S2 dataset and the Monash real-world time series dataset have a large overlapping area in statistical representation, indicating the high quality of our synthetic dataset (Dooley et al., 2023; Taga et al., 2024). Considering that our method can generate time series data without limitation, and the coverage of time series statistical characterization expands continuously with the increase of data volume, our synthetic dataset can uniformly cover the basic representations of all types of time series (Wu et al., 2023; Zhou et al., 2023; Cini et al., 2024; Turrero et al., 2024; Varambally et al., 2024).

C. Model Pre-training and Representation Learning

In this section, we analyze and present the model’s pre-training status and the learned representations (Radford et al., 2021; Wang et al., 2023b). We first examine the masked time series modeling (MTM) (Nie et al., 2023; Dong et al., 2023) of

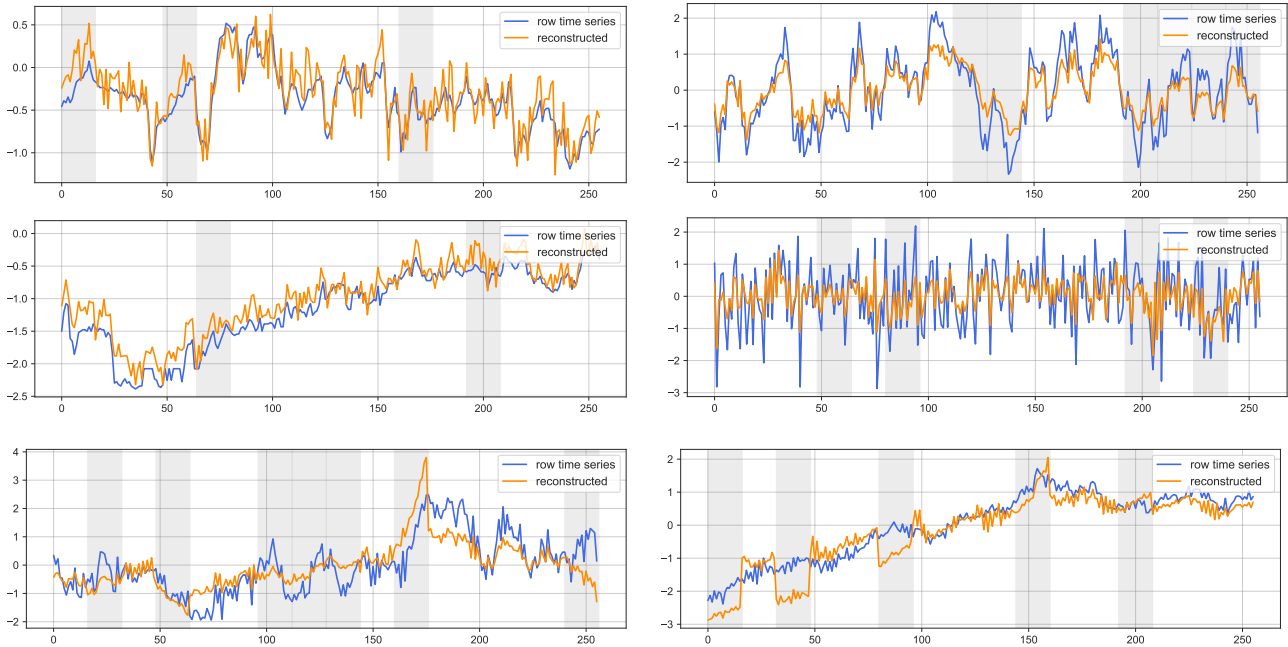


Figure 10. Zero-shot time series imputation in S2 out-of-domain data.

the time series encoder in *SymTime* and test its zero-shot imputation capability on both newly generated data and real time series data. Then, we analyze and visualize the cross-modal representations learned by the time series encoder and the symbol encoder through series-to-symbol and symbol-to-series contrastive loss (Li et al., 2021; He et al., 2020). By comparing the representation learning effects before and after model pre-training (Cini et al., 2024), we demonstrate that the time series encoder in *SymTime* can not only learn the basic representations of time series data through masked time series modeling but also acquire semantic information of symbolic expressions through contrastive losses.

C.1. Masked Time Series Modeling and Zero-shot Imputation

Setup. Since we incorporate MTM loss in the pre-training process of *SymTime*, in this section, we assess the specific learning effects of the time series encoder in *SymTime* through masked modeling (Nie et al., 2023; Dong et al., 2023; 2024; Wang et al., 2024b). We test the model’s performance using both pre-trained synthetic data not in the S2 dataset and real datasets from time series imputation tasks (Meidani et al., 2023; Kamienny et al., 2022; Lample & Charton, 2020). As *SymTime* adds masks in units of patches of length 16 during pre-training, we also add masks in the form of 16-length patches. The reconstruction effect of the masked parts by the time series encoder is shown in Figure 10 and 11.

S2 Dataset Out-of-Domain Data. In Figure 10, we generate new data using the method from the S2 dataset and add masks to test the reconstruction ability of the time series encoder (Meidani et al., 2023; Kamienny et al., 2022; Lample & Charton, 2020). The gray sections represent the masked segments, while blue and orange represent the original and reconstructed series, respectively. We input time series outside the gray parts in patches and have the model reconstruct the gray sections based on the remaining information. Since we only calculate the MTM loss on the masked parts (Dong et al., 2023; 2024), the visible reconstruction does not overlap with the original input series (Liu et al., 2024d; Das et al., 2024; Goswami et al., 2024). From the Figure 10, it can be observed that the time series encoder in *SymTime* performs well in fitting the fluctuations and trends of time series, demonstrating that our encoder successfully learned the fundamental representations of time series during pre-training (Woo et al., 2024; Ilbert et al., 2024; Varambally et al., 2024).

Real-world Time Series Data. In Figure 11, we conduct representation learning tests on 6 real datasets: ETTm1, ETTm2, ETTh1, ETTh2 (Zhou et al., 2021), Electricity (UCI), and Weather (Wetterstation). Since no real data are used for model pre-training, these datasets are also considered as out of domain data. We similarly add masks in patch units (gray sections). It can be observed that the time series encoder in *SymTime* also performs well in zero-shot reconstruction on real-world

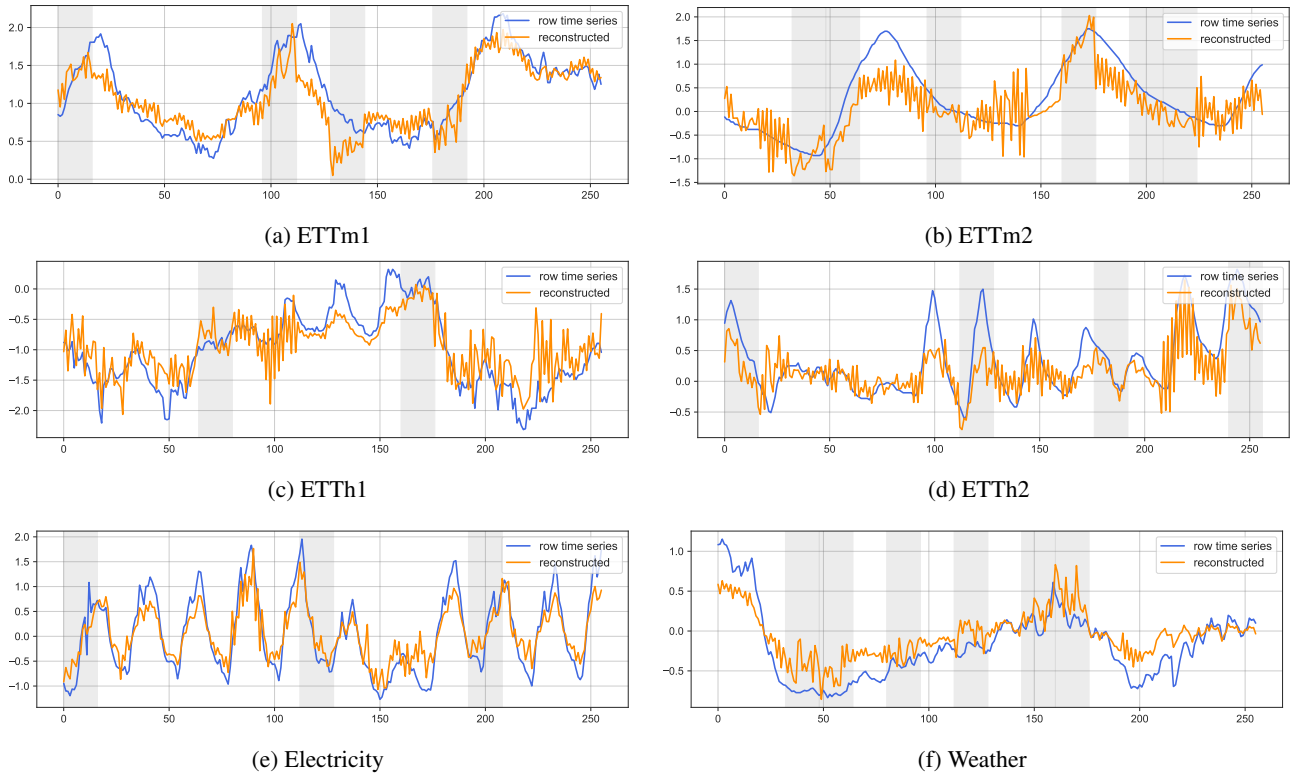


Figure 11. Zero-shot time series imputation in real world time series dataset in ETTm1, ETTm2, ETTh1, ETTh2 (Zhou et al., 2021), Electricity (UCI) and Weather (Wetterstation).

data (Dong et al., 2023; Zerveas et al., 2021).

C.2. Series-Symbol Representation Learning of Time Series Encoder

Setup. To evaluate the cross-modal representations (Li et al., 2021) and semantic information (Radford et al., 2021; Pan et al., 2024; Jin et al., 2024) by the time series encoder in `SymTime`, we select 20K single-input single-output channel symbolic expressions containing only one type of unary operator and their corresponding sampled series from the S2 dataset (Meidani et al., 2023). These symbolic expressions include only one specific math operator from the set $\{\text{inv}, \text{abs}, \text{pow2}, \text{pow3}, \text{sqrt}, \text{sin}, \text{cos}, \text{tan}, \text{arctan}, \text{log}, \text{exp}\}$, using this operator as the category label for the entire series data (Kamienny et al., 2022; Lample & Charton, 2020). Then, we do patching on the sampled time series and input them into the `SymTime` time series encoder, both pre-trained and without pre-trained (Nie et al., 2023). Finally, we use the series representations reconstructed by the time series encoder and apply t-SNE (Wattenberg et al., 2016) to reduce them to a two-dimensional space to observe the distribution of representations for series generated by different types of symbols. The specific results are shown in Figure 12.

Results. From Figure 12 (a), it can be observed that the time series encoder without pre-training cannot effectively distinguish different series-symbol categories. Only a few symbols, such as `inv` and `exp`, which may have more distinct data representations, form certain clusters even without pre-training. Due to we introduce both series-to-symbol and symbol-to-series contrastive losses in the pre-training of `SymTime`, contrastive learning can make positive samples as close as possible in the representation space and negative samples as distant as possible (Radford et al., 2021; Wang et al., 2023c; He et al., 2020; Chen et al., 2020). Through this form of learning, as shown in Figure 12 (b), the pre-trained time series encoder can clearly form simple clusters for series of the same type of unary symbol operator. Similar symbols like `sin` and `cos` are relatively close in the two-dimensional representation space after t-SNE dimensionality reduction (Wattenberg et al., 2016). The three polynomial operations, `pow2`, `pow3`, and `sqrt`, which are the most numerous, also show a certain pattern in the representation space. The `log` operation is surrounded by polynomial operations and also forms a distinct cluster.

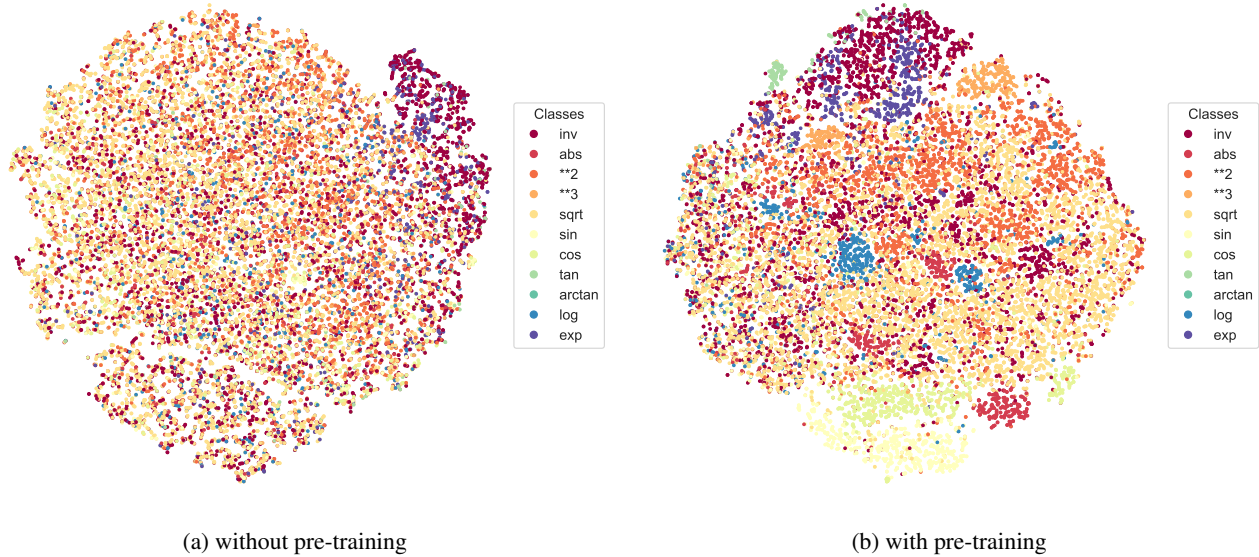


Figure 12. The t-SNE visualization of time series encoder in SymTime representation space.

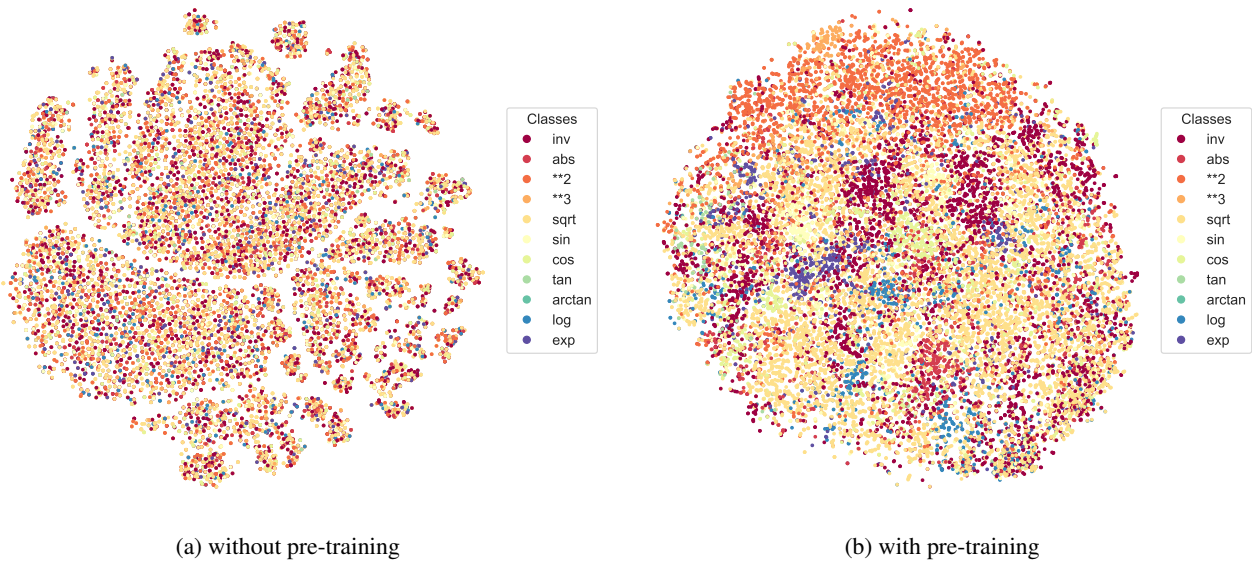


Figure 13. The t-SNE visualization of symbol encoder representation space.

This indicates that SymTime has successfully brought samples of the same category closer together in the latent space through contrastive learning, and thus our time series encoder has learned the semantic information of symbols (Meidani et al., 2023). Finally, ablation experiments reveal that learning with both contrastive losses simultaneously enhances the performance of downstream time series tasks.

C.3. Series-Symbol Representation Learning of Symbol Encoder

Setup. To capture the features of symbolic expressions and provide representation data for the contrastive learning of the time series encoder, we introduce a pre-trained distilled BERT as the symbol encoder (Devlin et al., 2019; Sanh et al., 2020). This approach pre-trains the time series encoder and equips it with semantic information from symbolic expressions. To

examine the cross-modal representation learned by the symbol encoder, we employ the same method as above, using 20K symbolic expressions with a single mathematical operator for our experiment. We first tokenize this series of symbolic expressions and then input them into both the pre-trained and non-pre-trained symbol encoders to obtain the [CLS] token from the last layer output. Finally, we use t-SNE to reduce the obtained [CLS] tokens and project them onto a two-dimensional representation space. The results are shown in Figure 13.

Results. Since the generated symbolic expressions contain specific unary operators, random constants, and binary operators such as $\{+, -, \times\}$ (Meidani et al., 2023), it can be observed from the symbol encoder without pre-training in Figure 13 (a) that the embeddings of various symbols exhibit certain distinctive shapes but are not sensitive to the influence of specific unary operators. All types of symbols are chaotically mixed together. However, after masked language modeling (MLM) generative pre-training and contrastive learning (Radford et al., 2019; Devlin et al., 2019; Wang et al., 2023b), the symbol encoder, composed of a LLM, becomes more sensitive to specific symbolic data, and similar types of symbolic expressions converge to form distinct cluster structures in Figure 13 (b).

D. Implementation Details

In this section, we first provide a detailed introduction to the datasets and evaluation metrics used for the five TSA tasks. Subsequently, we elaborate on the training details of our experiments, including how we pre-trained `SymTime` on the S2 dataset and how we fine-tuned it on downstream task datasets. All experiments and deep neural networks training are implemented in PyTorch on NVIDIA A6000 48GB GPU.

D.1. Downstream Tasks Datasets Details

We conduct experiments using the TimesNet benchmark (Wu et al., 2023), with a detailed description of the dataset provided in Table 12. Specifically, we utilize 8 datasets including ETTh1, ETTh2, ETTm1, ETTm2 (Zhou et al., 2021), Electricity (UCI), Traffic (PeMS), Weather (Wetterstation), and Exchange (Lai et al., 2018) to conduct long-term time series forecasting experiments. Our model, `SymTime`, employ input series of lookback lengths 96 and 512, with forecast horizons of 96, 192, 336, and 720. For short-term forecasting experiments, we employ the M4 benchmark dataset, predicting data of various frequencies (Spyros Makridakis, 2018). In the time series imputation task, we test on 6 datasets—ETTh1, ETTh2, ETTm1, ETTm2 (Zhou et al., 2021), Electricity (UCI), and Weather (Wetterstation)—with mask rates of 12.5%, 25%, 37.5%, and 50%. For time series classification, we utilize ten UEA multivariate time series classification benchmark datasets (Bagnall et al., 2018). For anomaly detection in time series, we experiment with five datasets: SMD (Su et al., 2019), MSL (Hundman et al., 2018), SMAP (Hundman et al., 2018), SWaT (Mathur & Tippenhauer, 2016), and PSM (Abdulaal et al., 2021).

D.2. Metrics

We assess the five TSA tasks using various metrics. For long-term forecasting and imputation tasks, we employ mean squared error (MSE) and mean absolute error (MAE). For short-term forecasting, we utilize symmetric mean absolute percentage error (SMAPE), mean absolute scaled Error (MASE), and overall weighted average (OWA), with OWA being a metric unique to the M4 competition. For time series classification tasks, we use classification accuracy as the metric. For anomaly detection tasks, we adopt precision, recall, and F1-score as our evaluation metrics. The calculations for these metrics are as follows.

$$\text{MSE} = \sum_{i=1}^n (y_i - \hat{y}_i)^2, \tag{12}$$

$$\text{MAE} = \sum_{i=1}^n |y_i - \hat{y}_i|, \tag{13}$$

$$\text{SMAPE} = \frac{200}{T} \sum_{i=1}^T \frac{|\mathbf{X}_i - \hat{\mathbf{Y}}_i|}{|\mathbf{X}_i| + |\hat{\mathbf{Y}}_i|}, \tag{14}$$

$$\text{MAPE} = \frac{100}{T} \sum_{i=1}^T \frac{|\mathbf{X}_i - \hat{\mathbf{Y}}_i|}{|\mathbf{X}_i|}, \tag{15}$$

Table 12. Dataset descriptions. The dataset size is organized in (Train, Validation, Test).

Tasks	Dataset	Dim	Series Length	Dataset Size	Information (Frequency)
Forecasting (Long-term)	ETTm1, ETTm2	7	{96, 192, 336, 720}	(34465, 11521, 11521)	Electricity (15 mins)
	ETTh1, ETTh2	7	{96, 192, 336, 720}	(8545, 2881, 2881)	Electricity (15 mins)
	Electricity	321	{96, 192, 336, 720}	(18317, 2633, 5261)	Electricity (Hourly)
	Traffic	862	{96, 192, 336, 720}	(12185, 1757, 3509)	Transportation (Hourly)
	Weather	21	{96, 192, 336, 720}	(36792, 5271, 10540)	Weather (10 mins)
	Exchange	8	{96, 192, 336, 720}	(5120, 665, 1422)	Exchange rate (Daily)
Forecasting (short-term)	M4-Yearly	1	6	(23000, 0, 23000)	Demographic
	M4-Quarterly	1	8	(24000, 0, 24000)	Finance
	M4-Monthly	1	18	(48000, 0, 48000)	Industry
	M4-Weakly	1	13	(359, 0, 359)	Macro
	M4-Daily	1	14	(4227, 0, 4227)	Micro
	M4-Hourly	1	48	(414, 0, 414)	Other
Imputation	ETTm1, ETTm2	7	96	(34465, 11521, 11521)	Electricity (15 mins)
	ETTh1, ETTh2	7	96	(8545, 2881, 2881)	Electricity (15 mins)
	Electricity	321	96	(18317, 2633, 5261)	Electricity (15 mins)
	Weather	21	96	(36792, 5271, 10540)	Weather (10 mins)
Classification (UEA)	EthanolConcentration	3	1751	(261, 0, 263)	Alcohol Industry
	FaceDetection	144	62	(5890, 0, 3524)	Face (250Hz)
	Handwriting	3	152	(150, 0, 850)	Handwriting
	Heartbeat	61	405	(204, 0, 205)	Heart Beat
	JapaneseVowels	12	29	(270, 0, 370)	Voice
	PEMS-SF	963	144	(267, 0, 173)	Transportation (Daily)
	SelfRegulationSCP1	6	896	(268, 0, 293)	Health (256Hz)
	SelfRegulationSCP2	7	1152	(200, 0, 180)	Health (256Hz)
	SpokenArabicDigits	13	93	(6599, 0, 2199)	Voice (11025Hz)
	UWaveGestureLibrary	3	315	(120, 0, 320)	Gesture
Anomaly Detection	SMD	38	100	(566724, 141681, 708420)	Server Machine
	MSL	55	100	(44653, 11664, 73729)	Spacecraft
	SMAP	25	100	(108146, 27037, 427617)	Spacecraft
	SWaT	51	100	(396000, 99000, 449919)	Infrastructure
	PSM	25	100	(105984, 26497, 87841)	Server Machine

$$\text{MASE} = \frac{1}{T} \sum_{i=1}^T \frac{|\mathbf{X}_i - \hat{\mathbf{Y}}_i|}{\frac{1}{T-q} \sum_{j=q+1}^T |\mathbf{X}_j - \mathbf{X}_{j-q}|}, \quad (16)$$

$$\text{OWA} = \frac{1}{2} \left[\frac{\text{SMAPE}}{\text{SMAPE}_{\text{Naive2}}} + \frac{\text{MASE}}{\text{MASE}_{\text{Naive2}}} \right], \quad (17)$$

where, y_i is the ground true value, \hat{y}_i is the model prediction, q is the periodicity of the time series data. $\mathbf{X}, \hat{\mathbf{Y}} \in \mathbb{R}^{T \times C}$ are the ground truth and prediction results of the future with T time points and C dimensions. \mathbf{X}_i means the i -th future time point.

D.3. Pre-training

Model Hyper-parameter. The parameter configurations for the time series encoder and symbol encoder in `SymTime` are shown in Table 1. During model pre-training, we primarily set three hyperparameters: (1) the masking ratio of time series patches, (2) the masking ratio for natural language symbols, and (3) the proportion factor α used to balance pseudo-targets in momentum distillation. Based on the masked time series modeling pre-training experimental configuration of PatchTST (Nie et al., 2023) and SimMTM (Dong et al., 2023), we set the masking ratio for time series to 40%. Following the experimental configuration of BERT in masked language modeling (Devlin et al., 2019; Sanh et al., 2020), we set the masking ratio for symbolic data to 15%. Based on the experimental configuration of momentum distillation in ALBEF (Li et al., 2021; Lin & Hu, 2024; He et al., 2020), we set α to 0.6.

Training Configurations. During the pre-training of `SymTime`, we employ AdamW (Kingma & Ba, 2017; Loshchilov & Hutter, 2019) as the optimizer with the default hyperparameter configuration for (β_1, β_2) as (0.9, 0.999). Then, we utilize the OneCycle policy to dynamically adjust the learning rate. We set the warmup epochs to 10, during which the learning rate gradually grows up to an initial value of 5×10^{-5} , and then adjust it dynamically using a cosine annealing schedule, with the minimum learning rate set at 1×10^{-7} . We conduct pre-training using data parallelism on a hardware setup consisting of 8 NVIDIA RTX A6000 GPUs with 48GB of memory each. We set the batch size to 128 and trained for a total of 85 epochs. Unlike SNIP (Meidani et al., 2023), we do not generate data on-the-fly during training for pre-training. Instead, we prepare the data in advance and then load it into the device for pre-training. Due to the large size of our generat S2 dataset, we load data into the GPU in batches during each epoch for pre-training.

D.4. Fine-tuning

For the five major tasks in TSA, we conduct downstream task fine-tuning experiments using the configurations in Table 13. For all downstream task fine-tuning experiments, we employ the Adam optimizer (Kingma & Ba, 2017; Loshchilov & Hutter, 2019) with hyperparameters (β_1, β_2) set to (0.9, 0.999). The LR in the table represents the initial learning rate and we utilize the dynamic learning rate adjustment strategy from TimesNet (Wu et al., 2023).

Table 13. Experiment configuration of `SymTime` fine-tuning.

Tasks / Configurations	Model Parameter			Training Configurations			
	d_{model}	d_{fit}	Layers	LR	Loss	Batch Size	Epochs
Long-term Forecasting	512	2048	3, 6	$10^{-4} - 5 \times 10^{-4}$	MSE	4-64	20
Short-term Forecasting			2, 3	$10^{-4} - 2 \times 10^{-4}$	SMAPE	8-32	16
Classification			1-6	$10^{-4} - 5 \times 10^{-3}$	Cross Entropy	4-64	64
Imputation			2, 3, 6	$10^{-4} - 5 \times 10^{-4}$	MSE	4-64	32
Anomaly Detection			3, 6	$10^{-4} - 5 \times 10^{-4}$	MSE	4-64	12

D.5. Ablation Experiments Details

Ablation study on pre-training strategies and objectives. To further verify the effectiveness of our series-symbol pre-training strategy and objectives, we establish 8 distinct ablation experiment groups and a control group. The specific configurations of these 8 ablation experiment groups are as follows.

1. **Freeze:** All parameters in the pre-trained time series encoder are frozen, with only the linear projection layer for outputting prediction results fine-tuned.

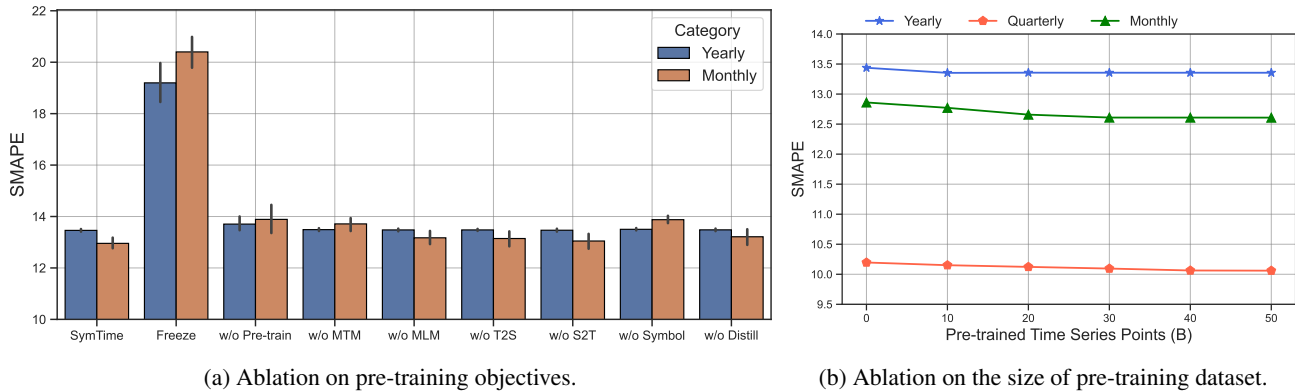


Figure 14. Ablation experiments on short-term forecasting task.

2. **w/o Pretrain:** No series-symbol pre-training is conducted; the time series encoder with initialized parameters is used for downstream task experiments.
3. **w/o MTM:** The masked time series modeling (MTM) is removed from the pre-training objectives.
4. **w/o MLM:** The masked language modeling (MLM) is removed from the pre-training objectives.
5. **w/o T2S:** The contrastive loss from time series to symbols is removed from the pre-training objectives.
6. **w/o S2T:** The contrastive loss from symbols to time series is removed from the pre-training objectives.
7. **w/o Symbol:** Only time series data from the S2 dataset are used to pre-train the time series encoder via MTM, disregarding the correspondence with symbols.
8. **w/o Distill:** The contrastive loss in pre-training does not use the pseudo objective of momentum distillation.

D.6. Ablation Experiments on Short-term Forecasting

Setup. We adopt the same experimental setup as in Section 4.6 to conduct ablation studies on short-term time series forecasting tasks. We first select the Yearly and Monthly sub-datasets from the M4 benchmark dataset (Spyros Makridakis, 2018) to perform ablation experiments on SymTime’s pre-training objectives. We choose SMAPE as the evaluation metric and the results are shown in Figure 14 (a). Subsequently, we select the Yearly, Quarterly and Monthly sub-datasets to verify the impact of the pre-training dataset size on downstream task performance. The results are shown in Figure 14 (b), where 0 indicates no pre-training.

Results. Figure 14 (a) indicates that SymTime’s performance drops sharply when the backbone encoder is frozen and no pre-training is conducted. When some pre-training objectives are removed, the model’s performance in short-term time series forecasting also declines, but the sensitivity of performance degradation is not as pronounced as in long-term forecasting experiments. Figure 14 (a) shows that as the size of the pre-training dataset increases, SymTime’s performance on the Quarterly dataset improves significantly.

D.7. The Impact and Ablation of Pre-interpolation on Time Series Imputation Task

SymTime adds masks randomly at the patch level during pre-training for time series reconstruction. While in the imputation task, masks are added randomly at the data point level. Additionally, high masking rates may disrupt the original trend and periodic features of the time series. Therefore, we use Peri-midFormer’s method to apply per-interpolation to the masked time series to restore the disrupted periodic features (Wu et al., 2024b; 2023; Wang et al., 2024b; 2025; Han et al., 2024; junxin lu & Sun, 2024). It is important to note that this method is general and independent of deep learning models. The use of this method aims to further enhance the potential of deep learning models. To further verify the effectiveness and impact of the per-interpolation method, we conduct experiments on the ECL time series imputation dataset, with results shown in Table 14. Taking the ECL time series dataset 0.5 mask ratio as an example, the effect of pre-interpolation is shown in Figure

Table 14. Ablation Experiments of pre-interpolation in inputation task on ECL dataset. The per-interpolation results for Peri-midFormer, TimesNet, PatchTST, DLinear and Pyraformer are copied from (Wu et al., 2024b).

Methods	Metric	w/o per-interpolation				with per-interpolation			
		0.125	0.25	0.375	0.5	0.125	0.25	0.375	0.5
Per-interpolation	MSE	-	-	-	-	0.086	0.110	0.149	0.206
	MAE	-	-	-	-	0.188	0.213	0.251	0.301
SymTime (Ours)	MSE	0.050	0.064	0.074	0.092	0.037	0.047	0.060	0.075
	MAE	0.145	0.169	0.181	0.206	0.122	0.139	0.160	0.181
Peri-midFormer (Wu et al., 2024b)	MSE	0.073	0.092	0.107	0.122	0.047	0.053	0.067	0.085
	MAE	0.187	0.214	0.231	0.248	0.140	0.162	0.179	0.195
TimesNet (Wu et al., 2023)	MSE	0.088	0.092	0.096	0.102	0.081	0.083	0.086	0.091
	MAE	0.203	0.208	0.214	0.221	0.196	0.198	0.201	0.207
PatchTST (Nie et al., 2023)	MSE	0.061	0.072	0.082	0.097	0.050	0.059	0.070	0.087
	MAE	0.170	0.185	0.198	0.216	0.148	0.164	0.181	0.202
DLinear (Zeng et al., 2023)	MSE	0.084	0.113	0.141	0.173	0.050	0.062	0.789	0.105
	MAE	0.206	0.243	0.273	0.303	0.144	0.164	0.189	0.225
Pyraformer (Liu et al., 2022a)	MSE	0.297	0.294	0.296	0.299	0.165	0.165	0.171	0.173
	MAE	0.383	0.380	0.381	0.383	0.290	0.291	0.293	0.295

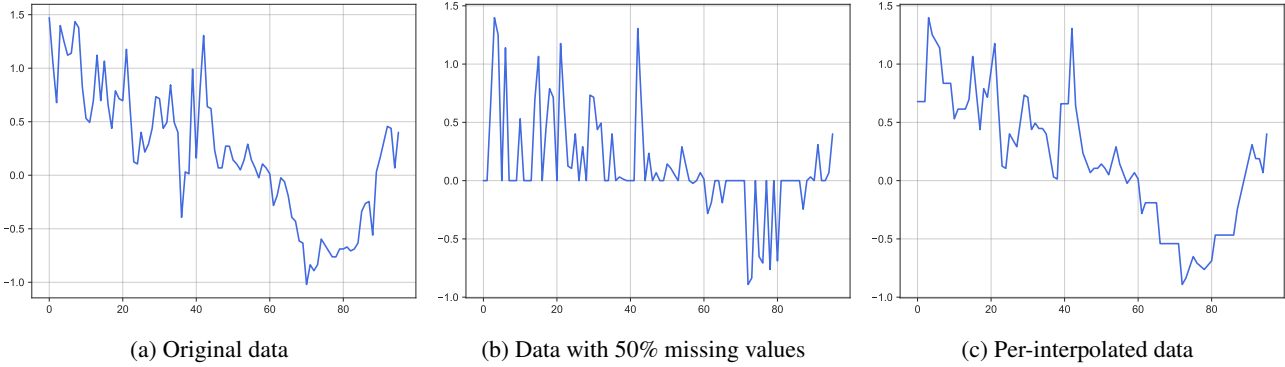


Figure 15. Visualization of original data, data with 50% missing values and pre-interpolated data of ECL dataset.

15. We perform experiments with masking rate of $\{0.125, 0.25, 0.375, 0.50\}$ and compare models such as Peri-midFormer (Wu et al., 2024b), TimesNet (Wu et al., 2023), PatchTST (Nie et al., 2023), DLinear (Zeng et al., 2023) and Pyraformer (Liu et al., 2022a). Per-interpolation represents the experimental results obtained using only linear interpolation. For a missing time series x_t at time t , the method can be described as:

$$x_t = \begin{cases} \frac{x_{t-1} + x_{t+1}}{2}, & \text{if } (x_{t-1} \neq \text{None} \ \& \ x_{t+1} \neq \text{None}) \\ x_{t+1}, & \text{if } (x_{t-1} = \text{None} \ \& \ x_{t+1} \neq \text{None}) , \\ x_{t-1}, & \text{if } (x_{t-1} \neq \text{None} \ \& \ x_{t+1} = \text{None}) \end{cases} \tag{18}$$

where, x_{t-1} and x_{t+1} represent the values at the previous and next time points, respectively, while None indicates a missing value. The results in Table 14 show that this method significantly improves the performance of all models in a model-independent manner.

E. Related Work

E.1. Time Series Foundation Models

In CV and NLP (Radford et al., 2021), PTFMs have been demonstrated to adapt to a variety of downstream tasks after fine-tuning on specific datasets, exhibiting excellent generalization and scalability. Inspired by this, recent years have seen significant progress in PTFMs for TSA (Ahmed et al., 2023; Liang et al., 2024), with the emergence of various pre-training methods. MOIRAI, through MTSM and reconstruction, has been pre-trained on large datasets (27B), yielding a universal forecasting model with significant zero-shot advantages (Woo et al., 2024). Timer, after generative pre-training on large datasets (1B), has performed well in forecasting (Liu et al., 2024d). TimeGPT trained a encoder-decoder Transformer with 100B data (Garza et al., 2024). COMET, using multi-level contrastive learning on a large ECG dataset, has obtained a medical time series PTFMs with few-shot advantages (Wang et al., 2023c).

As discussed in Appendix Section B.2, these baseline models still face challenges related to data scarcity and data imbalance. In the next section, we introduce the proposed data generation mechanism and the corresponding dual-modality foundation model designed to address these issues.

E.2. Deep Learning and Symbolic Regression

The central thesis of this paper is to regard time series as representations of complex dynamical systems (Udrescu & Tegmark, 2020). Traditionally, complex systems are modeled by observing time series utilizing ODE and PDE (Doering, 2018). With the advancement of machine learning, symbolic regression (SR) (Bartlett et al., 2024), as a supervised learning method, can discover hidden mathematical expressions from numerical series. Although genetic algorithms (GAs) are the mainstream approach for SR (Virgolin et al., 2021; de Franca & Aldeia, 2021), deep learning-based methods have also made significant progress. (Kamienny et al., 2022) constructed an end-to-end SR model using Transformers, while SNIP built a large-scale pre-trained model through contrastive learning on symbolic expressions and numerical observations (Meidani et al., 2023). Both methods treat symbolic expressions as nature language and use deep neural networks to learn their features. Therefore, this paper employs a pre-trained LLM as a symbol encoder to learn the features of symbolic expressions and jointly trains a time series foundation model imbued with semantic information through contrastive learning (junxin lu & Sun, 2024).

E.3. Time Series Forecasting Models Based on Synthetic Data

Unlike the representation pre-training conducted on the large synthetic S2 dataset in this paper, previous TSA models trained on synthetic data were mainly based on Prior-data Fitted Networks (PFN) (Müller et al., 2022; Nagler, 2023). This model learns prior distributions from synthetic data using Bayesian methods, enabling zero-shot inference. ForecastPFN generated a large number of synthetic time series by separately modeling the seasonal trend, global trend and noise based on given constraint expressions (Dooley et al., 2023). Although PFN trained in this way offered certain zero-shot and few-shot advantages, this approach was limited to generating time series through sampling fixed expressions and performing linear combinations. In contrast, the S2 data generation mechanism proposed in this paper can sample an infinite variety of symbolic expressions (Meidani et al., 2023; Kamienny et al., 2022; Lample & Charton, 2020; junxin lu & Sun, 2024). TimePFN constructed synthetic datasets by filtering real time series with linear and periodic convolution kernels, training PFN for zero-shot inference (Taga et al., 2024). However, this method depends on real-world time series for filtering and linear transformations between channels. Compared to the S2 data generation mechanism, it can not create large-scale and fully representative synthetic datasets for model pre-training.

F. Visualization

F.1. Long-term Time Series Forecasting with 96 Prediction on ETTh1 (Figure 16) and ECL (Figure 17)

F.2. Short-term Time Series Forecasting on M4 Weekly (Figure 18) and Monthly (Figure 19)

F.3. Time Series Imputation with 50% mask rate on ETTh1 (Figure 20) and ETTm1 (Figure 21)

G. Full Results

For the five downstream TSA tasks results, we use (1) Peri-midFormer for Peri-midFormer (Wu et al., 2024b), (2) uni2ts for Moirai (Woo et al., 2024), (3) Large-Time-Series-Model for Timer (Liu et al., 2024d), (4) Time-LLM for Time-LLM

(Jin et al., 2024), (5) TSLANet for TSLANet (Eldele et al., 2024), (6) S2IP-LLM for S^2 IP-LLM (Pan et al., 2024), (7) NeurIPS2023-One-Fits-All for GPT4TS (Zhou et al., 2023), (8) UniTS for UniTS (Gao et al., 2024), (9) moment for Moment (Goswami et al., 2024), (10) FilterNet for FilterNet (Yi et al., 2024), (11) RTSF for RLinear (Li et al., 2023b), and (12) Time-Series-Library for other models, such as TimesNet (Wu et al., 2023), PatchTST (Nie et al., 2023), TimeMixer (Wang et al., 2024b), iTransformer (Liu et al., 2024b), DLinear (Zeng et al., 2023), Autoformer (Wu et al., 2021) and Informer (Zhou et al., 2021). To ensure a fair comparison, we use the original experimental configuration in the project scripts.

G.1. Time Series Long-term Forecasting (Table 15, Table 16 and Table 17)

G.2. Time Series Short-term Forecasting (Table 18 and Table 19)

G.3. Time Series Classification (Table 20 and Table 21)

G.4. Time Series Imputation (Table 22 and Table 23)

G.5. Time Series Anomaly Detection (Table 24)

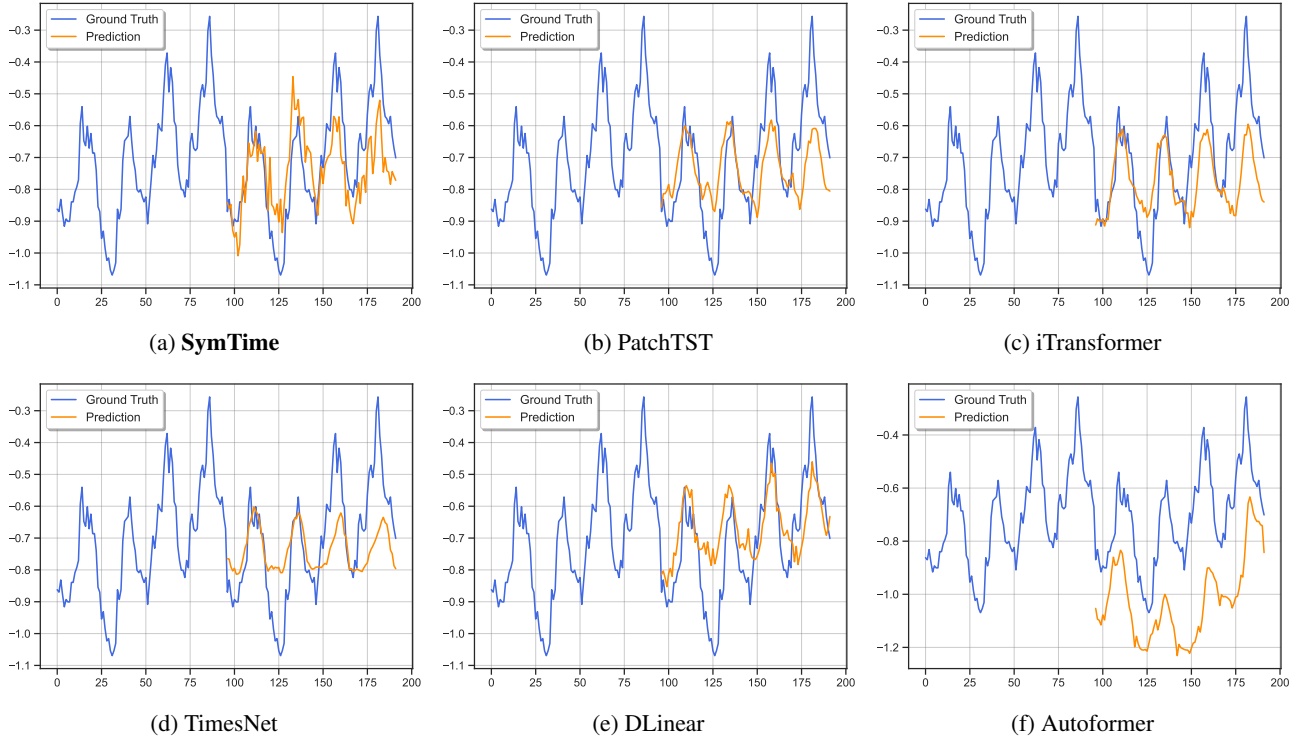


Figure 16. Visualization of long-term forecasting with 96 prediction length of ETTh1 dataset.

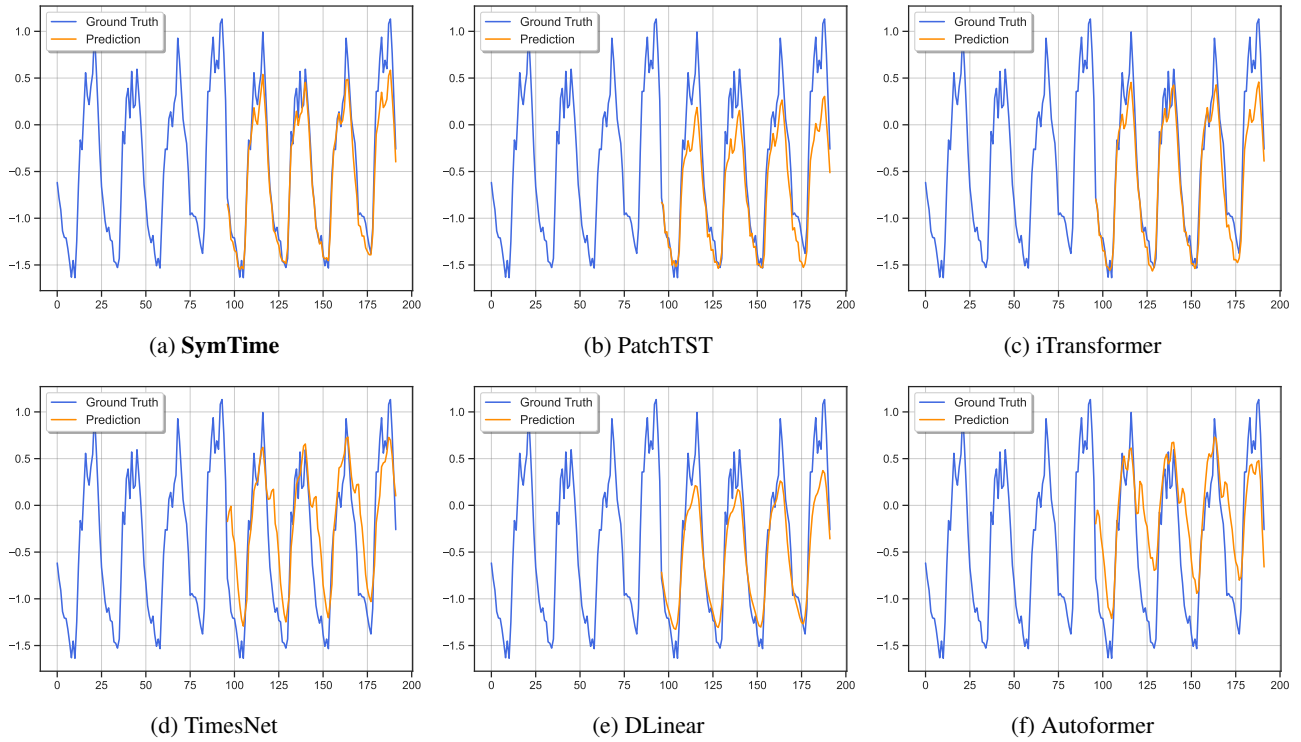


Figure 17. Visualization of long-term forecasting with 96 prediction length of Electricity dataset.

Mitigating Data Scarcity in Time Series Analysis: A Foundation Model with Series-Symbol Data Generation

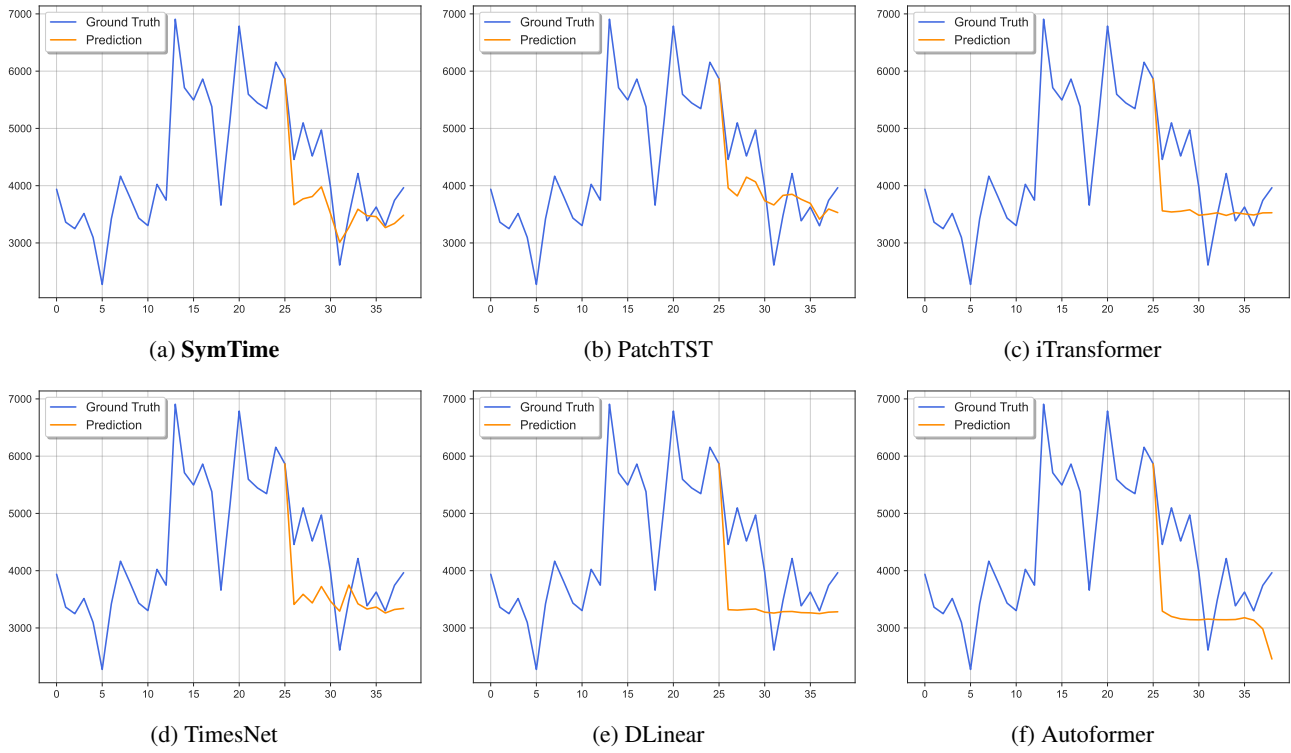


Figure 18. Visualization of time series short-term forecasting in M4 dataset Weekly.

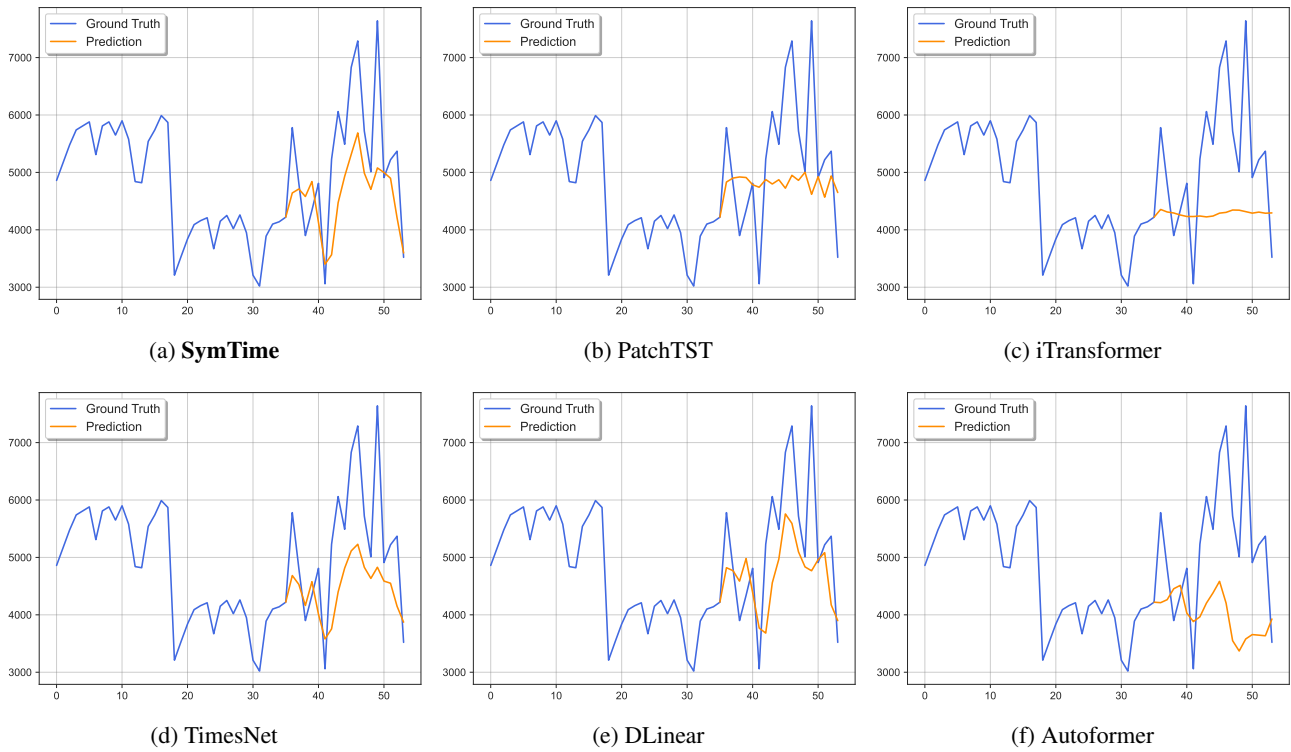


Figure 19. Visualization of time series short-term forecasting in M4 dataset Monthly.

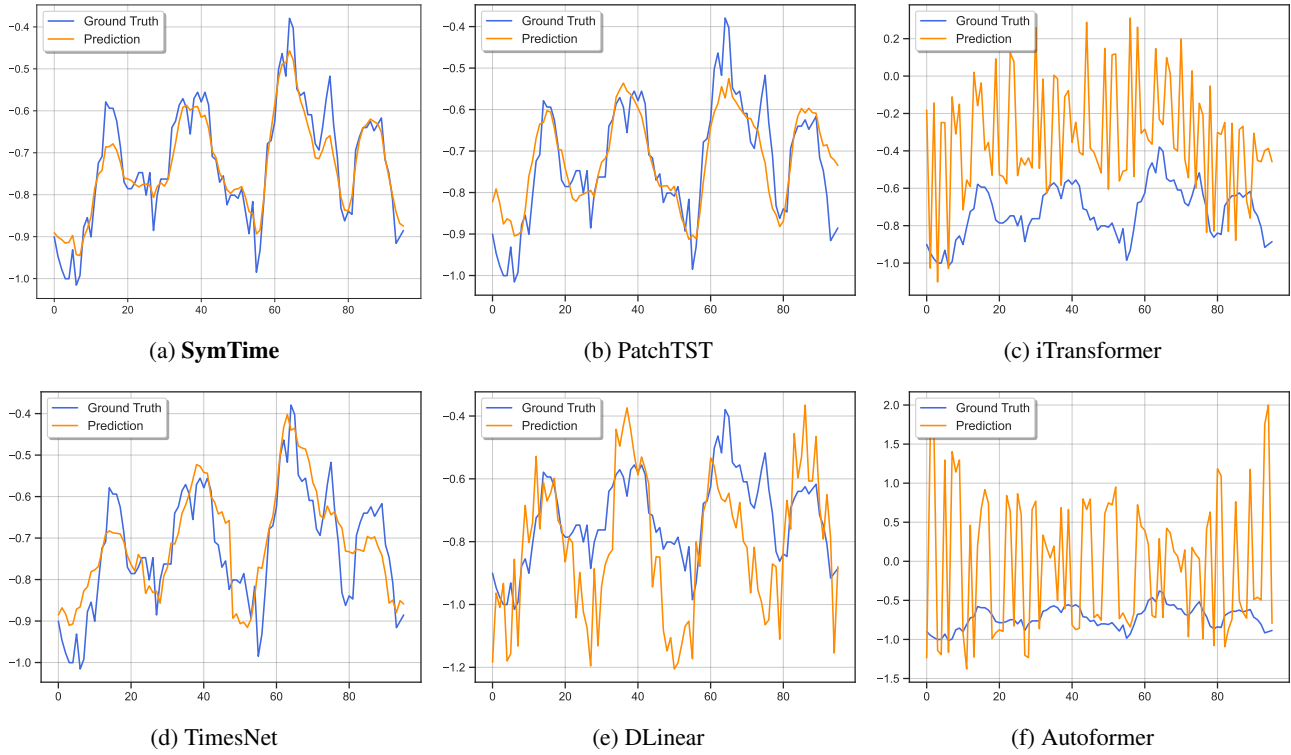


Figure 20. Visualization of time series imputation with 50% mask rate of ETTh1 dataset.

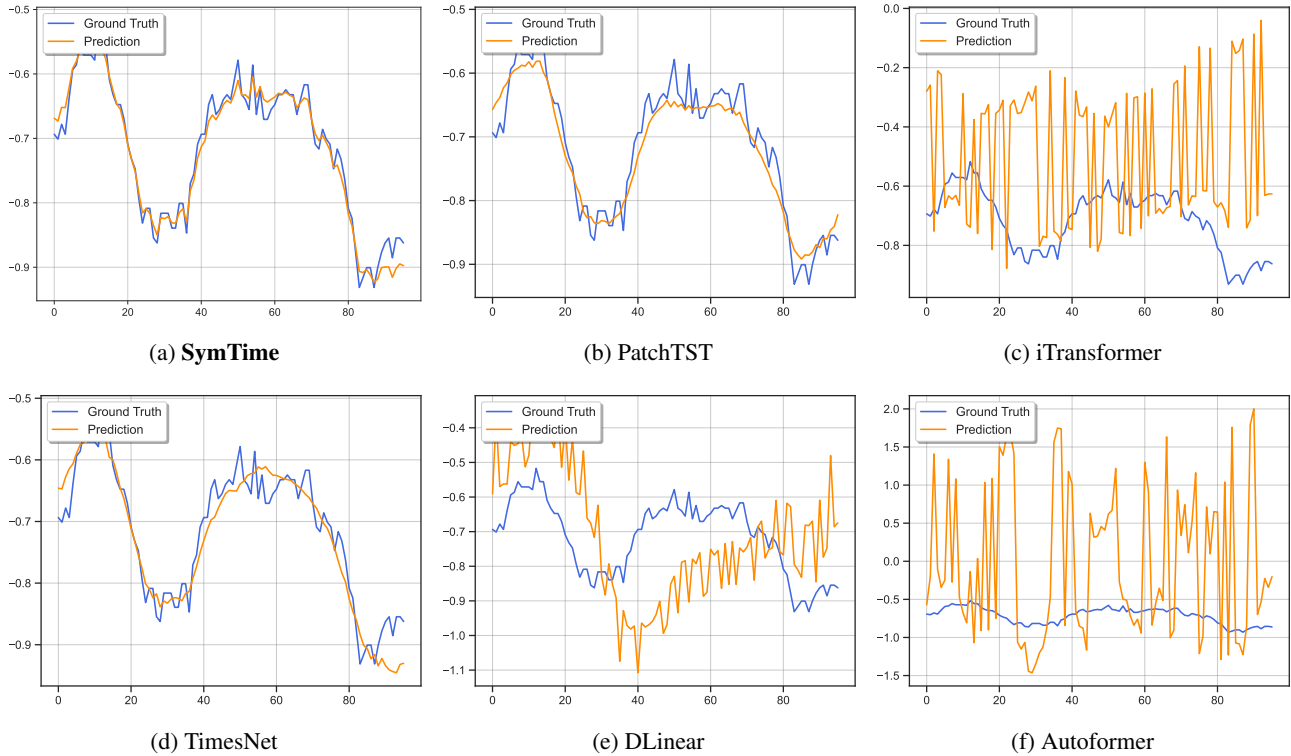


Figure 21. Visualization of time series imputation with 50% mask rate of ETTm1 dataset.

Mitigating Data Scarcity in Time Series Analysis: A Foundation Model with Series-Symbol Data Generation

Table 15. Full results for the long-term forecasting task compared with Peri-midFormer (Wu et al., 2024b), Moirai (Woo et al., 2024), Timer (Liu et al., 2024d), Time-LLM (Jin et al., 2024), TSLANet (Eldele et al., 2024), S²IP-LLM (Pan et al., 2024) and GPT4TS (Zhou et al., 2023). (* means former.) To ensure fairness in the comparison, we set the look-back window length of all models to **96**. Since the Timer and Moirai need to input a longer series to build a token, their windows are **672**. S2IP-LLM has a gradient explosion when the window is **96**, so its look-back window is **512**. **Red**: best, **Blue**: second best.

Methods	SymTime Ours		Peri-mid* (2024b)		Moirai (2024)		Timer (2024d)		Time-LLM (2024)		TSLANet (2024)		S ² IP-LLM (2024)		GPT4TS (2023)		
	MSE	MAE	MSE	MAE	MSE	MAE	MSE	MAE	MSE	MAE	MSE	MAE	MSE	MAE	MSE	MAE	
ETTm1	96	0.322	0.362	0.334	0.370	0.311	0.358	0.315	0.354	0.304	0.359	0.321	0.362	0.325	0.371	0.293	0.362
	192	0.362	0.380	0.382	0.391	0.381	0.402	0.369	0.378	0.368	0.396	0.361	0.383	0.361	0.397	0.374	0.392
	336	0.386	0.402	0.417	0.418	0.436	0.432	0.425	0.428	0.383	0.393	0.383	0.404	0.385	0.403	0.389	0.404
	720	0.419	0.423	0.501	0.461	0.466	0.476	0.442	0.447	0.420	0.429	0.445	0.437	0.426	0.446	0.421	0.423
	Avg	0.372	0.392	0.409	0.410	0.398	0.417	0.388	0.402	0.369	0.394	0.377	0.397	0.374	0.404	0.369	0.395
ETTm2	96	0.176	0.260	0.174	0.255	0.179	0.267	0.168	0.254	0.177	0.269	0.179	0.261	0.174	0.263	0.171	0.265
	192	0.244	0.306	0.249	0.305	0.244	0.311	0.429	0.425	0.239	0.305	0.243	0.303	0.232	0.306	0.226	0.304
	336	0.306	0.343	0.319	0.349	0.335	0.371	0.476	0.457	0.301	0.340	0.308	0.345	0.300	0.344	0.288	0.345
	720	0.405	0.401	0.418	0.405	0.425	0.444	0.545	0.497	0.382	0.381	0.403	0.401	0.359	0.386	0.372	0.398
	Avg	0.283	0.328	0.290	0.328	0.296	0.348	0.405	0.408	0.275	0.324	0.283	0.327	0.266	0.325	0.264	0.328
ETTth1	96	0.376	0.400	0.382	0.403	0.369	0.408	0.374	0.404	0.386	0.395	0.387	0.405	0.380	0.403	0.388	0.399
	192	0.428	0.431	0.436	0.435	0.441	0.450	0.430	0.438	0.421	0.424	0.448	0.436	0.410	0.427	0.425	0.429
	336	0.463	0.456	0.492	0.455	0.469	0.469	0.458	0.453	0.438	0.450	0.451	0.437	0.426	0.442	0.444	0.455
	720	0.450	0.458	0.508	0.490	0.486	0.490	0.475	0.480	0.506	0.510	0.505	0.485	0.610	0.543	0.479	0.477
	Avg	0.430	0.436	0.455	0.446	0.441	0.454	0.434	0.444	0.438	0.445	0.448	0.441	0.456	0.454	0.434	0.440
ETTth2	96	0.293	0.347	0.312	0.358	0.288	0.350	0.315	0.360	0.307	0.369	0.289	0.345	0.292	0.353	0.292	0.351
	192	0.376	0.397	0.388	0.403	0.390	0.426	0.411	0.423	0.349	0.384	0.362	0.391	0.355	0.388	0.351	0.394
	336	0.410	0.431	0.443	0.443	0.441	0.435	0.465	0.467	0.394	0.420	0.350	0.389	0.368	0.417	0.380	0.421
	720	0.423	0.445	0.455	0.459	0.487	0.435	0.521	0.515	0.426	0.454	0.418	0.439	0.434	0.460	0.424	0.446
	Avg	0.375	0.405	0.400	0.416	0.402	0.411	0.428	0.441	0.369	0.407	0.355	0.391	0.362	0.405	0.359	0.403
Weather	96	0.166	0.213	0.157	0.201	0.156	0.206	0.289	0.331	0.172	0.221	0.177	0.216	0.162	0.213	0.184	0.224
	192	0.212	0.254	0.244	0.273	0.229	0.274	0.314	0.349	0.194	0.241	0.226	0.258	0.197	0.246	0.230	0.263
	336	0.267	0.294	0.283	0.303	0.282	0.316	0.339	0.363	0.286	0.282	0.279	0.588	0.281	0.299	0.285	0.302
	720	0.342	0.344	0.364	0.355	0.395	0.401	0.375	0.388	0.337	0.332	0.355	0.346	0.333	0.339	0.362	0.352
	Avg	0.247	0.276	0.262	0.283	0.265	0.299	0.329	0.358	0.247	0.269	0.259	0.352	0.243	0.274	0.265	0.285
ECL	96	0.162	0.253	0.151	0.245	0.137	0.221	0.150	0.244	0.149	0.242	0.176	0.261	0.149	0.251	0.186	0.272
	192	0.173	0.264	0.168	0.259	0.158	0.243	0.159	0.252	0.167	0.261	0.182	0.268	0.171	0.269	0.190	0.277
	336	0.194	0.285	0.184	0.268	0.167	0.255	0.190	0.271	0.188	0.270	0.199	0.285	0.199	0.291	0.205	0.292
	720	0.220	0.304	0.207	0.297	0.207	0.290	0.210	0.300	0.214	0.301	0.240	0.317	0.244	0.319	0.245	0.323
	Avg	0.187	0.276	0.178	0.267	0.167	0.252	0.177	0.267	0.180	0.269	0.199	0.283	0.191	0.283	0.206	0.291
Traffic	96	0.432	0.280	0.426	0.277	0.376	0.264	0.391	0.260	0.389	0.286	0.398	0.291	0.385	0.289	0.471	0.312
	192	0.444	0.287	0.440	0.283	0.410	0.279	0.426	0.271	0.405	0.306	0.430	0.307	0.403	0.308	0.478	0.312
	336	0.458	0.293	0.477	0.311	0.442	0.287	0.451	0.297	0.424	0.299	0.494	0.312	0.425	0.299	0.493	0.319
	720	0.492	0.303	0.487	0.308	0.470	0.328	0.475	0.307	0.453	0.334	0.528	0.332	0.454	0.326	0.523	0.335
	Avg	0.457	0.291	0.458	0.295	0.424	0.289	0.436	0.284	0.418	0.306	0.463	0.310	0.417	0.306	0.491	0.320
Exchange	96	0.084	0.201	0.083	0.199	0.089	0.211	0.098	0.228	0.090	0.209	0.082	0.200	0.147	0.279	0.087	0.218
	192	0.174	0.295	0.190	0.307	0.175	0.289	0.196	0.325	0.188	0.310	0.172	0.295	0.234	0.354	0.171	0.294
	336	0.331	0.416	0.401	0.458	0.345	0.423	0.359	0.433	0.342	0.427	0.329	0.415	0.403	0.474	0.349	0.418
	720	0.847	0.694	0.879	0.702	0.882	0.744	0.875	0.713	0.885	0.707	0.889	0.747	1.103	0.804	0.873	0.713
	Avg	0.359	0.401	0.388	0.417	0.373	0.417	0.382	0.425	0.376	0.414	0.368	0.414	0.472	0.478	0.370	0.411
Average	0.339	0.351	0.355	0.358	0.346	0.361	0.372	0.378	0.334	0.353	0.344	0.364	0.348	0.366	0.345	0.359	

Table 16. Full results for the long-term forecasting task compared with FilterNet (Yi et al., 2024), TimesNet (Wu et al., 2023), iTransformer (Liu et al., 2024b), PatchTST (Nie et al., 2023), RLinear (Li et al., 2023b), DLinear (Zeng et al., 2023) and TimeMixer (Wang et al., 2024b). To ensure fairness in the comparison, we set the look-back window length of all models to 96. **Red**: best, **Blue**: second best.

Methods	SymTime (Ours)		FilterNet (2024)		TimesNet (2023)		iTransformer (2024b)		PatchTST (2023)		RLinear (2023b)		DLinear (2023)		TimeMixer (2024b)		
	MSE	MAE	MSE	MAE	MSE	MAE	MSE	MAE	MSE	MAE	MSE	MAE	MSE	MAE	MSE	MAE	
ETTm1	96	0.322	0.362	0.321	0.361	0.331	0.372	0.343	0.377	0.324	0.365	0.355	0.376	0.345	0.372	0.323	0.361
	192	0.362	0.380	0.367	0.387	0.397	0.402	0.381	0.395	0.367	0.389	0.387	0.392	0.382	0.391	0.362	0.383
	336	0.386	0.402	0.401	0.409	0.427	0.427	0.419	0.418	0.400	0.409	0.424	0.415	0.414	0.414	0.388	0.403
	720	0.419	0.423	0.477	0.448	0.493	0.463	0.487	0.457	0.460	0.445	0.487	0.450	0.473	0.450	0.454	0.442
	Avg	0.372	0.392	0.392	0.401	0.412	0.416	0.407	0.412	0.388	0.402	0.413	0.408	0.403	0.407	0.382	0.397
ETTm2	96	0.176	0.260	0.175	0.258	0.185	0.265	0.185	0.271	0.182	0.266	0.182	0.265	0.194	0.293	0.177	0.259
	192	0.244	0.306	0.240	0.301	0.256	0.310	0.254	0.314	0.250	0.311	0.246	0.304	0.283	0.360	0.245	0.306
	336	0.306	0.343	0.311	0.347	0.314	0.345	0.315	0.352	0.313	0.350	0.307	0.342	0.376	0.423	0.298	0.338
	720	0.405	0.401	0.414	0.405	0.424	0.412	0.413	0.407	0.417	0.412	0.407	0.398	0.529	0.509	0.395	0.396
	Avg	0.283	0.328	0.285	0.328	0.295	0.333	0.292	0.336	0.291	0.335	0.286	0.327	0.346	0.396	0.279	0.325
ETTh1	96	0.376	0.400	0.382	0.402	0.409	0.425	0.394	0.409	0.381	0.400	0.386	0.395	0.396	0.411	0.385	0.400
	192	0.428	0.431	0.430	0.429	0.469	0.460	0.447	0.440	0.429	0.433	0.437	0.424	0.446	0.441	0.441	0.431
	336	0.463	0.456	0.472	0.451	0.507	0.478	0.491	0.464	0.475	0.460	0.479	0.446	0.490	0.468	0.482	0.450
	720	0.450	0.458	0.481	0.473	0.521	0.497	0.517	0.501	0.517	0.502	0.481	0.470	0.514	0.511	0.504	0.482
	Avg	0.430	0.436	0.441	0.439	0.476	0.465	0.462	0.454	0.451	0.449	0.446	0.434	0.461	0.458	0.453	0.441
ETTh2	96	0.293	0.347	0.293	0.343	0.331	0.372	0.300	0.350	0.301	0.351	0.318	0.363	0.348	0.401	0.293	0.343
	192	0.376	0.397	0.374	0.396	0.429	0.423	0.380	0.399	0.374	0.398	0.401	0.412	0.473	0.474	0.376	0.396
	336	0.410	0.431	0.417	0.430	0.450	0.451	0.422	0.432	0.429	0.439	0.436	0.442	0.588	0.539	0.425	0.432
	720	0.423	0.445	0.449	0.460	0.459	0.466	0.429	0.447	0.443	0.461	0.442	0.454	0.829	0.656	0.457	0.459
	Avg	0.375	0.405	0.383	0.407	0.417	0.428	0.383	0.407	0.387	0.412	0.399	0.418	0.559	0.518	0.388	0.408
Weather	96	0.166	0.213	0.162	0.207	0.171	0.222	0.176	0.215	0.177	0.219	0.192	0.232	0.197	0.258	0.172	0.220
	192	0.212	0.254	0.210	0.250	0.234	0.273	0.226	0.258	0.222	0.258	0.240	0.271	0.237	0.296	0.227	0.259
	336	0.267	0.294	0.265	0.290	0.284	0.306	0.281	0.299	0.281	0.299	0.292	0.307	0.282	0.332	0.266	0.294
	720	0.342	0.344	0.342	0.340	0.358	0.352	0.359	0.350	0.356	0.348	0.364	0.353	0.347	0.385	0.346	0.347
	Avg	0.247	0.276	0.245	0.272	0.262	0.288	0.260	0.281	0.259	0.281	0.272	0.291	0.266	0.318	0.253	0.280
ECL	96	0.162	0.253	0.147	0.245	0.167	0.271	0.148	0.240	0.180	0.272	0.201	0.281	0.210	0.302	0.157	0.249
	192	0.173	0.264	0.160	0.250	0.186	0.288	0.165	0.256	0.188	0.279	0.201	0.283	0.210	0.305	0.170	0.261
	336	0.194	0.285	0.173	0.267	0.203	0.304	0.179	0.271	0.204	0.296	0.215	0.298	0.223	0.319	0.186	0.276
	720	0.220	0.304	0.210	0.309	0.227	0.322	0.209	0.298	0.246	0.328	0.257	0.331	0.258	0.350	0.227	0.311
	Avg	0.187	0.276	0.173	0.268	0.196	0.296	0.175	0.267	0.204	0.294	0.219	0.298	0.225	0.319	0.185	0.274
Traffic	96	0.432	0.280	0.430	0.294	0.589	0.316	0.393	0.268	0.461	0.298	0.649	0.389	0.696	0.429	0.479	0.299
	192	0.444	0.287	0.452	0.307	0.616	0.328	0.413	0.277	0.467	0.301	0.601	0.366	0.647	0.407	0.490	0.303
	336	0.458	0.293	0.470	0.316	0.628	0.333	0.424	0.283	0.483	0.308	0.609	0.369	0.653	0.410	0.493	0.304
	720	0.492	0.303	0.498	0.323	0.667	0.352	0.458	0.300	0.517	0.325	0.647	0.387	0.695	0.429	0.534	0.319
	Avg	0.457	0.291	0.463	0.310	0.625	0.332	0.422	0.282	0.482	0.308	0.627	0.378	0.673	0.419	0.499	0.306
Exchange	96	0.084	0.201	0.091	0.211	0.115	0.246	0.094	0.216	0.088	0.205	0.093	0.217	0.093	0.226	0.091	0.210
	192	0.174	0.295	0.186	0.305	0.213	0.335	0.185	0.307	0.189	0.309	0.184	0.307	0.184	0.324	0.185	0.304
	336	0.331	0.416	0.380	0.449	0.367	0.440	0.336	0.422	0.327	0.415	0.351	0.432	0.328	0.436	0.361	0.435
	720	0.847	0.694	0.896	0.712	0.978	0.753	0.893	0.716	0.886	0.706	0.886	0.714	0.880	0.705	0.974	0.741
	Avg	0.359	0.401	0.388	0.419	0.418	0.443	0.377	0.415	0.373	0.409	0.379	0.418	0.371	0.423	0.403	0.423
Average	0.339	0.351	0.346	0.356	0.388	0.375	0.347	0.357	0.354	0.361	0.380	0.371	0.413	0.407	0.355	0.357	

Mitigating Data Scarcity in Time Series Analysis: A Foundation Model with Series-Symbol Data Generation

Table 17. Full results for the long-term forecasting task compared with Autoformer (Wu et al., 2021), Crossformer (Zhang & Yan, 2023), FEDformer (Zhou et al., 2022a), ETSformer (Woo et al., 2023), Stationary (Liu et al., 2022b), LightTS (Zhang et al., 2022), Informer (Zhou et al., 2021). (Stationary means Nonstationary Transformer.) To ensure fairness in the comparison, we set the look-back window length of all models to 96. **Red**: best, **Blue**: second best.

Methods	SymTime (Ours)		Autoformer (2021)		Crossformer (2023)		FEDformer (2022a)		ETSformer (2023)		Stationary (2022b)		LightTS (2022)		Informer (2021)		
	MSE	MAE	MSE	MAE	MSE	MAE	MSE	MAE	MSE	MAE	MSE	MAE	MSE	MAE	MSE	MAE	
ETTm1	96	0.322	0.362	0.501	0.479	0.360	0.399	0.378	0.418	0.375	0.398	0.418	0.415	0.390	0.411	0.619	0.549
	192	0.362	0.380	0.578	0.510	0.422	0.449	0.438	0.449	0.408	0.410	0.506	0.454	0.425	0.436	0.760	0.645
	336	0.386	0.402	0.668	0.552	0.589	0.557	0.456	0.462	0.435	0.428	0.530	0.482	0.463	0.464	1.093	0.812
	720	0.419	0.423	0.602	0.524	0.838	0.706	0.530	0.498	0.499	0.462	0.610	0.525	0.547	0.520	1.114	0.806
	Avg	0.372	0.392	0.587	0.516	0.552	0.528	0.450	0.457	0.429	0.425	0.516	0.469	0.456	0.458	0.896	0.703
ETTm2	96	0.176	0.260	0.245	0.323	0.274	0.268	0.196	0.284	0.189	0.280	0.240	0.308	0.226	0.323	0.467	0.533
	192	0.244	0.306	0.289	0.345	0.366	0.380	0.264	0.325	0.275	0.319	0.428	0.402	0.361	0.421	0.742	0.664
	336	0.306	0.343	0.342	0.378	0.437	0.453	0.324	0.363	0.314	0.357	0.521	0.449	0.474	0.488	1.184	0.825
	720	0.405	0.401	0.441	0.429	0.506	0.623	0.434	0.428	0.414	0.413	0.602	0.501	0.760	0.631	4.039	1.530
	Avg	0.283	0.328	0.329	0.369	0.396	0.431	0.305	0.350	0.298	0.342	0.448	0.415	0.455	0.466	1.608	0.888
ETTth1	96	0.376	0.400	0.453	0.459	0.462	0.473	0.376	0.417	0.494	0.479	0.550	0.503	0.448	0.450	0.926	0.741
	192	0.428	0.431	0.481	0.470	0.495	0.484	0.431	0.454	0.538	0.504	0.655	0.569	0.503	0.483	0.968	0.757
	336	0.463	0.456	0.519	0.495	0.693	0.626	0.461	0.469	0.574	0.521	0.791	0.639	0.554	0.513	1.144	0.849
	720	0.450	0.458	0.510	0.508	0.668	0.599	0.502	0.499	0.562	0.535	0.797	0.652	0.627	0.578	1.214	0.880
	Avg	0.430	0.436	0.491	0.483	0.580	0.545	0.442	0.460	0.542	0.510	0.698	0.591	0.533	0.506	1.063	0.807
ETTth2	96	0.293	0.347	0.383	0.416	0.367	0.347	0.346	0.390	0.340	0.391	0.417	0.432	0.417	0.448	3.132	1.425
	192	0.376	0.397	0.479	0.467	0.450	0.459	0.428	0.439	0.430	0.439	0.529	0.486	0.546	0.520	5.552	1.957
	336	0.410	0.431	0.476	0.481	0.532	0.521	0.469	0.474	0.485	0.479	0.591	0.517	0.619	0.554	4.926	1.873
	720	0.423	0.445	0.494	0.503	0.614	0.633	0.473	0.486	0.500	0.497	0.601	0.531	0.972	0.704	4.201	1.741
	Avg	0.375	0.405	0.458	0.467	0.491	0.490	0.429	0.447	0.439	0.452	0.534	0.491	0.639	0.556	4.453	1.749
Weather	96	0.166	0.213	0.276	0.343	0.174	0.243	0.218	0.299	0.197	0.281	0.184	0.233	0.174	0.235	0.357	0.415
	192	0.212	0.254	0.305	0.361	0.235	0.307	0.281	0.344	0.237	0.312	0.248	0.286	0.218	0.276	0.458	0.456
	336	0.267	0.294	0.372	0.405	0.277	0.342	0.337	0.375	0.298	0.353	0.337	0.349	0.267	0.316	0.520	0.501
	720	0.342	0.344	0.430	0.437	0.369	0.407	0.423	0.429	0.352	0.288	0.399	0.385	0.353	0.366	0.926	0.705
	Avg	0.247	0.276	0.346	0.387	0.264	0.325	0.315	0.362	0.271	0.309	0.292	0.313	0.253	0.298	0.565	0.519
ECL	96	0.162	0.253	0.198	0.313	0.146	0.249	0.202	0.314	0.187	0.304	0.167	0.270	0.211	0.313	0.342	0.423
	192	0.173	0.264	0.218	0.329	0.163	0.262	0.211	0.323	0.199	0.315	0.183	0.284	0.223	0.326	0.360	0.442
	336	0.194	0.285	0.253	0.352	0.198	0.296	0.222	0.335	0.212	0.329	0.194	0.295	0.243	0.346	0.365	0.445
	720	0.220	0.304	0.265	0.367	0.245	0.346	0.272	0.373	0.233	0.345	0.224	0.321	0.277	0.371	0.412	0.469
	Avg	0.187	0.276	0.233	0.340	0.188	0.288	0.227	0.337	0.208	0.323	0.192	0.292	0.239	0.339	0.370	0.445
Traffic	96	0.432	0.280	0.608	0.383	0.516	0.268	0.592	0.372	0.607	0.392	0.621	0.347	0.667	0.419	0.720	0.407
	192	0.444	0.287	0.630	0.397	0.541	0.283	0.598	0.371	0.621	0.399	0.643	0.355	0.662	0.425	0.738	0.414
	336	0.458	0.293	0.622	0.387	0.566	0.351	0.636	0.397	0.622	0.396	0.650	0.360	0.683	0.436	0.833	0.470
	720	0.492	0.303	0.689	0.396	0.610	0.403	0.639	0.395	0.632	0.396	0.670	0.365	0.700	0.455	0.854	0.491
	Avg	0.457	0.291	0.637	0.391	0.558	0.326	0.616	0.384	0.621	0.396	0.646	0.357	0.678	0.434	0.786	0.445
Exchange	96	0.084	0.201	0.191	0.318	0.276	0.383	0.162	0.291	0.085	0.204	0.132	0.254	0.128	0.266	0.896	0.761
	192	0.174	0.295	0.315	0.407	0.540	0.552	0.276	0.382	0.182	0.303	0.251	0.361	0.292	0.402	1.146	0.861
	336	0.331	0.416	0.480	0.519	1.229	0.873	0.442	0.488	0.348	0.428	0.467	0.507	0.500	0.536	1.628	1.017
	720	0.847	0.694	1.255	0.868	1.721	1.055	1.175	0.833	1.025	0.774	1.304	0.837	1.002	0.763	2.552	1.299
	Avg	0.359	0.401	0.560	0.528	0.942	0.716	0.514	0.498	0.410	0.427	0.538	0.490	0.480	0.492	1.555	0.984
Average	0.339	0.351	0.455	0.435	0.496	0.456	0.456	0.412	0.402	0.398	0.483	0.427	0.467	0.444	1.412	0.818	

Mitigating Data Scarcity in Time Series Analysis: A Foundation Model with Series-Symbol Data Generation

Table 18. Full results for the short-term forecasting task in the M4 dataset compared with Peri-midFormer (Wu et al., 2024b), S^2 IP-LLM (Pan et al., 2024), Time-LLM (Jin et al., 2024), GPT4TS (Zhou et al., 2023), TimeMixer (Wang et al., 2024b), PatchTST (Nie et al., 2023), iTransformer (Liu et al., 2024b), TimesNet (Wu et al., 2023), DLinear (Zeng et al., 2023), Informer (Zhou et al., 2021). (* means former.) **Red**: best, **Blue**: second best.

	Methods	SymTime	Peri-mid*	S^2 IP-LLM	Time-LLM	GPT4TS	TimeMixer	PatchTST	iTrans*	TimesNet	DLinear	In*
	Metric	(Ours)	(2024b)	(2024)	(2024)	(2023)	(2024b)	(2023)	(2024b)	(2023)	(2023)	(2021)
Yearly	SMAPE	13.355	13.483	14.931	13.450	14.847	13.369	13.677	13.724	13.463	14.340	14.698
	MASE	2.997	3.080	3.345	3.184	3.628	3.009	3.049	3.157	3.058	3.112	3.293
	OWA	0.786	0.800	0.878	0.819	0.911	0.787	0.802	0.817	0.797	0.830	0.864
Quarterly	SMAPE	10.060	10.037	10.655	10.671	10.389	10.131	10.922	13.473	10.069	10.510	16.172
	MASE	1.183	1.170	1.249	1.276	1.228	1.186	1.326	1.722	1.175	1.241	2.136
	OWA	0.872	0.882	0.939	0.950	0.919	0.893	0.979	1.240	0.886	0.930	1.513
Monthly	SMAPE	12.608	12.795	13.012	13.416	12.907	12.762	14.200	13.674	12.760	13.382	15.446
	MASE	0.925	0.948	0.973	1.045	0.954	0.940	1.111	1.068	0.947	1.007	1.247
	OWA	0.872	0.889	0.909	0.957	0.896	0.884	1.015	0.976	0.887	0.937	1.122
Others	SMAPE	4.941	4.912	5.540	4.973	5.266	5.085	5.658	5.598	4.995	5.122	6.839
	MASE	3.327	3.260	8.426	3.412	3.595	3.403	3.626	3.957	3.346	3.608	4.536
	OWA	1.045	1.031	3.792	1.059	1.121	1.072	1.167	1.213	1.053	1.108	1.435
Average	SMAPE	11.785	11.897	12.514	12.584	12.367	11.885	12.866	13.233	11.888	12.500	15.018
	MASE	1.584	1.607	1.726	1.763	1.767	1.598	1.734	1.850	1.607	1.678	2.096
	OWA	0.849	0.859	0.913	0.915	0.918	0.856	0.928	0.972	0.858	0.899	1.102

Table 19. Full results for the short-term forecasting task in the M4 dataset compared with LightTS (Zhang et al., 2022), Autoformer (Wu et al., 2021), Crossformer (Zhang & Yan, 2023), FEDformer (Zhou et al., 2022a), ETSformer (Woo et al., 2023), Nonstationary Transformer (Stationary) (Liu et al., 2022b), FiLM (Zhou et al., 2022b), MICN (Wang et al., 2023a), Reformer (Kitaev et al., 2020), Pyraformer (Liu et al., 2022a). (* means former.) **Red**: best, **Blue**: second best.

	Methods	SymTime	LightTS	Auto*	Cross*	FED*	ETS*	Stationary	FiLM	MICN	Re*	Pyra*
	Metric	(Ours)	(2022)	(2021)	(2023)	(2022a)	(2023)	(2022b)	(2022b)	(2023a)	(2020)	(2022a)
Yearly	SMAPE	13.355	13.444	17.764	79.308	13.508	18.009	13.717	14.076	14.557	13.752	14.594
	MASE	2.997	3.022	3.919	18.692	3.051	4.487	3.078	3.017	3.380	3.088	3.269
	OWA	0.786	0.792	1.037	4.778	0.797	1.115	0.807	0.810	0.871	0.809	0.858
Quarterly	SMAPE	10.060	10.252	13.968	74.943	10.706	13.376	10.958	10.711	11.408	10.900	11.654
	MASE	1.183	1.183	1.754	13.133	1.263	1.906	1.325	1.292	1.384	1.316	1.392
	OWA	0.872	0.897	1.274	8.191	0.947	1.302	0.981	0.957	1.022	0.975	1.037
Monthly	SMAPE	12.608	12.798	18.200	68.892	13.925	14.588	13.917	13.362	13.803	13.949	14.963
	MASE	0.925	0.957	1.574	11.199	1.062	1.368	1.097	1.016	1.078	1.096	1.165
	OWA	0.872	0.894	1.371	7.654	0.982	1.149	0.998	0.941	0.985	0.999	1.066
Others	SMAPE	4.941	5.324	6.738	176.164	4.888	7.267	6.302	5.387	6.090	6.611	5.605
	MASE	3.327	3.410	4.853	116.723	3.244	5.240	4.064	3.670	4.203	4.492	3.966
	OWA	1.045	1.098	1.474	36.941	1.026	1.591	1.304	1.146	1.304	1.404	1.215
Average	SMAPE	11.785	11.962	16.511	78.103	12.605	14.718	12.780	12.491	13.016	12.805	13.616
	MASE	1.584	1.609	2.321	18.663	1.677	2.408	1.756	1.675	1.837	1.777	1.843
	OWA	0.849	0.862	1.215	7.759	0.903	1.172	0.930	0.899	0.960	0.937	0.984

Table 20. Full results for time series classification task compared with (1) classical methods: DTW (Berndt & Clifford, 1994), XGBoost (Chen & Guestrin, 2016), Rocket (Dempster et al., 2020); (2) RNN-based methods: LSTM (Hochreiter & Schmidhuber, 1997), LSTNet (Lai et al., 2018), LSSL (Gu et al., 2022); (3) CNN-based methods: InceptionTime (InTime) (Ismail Fawaz et al., 2020), TCN (Franceschi et al., 2019), TimesNet (Wu et al., 2023), TSLANet (Eldele et al., 2024). We report the classification accuracy (%) as the result. **Red**: best, **Blue**: second best.

Datasets / Methods	Classical Methods			RNN-based			CNN-based				SymTime (Ours)
	DTW (1994)	XGBoost (2016)	Rocket (2020)	LSTM (1997)	LSTNet (2018)	LSSL (2022)	InTime (2020)	TCN (2019)	TimesNet (2023)	TSLANet (2024)	
EthanolConcentration	32.3	43.7	45.2	32.3	39.9	31.1	39.1	28.9	35.7	30.4	37.3
FaceDetection	52.9	63.3	64.7	57.7	65.7	66.7	65.4	52.8	68.6	66.7	69.2
Handwriting	28.6	15.8	58.8	15.2	25.8	24.6	46.9	53.3	32.1	57.9	36.7
Heartbeat	71.7	73.2	75.6	72.2	77.1	72.7	75.2	75.6	78.0	77.5	74.1
JapaneseVowels	94.9	86.5	96.2	79.7	98.1	98.4	95.1	98.9	98.4	95.1	98.1
PEMS-SF	71.1	98.3	75.1	39.9	86.7	86.1	79.6	68.8	89.6	83.8	92.5
SelfRegulationSCP1	77.7	84.6	90.8	68.9	84.0	90.8	87.2	84.6	91.8	91.8	89.8
SelfRegulationSCP2	53.9	48.9	53.3	46.6	52.8	52.2	53.6	55.6	57.2	53.3	58.9
SpokenArabicDigits	96.3	69.6	71.2	31.9	100.0	100.0	96.3	95.6	99.0	98.0	98.9
UWaveGestureLibrary	90.3	75.9	94.4	41.2	87.8	85.9	92.4	88.4	85.3	89.4	89.4
Average Accuracy	67.0	66.0	72.5	48.6	71.8	70.9	73.1	70.3	73.6	74.4	74.5

Table 21. Full results for time series classification task compared with (1) Transformer-based methods: Autoformer (Wu et al., 2021), FEDformer (Zhou et al., 2022a), ETSformer (Woo et al., 2023), Informer (Zhou et al., 2021), iTransformer (Liu et al., 2024b), PatchTST (Patch) (Nie et al., 2023), GPT4TS (GPT) (Zhou et al., 2023), UniTS (Gao et al., 2024), Peri-midformer (Wu et al., 2024b) and (2) MLP-based methods: DLinear (Zeng et al., 2023), LightTS (Zhang et al., 2022). We report the classification accuracy (%) as the results. * means former. **Red**: best, **Blue**: second best.

Datasets / Methods	Transformer-based							MLP-based			SymTime (Ours)	
	Auto* (2021)	FED* (2022a)	ETS* (2023)	In* (2021)	iTrans* (2024b)	Patch (2023)	GPT (2023)	UniTS (2024)	Peri-mid* (2024b)	DLinear (2023)		LightTS (2022)
EthanolConcentration	31.6	31.2	28.1	31.6	27.0	29.6	34.2	37.3	47.3	32.6	29.7	37.3
FaceDetection	68.4	66.0	66.3	67.0	67.0	67.8	69.2	67.5	68.7	68.0	67.5	69.2
Handwriting	36.7	28.0	32.5	32.8	27.2	23.2	32.7	27.0	31.5	27.0	26.1	36.7
Heartbeat	74.6	73.7	71.2	80.5	75.6	75.7	77.2	80.5	86.3	75.1	75.1	74.1
JapaneseVowels	96.2	98.4	95.9	98.9	97.6	94.0	98.6	97.8	96.8	96.2	96.2	98.1
PEMS-SF	82.7	80.9	86.0	81.5	85.5	80.9	87.9	93.1	88.2	75.1	88.4	92.5
SelfRegulationSCP1	84.0	88.7	89.6	90.1	92.2	82.2	87.2	89.6	87.4	87.3	89.8	89.8
SelfRegulationSCP2	50.6	54.4	55.0	53.3	54.4	53.6	59.4	61.1	55.4	50.5	51.1	58.9
SpokenArabicDigits	100.0	100.0	100.0	100.0	98.0	98.0	95.2	98.9	98.0	81.4	100.0	98.9
UWaveGestureLibrary	85.9	85.3	85.0	85.6	85.9	81.7	85.1	87.8	84.3	82.1	80.3	89.4
Average Accuracy	71.1	70.7	71.0	72.1	71.1	68.7	72.7	74.1	74.4	67.5	70.4	74.5

Table 22. Full results for time series imputation task, where we randomly mask {12.5%, 25%, 37.5%, 50%} time points of length-96 time series to compare the model performance under different missing degrees. We compare with GPT4TS (Zhou et al., 2023), TimesNet (Wu et al., 2023), Peri-midFormer (Wu et al., 2024b), Moment (Goswami et al., 2024), iTransformer (Liu et al., 2024b), PatchTST (Nie et al., 2023), DLinear (Zeng et al., 2023) in this table. (* means former.) The standard deviation is within 0.5%. **Red**: best, **Blue**: second best.

Models		SymTime (Ours)		GPT4TS (2023)		TimesNet (2023)		Peri-mid* (2024b)		Moment (2024)		iTrans* (2024b)		PatchTST (2023)		DLinear (2023)	
Mask Ratio		MSE	MAE	MSE	MAE	MSE	MAE	MSE	MAE	MSE	MAE	MSE	MAE	MSE	MAE	MSE	MAE
ETTm1	12.5%	0.032	0.110	0.018	0.090	0.019	0.091	0.032	0.109	0.069	0.170	0.046	0.147	0.045	0.137	0.056	0.162
	25%	0.034	0.113	0.024	0.102	0.024	0.101	0.034	0.112	0.071	0.169	0.060	0.171	0.046	0.139	0.077	0.191
	37.5%	0.037	0.118	0.029	0.111	0.029	0.112	0.037	0.117	0.069	0.163	0.077	0.195	0.049	0.143	0.100	0.218
	50%	0.041	0.126	0.042	0.132	0.036	0.124	0.042	0.126	0.086	0.169	0.104	0.228	0.055	0.152	0.129	0.247
	Avg	0.036	0.116	0.028	0.109	0.027	0.107	0.036	0.116	0.074	0.168	0.072	0.185	0.049	0.143	0.090	0.204
ETTm2	12.5%	0.024	0.084	0.018	0.081	0.019	0.081	0.023	0.081	0.032	0.108	0.052	0.151	0.026	0.094	0.067	0.171
	25%	0.024	0.086	0.021	0.082	0.021	0.086	0.024	0.084	0.029	0.105	0.070	0.179	0.028	0.099	0.089	0.200
	37.5%	0.027	0.089	0.023	0.090	0.023	0.091	0.026	0.089	0.032	0.109	0.091	0.204	0.031	0.104	0.112	0.226
	50%	0.030	0.093	0.027	0.098	0.026	0.098	0.030	0.095	0.031	0.110	0.117	0.232	0.034	0.109	0.140	0.253
	Avg	0.026	0.088	0.022	0.088	0.022	0.089	0.026	0.087	0.031	0.108	0.082	0.191	0.030	0.101	0.102	0.212
ETTth1	12.5%	0.074	0.179	0.063	0.171	0.062	0.169	0.069	0.173	0.160	0.239	0.098	0.220	0.097	0.203	0.111	0.232
	25%	0.082	0.190	0.080	0.190	0.081	0.191	0.079	0.185	0.142	0.238	0.125	0.249	0.115	0.221	0.149	0.269
	37.5%	0.100	0.205	0.107	0.218	0.098	0.210	0.096	0.202	0.121	0.228	0.156	0.278	0.134	0.239	0.187	0.301
	50%	0.123	0.230	0.121	0.221	0.116	0.227	0.122	0.226	0.132	0.231	0.213	0.327	0.160	0.260	0.229	0.332
	Avg	0.095	0.201	0.093	0.200	0.089	0.199	0.091	0.196	0.139	0.234	0.148	0.269	0.126	0.231	0.169	0.283
ETTth2	12.5%	0.051	0.138	0.041	0.129	0.040	0.132	0.051	0.139	0.051	0.150	0.095	0.210	0.058	0.153	0.109	0.223
	25%	0.055	0.146	0.046	0.138	0.047	0.144	0.054	0.142	0.079	0.177	0.120	0.239	0.063	0.160	0.146	0.260
	37.5%	0.059	0.152	0.060	0.160	0.054	0.154	0.058	0.148	0.056	0.155	0.149	0.266	0.068	0.167	0.180	0.290
	50%	0.064	0.157	0.061	0.160	0.061	0.164	0.064	0.159	0.056	0.154	0.192	0.302	0.074	0.175	0.217	0.319
	Avg	0.058	0.148	0.052	0.147	0.050	0.148	0.057	0.147	0.061	0.159	0.139	0.254	0.066	0.164	0.163	0.273
ECL	12.5%	0.037	0.122	0.080	0.195	0.088	0.203	0.047	0.140	0.095	0.211	0.073	0.190	0.061	0.170	0.084	0.206
	25%	0.046	0.139	0.089	0.205	0.092	0.208	0.053	0.162	0.093	0.211	0.090	0.214	0.072	0.185	0.113	0.243
	37.5%	0.060	0.160	0.094	0.217	0.096	0.214	0.067	0.179	0.094	0.211	0.107	0.235	0.082	0.198	0.141	0.273
	50%	0.075	0.181	0.108	0.231	0.102	0.221	0.085	0.195	0.092	0.210	0.127	0.257	0.097	0.216	0.173	0.303
	Avg	0.054	0.151	0.093	0.212	0.094	0.211	0.063	0.169	0.094	0.211	0.099	0.224	0.078	0.192	0.128	0.256
Weather	12.5%	0.025	0.035	0.026	0.047	0.026	0.049	0.025	0.037	0.033	0.073	0.038	0.087	0.028	0.049	0.039	0.091
	25%	0.027	0.037	0.030	0.055	0.030	0.056	0.026	0.037	0.036	0.078	0.046	0.106	0.032	0.055	0.049	0.112
	37.5%	0.029	0.039	0.033	0.061	0.032	0.058	0.029	0.041	0.034	0.075	0.055	0.122	0.035	0.059	0.057	0.125
	50%	0.032	0.042	0.039	0.070	0.034	0.062	0.034	0.048	0.035	0.075	0.068	0.142	0.039	0.064	0.067	0.139
	Avg	0.028	0.038	0.032	0.058	0.030	0.056	0.029	0.041	0.035	0.075	0.052	0.114	0.033	0.057	0.053	0.116
Average	0.050	0.125	0.053	0.136	0.052	0.135	0.050	0.126	0.072	0.159	0.099	0.206	0.064	0.148	0.118	0.224	

Table 23. Full results for time series imputation task, where we randomly mask {12.5%, 25%, 37.5%, 50%} time points of length-96 time series to compare the model performance under different missing degrees. We compare with Stationary (Liu et al., 2022b), LightTS (Zhang et al., 2022), ETSformer (Woo et al., 2023), FEDformer (Zhou et al., 2022a), Informer (Zhou et al., 2021), Reformer (Kitaev et al., 2020) and Pyraformer (Liu et al., 2022a) in this table. (Stationary means Nonstationary Transformer.) The standard deviation is within 0.5%. **Red**: best, **Blue**: second best.

Methods	SymTime (Ours)		Stationary		LightTS		ETSformer		FEDformer		Informer		Reformer		Pyraformer		
	MSE	MAE	MSE	MAE	MSE	MAE	MSE	MAE	MSE	MAE	MSE	MAE	MSE	MAE	MSE	MAE	
ETTm1	12.5%	0.032	0.110	0.026	0.107	0.054	0.158	0.034	0.130	0.068	0.188	0.027	0.115	0.032	0.126	0.670	0.541
	25%	0.034	0.113	0.032	0.119	0.061	0.173	0.053	0.162	0.097	0.230	0.040	0.140	0.042	0.146	0.689	0.553
	37.5%	0.037	0.118	0.039	0.131	0.073	0.189	0.082	0.201	0.134	0.287	0.071	0.189	0.063	0.182	0.737	0.581
	50%	0.041	0.126	0.047	0.145	0.086	0.207	0.130	0.257	0.188	0.323	0.091	0.208	0.082	0.208	0.770	0.605
	Avg	0.036	0.116	0.036	0.126	0.068	0.182	0.075	0.187	0.121	0.257	0.057	0.163	0.055	0.166	0.717	0.570
ETTm2	12.5%	0.024	0.084	0.021	0.088	0.051	0.150	0.061	0.169	0.109	0.239	0.196	0.326	0.108	0.228	0.394	0.470
	25%	0.024	0.086	0.024	0.096	0.069	0.176	0.093	0.214	0.166	0.295	0.295	0.414	0.136	0.262	0.421	0.482
	37.5%	0.027	0.089	0.027	0.103	0.074	0.185	0.137	0.253	0.237	0.356	0.155	0.293	0.175	0.300	0.478	0.521
	50%	0.030	0.093	0.030	0.108	0.078	0.192	0.237	0.332	0.323	0.412	0.214	0.325	0.211	0.329	0.568	0.560
	Avg	0.026	0.088	0.026	0.099	0.068	0.176	0.132	0.242	0.209	0.326	0.215	0.340	0.157	0.280	0.465	0.508
ETTh1	12.5%	0.074	0.179	0.060	0.165	0.119	0.239	0.073	0.195	0.126	0.265	0.068	0.187	0.074	0.194	0.857	0.609
	25%	0.082	0.190	0.080	0.189	0.144	0.266	0.105	0.234	0.169	0.305	0.096	0.220	0.102	0.227	0.829	0.672
	37.5%	0.100	0.205	0.102	0.212	0.171	0.292	0.144	0.276	0.220	0.348	0.128	0.253	0.135	0.261	0.830	0.675
	50%	0.123	0.230	0.133	0.240	0.201	0.317	0.200	0.327	0.298	0.403	0.166	0.287	0.179	0.298	0.854	0.691
	Avg	0.095	0.201	0.094	0.201	0.159	0.278	0.130	0.258	0.204	0.330	0.115	0.237	0.122	0.245	0.842	0.682
ETTh2	12.5%	0.051	0.138	0.042	0.133	0.094	0.208	0.134	0.251	0.187	0.319	0.271	0.384	0.163	0.289	0.976	0.754
	25%	0.055	0.146	0.049	0.147	0.140	0.255	0.180	0.294	0.279	0.396	0.362	0.450	0.206	0.331	1.037	0.774
	37.5%	0.059	0.152	0.056	0.158	0.159	0.274	0.243	0.341	0.402	0.465	0.401	0.469	0.252	0.370	1.107	0.800
	50%	0.064	0.157	0.065	0.170	0.180	0.293	0.353	0.408	0.604	0.504	0.437	0.487	0.316	0.419	1.193	0.838
	Avg	0.058	0.148	0.053	0.152	0.143	0.258	0.228	0.324	0.368	0.421	0.368	0.448	0.234	0.352	1.079	0.792
ECL	12.5%	0.037	0.122	0.093	0.210	0.077	0.198	0.185	0.323	0.197	0.324	0.152	0.279	0.190	0.308	0.297	0.383
	25%	0.046	0.139	0.097	0.214	0.099	0.228	0.207	0.340	0.208	0.345	0.166	0.290	0.197	0.312	0.294	0.380
	37.5%	0.060	0.160	0.102	0.220	0.120	0.252	0.226	0.355	0.219	0.337	0.178	0.297	0.203	0.315	0.296	0.381
	50%	0.075	0.181	0.108	0.228	0.138	0.272	0.251	0.372	0.235	0.357	0.189	0.305	0.210	0.319	0.299	0.383
	Avg	0.049	0.151	0.100	0.218	0.108	0.238	0.217	0.347	0.215	0.341	0.171	0.293	0.200	0.313	0.297	0.382
Weather	12.5%	0.025	0.035	0.027	0.051	0.039	0.092	0.042	0.103	0.057	0.141	0.040	0.108	0.031	0.076	0.140	0.220
	25%	0.027	0.037	0.029	0.056	0.045	0.105	0.056	0.131	0.066	0.155	0.045	0.130	0.035	0.082	0.147	0.229
	37.5%	0.029	0.039	0.033	0.062	0.049	0.110	0.081	0.180	0.083	0.180	0.049	0.101	0.040	0.091	0.156	0.240
	50%	0.032	0.042	0.037	0.068	0.054	0.117	0.102	0.207	0.103	0.207	0.054	0.114	0.046	0.099	0.164	0.249
	Avg	0.028	0.038	0.032	0.059	0.047	0.106	0.071	0.155	0.077	0.171	0.047	0.113	0.038	0.087	0.152	0.235
Average	0.049	0.124	0.057	0.143	0.099	0.206	0.142	0.252	0.199	0.308	0.162	0.265	0.134	0.241	0.592	0.528	

Table 24. Full results for time series anomaly detection task, where P, R and F1 represent the precision, recall and F1-score (%) respectively. F1-score is the harmonic mean of precision and recall. A higher value of P, R and F1 indicates a better performance. We compare with: Transformer (Vaswani, 2017), Reformer (Kitaev et al., 2020), Informer (Zhou et al., 2021), Autoformer (Wu et al., 2021), Crossformer (Zhang & Yan, 2023), iTransformer (Liu et al., 2024b), Anomaly (Xu et al., 2022), Stationary (Liu et al., 2022b), DLinear (Zeng et al., 2023), LightTS (Zhang et al., 2022), ETSformer (Woo et al., 2023), FEDformer (Zhou et al., 2022a), PatchTST (Nie et al., 2023), TimesNet (Wu et al., 2023), GPT4TS (Zhou et al., 2023), Peri-midFormer (Wu et al., 2024b), UniTS (Gao et al., 2024), where Anomaly means the Anomaly Transformer and Stationary means the Non-stationary Transformer. The standard deviation is within 1%. **Red**: best, **Blue**: second best.

Datasets	SMD			MSL			SMAP			SWaT			PSM			Avg F1 (%)
	P	R	F1													
Transformer (2017)	78.44	65.26	71.24	89.85	73.71	80.99	90.77	61.76	73.50	96.82	66.41	79.76	99.31	83.18	90.53	79.20
Reformer (2020)	72.50	84.19	77.90	90.24	73.78	81.18	90.63	62.48	73.97	99.94	66.75	80.04	99.73	83.03	90.62	80.74
Informer (2021)	72.51	84.13	77.88	90.10	73.68	81.07	90.57	61.51	73.26	99.83	67.24	80.35	99.03	83.21	90.43	80.60
Autoformer (2021)	78.46	65.11	71.17	90.59	75.26	82.22	90.84	62.39	73.97	99.95	65.57	79.19	99.99	78.96	88.24	78.96
Crossformer (2023)	71.89	83.41	77.22	90.32	72.74	80.59	89.68	53.63	67.12	98.00	83.59	90.22	97.49	88.02	92.52	81.53
iTransformer (2024b)	76.13	84.70	80.19	86.15	62.54	72.47	90.68	52.78	66.72	92.23	93.05	92.64	97.92	92.03	94.88	81.38
Anomaly (2022)	88.91	82.23	85.49	79.61	87.37	83.31	91.85	58.11	71.18	72.51	97.32	83.10	68.35	94.72	79.40	80.50
Stationary (2022b)	78.51	87.98	82.97	86.86	68.63	76.68	90.62	55.74	69.02	89.26	95.42	92.24	98.17	96.30	97.23	83.63
DLinear (2023)	75.91	84.02	79.76	89.68	75.31	81.87	89.87	53.79	67.30	92.26	93.05	92.66	98.65	94.70	96.64	83.64
LightTS (2022)	87.10	78.42	82.53	82.40	75.78	78.95	92.58	55.27	69.21	91.98	94.72	93.33	98.37	95.97	97.15	84.23
ETSformer (2023)	87.44	79.23	83.13	85.13	84.93	85.03	92.25	55.75	69.50	90.02	80.36	84.91	99.31	85.28	91.76	82.87
FEDformer (2022a)	72.82	81.68	76.99	90.72	75.41	82.36	90.47	58.10	70.76	99.95	65.55	79.18	99.98	81.92	90.05	79.46
PatchTST (2023)	87.26	82.14	84.62	88.34	70.96	78.70	90.64	55.46	68.82	91.10	80.94	85.72	98.84	93.47	96.08	82.79
TimesNet (2023)	88.07	80.97	84.37	88.83	74.68	81.14	89.98	56.02	69.05	91.99	93.24	92.61	98.46	95.70	97.06	84.85
GPT4TS (2023)	87.68	81.52	84.49	82.09	81.97	82.03	90.12	55.70	68.85	92.12	93.09	92.60	98.36	95.85	97.09	85.01
Peri-midFormer (2024b)	86.97	81.37	84.08	88.66	74.02	80.68	90.02	54.03	67.53	90.74	92.55	91.64	98.46	94.06	96.21	84.03
UniTS (2024)	82.42	84.99	83.69	91.32	73.04	81.16	90.58	62.55	74.00	92.60	92.42	92.51	98.45	96.19	97.31	85.73
SymTime (Ours)	87.93	81.56	84.62	89.46	75.31	81.77	90.34	56.96	69.87	95.94	91.39	93.61	98.89	95.32	97.07	85.39